NISTIR 6760

Evaluation of a Fast, Simplified Computational Fluid Dynamics Model for Solving Room Airflow Problems

Amy Musser
Kevin McGrattan
Jeanne Palmer

NIST
National Institute of Standards and Technology
Technology Administration, U.S. Department of Commerce

NISTIR 6760

Evaluation of a Fast, Simplified Computational Fluid Dynamics Model for Solving Room Airflow Problems

Amy Musser
Kevin McGrattan
Jeanne Palmer
Building and Fire Research Laboratory
National Institute of Standards and Technology
Gaithersburg, MD 20899

June 2001

U.S. Department of Commerce
Donald L. Evans, Secretary

National Institute of Standards and Technology
Karen H. Brown, Acting Director

ABSTRACT

This report investigates the use of the Fire Dynamics Simulator (FDS), for coarse grid modeling of non-fire and fire situations. FDS is a large eddy simulation computational fluid dynamics program that was developed to model fires in enclosures. One goal of this study was to compare its predictions with experimental data and other published CFD studies of test rooms without fires in them. Four such experiments are considered. The first three are idealized test rooms designed to demonstrate forced, natural, and mixed convection. The fourth is a more realistic room setup with furniture, a displacement ventilation system, and a contaminant release. The results of these simulations agree reasonably with the experimental data, provided that care is taken in defining boundary conditions and inputs in a way that is consistent with the intention and capabilities of the model. In particular, some care is needed to define convection coefficients for heated or cooled surfaces. A second goal of this study was to determine the effects of using very coarse grids on both the computational results and computing time. The results of this comparison show that non-fire simulations are generally much faster than fires because the simulation times step is limited by the convective motion. In many cases, the coarse grid solutions agreed with the experimental data nearly as well as could be accomplished with a much finer grid and could be modeled in real time or faster. However, accurate contaminant dispersal modeling did require a significantly finer grid.

ACKNOWLEDGEMENT

The work described in this report was undertaken while the first author held a National Research Council Postdoctoral Research Associateship. The assistance of that program is gratefully acknowledged.

Evaluation of a Fast, Simplified Computational Fluid Dynamics Model for Solving Room Airflow Problems

TABLE OF CONTENTS

FIGURE LIST

TABLE LIST

1. INTRODUCTION

Many types of building design and analysis would benefit from a more detailed understanding of building airflow patterns, contaminant dispersal, and thermal stratification. Computational Fluid Dynamics (CFD) models provide this type of information and have been available for many years, however, their application has historically been limited by their need for extensive computational resources. Historically, then, two modeling techniques have evolved: CFD models to represent a single room or small set of rooms when much detail is needed, and whole-building models that are less detailed but consume fewer computational resources.

Many airflow problems require analysis of the entire building, since pressure-driven flows generated by forces such as weather and the building mechanical system influence the migration of contaminants between rooms. Often, this macroscopic view of building airflows is adequate to characterize contaminant behavior. However, when stratified or poorly mixed spaces are present within the building, the details of contaminant migration within these rooms begin to influence its interaction with surrounding rooms. A CFD modeling approach allows this room or group of rooms to be modeled in a more detailed way. A fast, simplified CFD simulation could be integrated into the whole-building simulation or possibly used on its own to model many rooms simultaneously.

This sort of integrated simulation approach would offer the building design community an enhanced ability to predict and model the performance of complicated spaces, and to simulate events more realistically. As computing time and resources become faster and less costly, emulation of building or system behavior in response to an event such as a fire or a contaminant release also becomes possible. However, before such an undertaking is begun, the CFD software must first be evaluated for its intended usage. In addition to the verification of results with experimental data, issues such as computing time, model construction, and output data must be investigated.

This report compares results of simulations performed using the Fire Dynamics Simulator (FDS) with published experimental data, covering a wide range of conditions that are encountered in buildings. Whenever possible, these results have also been qualitatively compared with published simulations from other CFD programs. The issues of computing time and model assembly have also been investigated in detail. The overall focus is to simultaneously consider both experimental verification and computing time, allowing users to build improved models and develop realistic expectations regarding speed and accuracy.

Issues of concern with regard to FDS model development, execution, and application are documented for situations relevant to the modeling of fire scenarios, indoor air quality, and thermal comfort. The report offers guidance, identifies weaknesses, and evaluates the effectiveness of the model for situations beyond the fire and smoke applications for which it was originally developed. Verification of results with experimental data and qualitative comparison with published predictions of other CFD programs provide a context from which potential users may evaluate FDS according to the needs of a specific project.

2. SIMPLIFIED CFD MODELING OF ROOM AIRFLOW

Computational fluid dynamics (CFD) models have been used to predict room air motion since the mid-1970s. Since they provide a very detailed prediction of velocities, temperatures, and species concentration in rooms, CFD models are potentially useful for many types of building analysis. Some examples include indoor air quality studies, fire modeling, thermal comfort evaluations, and predicting air distribution patterns. Unfortunately, it can be difficult to construct realistic CFD models of building airflows because diffuser flows, heat fluxes, and other boundary conditions may not be well understood or easily defined (Chen 1997). In addition, room airflows typically require turbulence modeling.

2.1. Types of CFD Models

CFD models are often categorized according to the way in which turbulence is addressed. Direct numerical simulation of the Navier-Stokes equations is possible, but requires very fine grid resolution and small time steps that demand computing capacity far exceeding what is currently available. Therefore, two groups of methods have been developed to reduce the computing effort associated with turbulence. These methods differ in the way that turbulence is approximated. The first solves a time averaged set of Navier-Stokes equations. The other method solves directly for the transient behavior of the large scale turbulent motion and approximates small scale activity to reduce computing time.

Reynolds Averaged Navier-Stokes (RANS) methods divide the flow into mean and fluctuating components, solving a time averaged set of Navier-Stokes equations. These methods save computing time by allowing coarser grids to be used and because they produce time independent solutions for steady flows. If a transient solution is desired, a quasi-steady solution is obtained at each time step. While the standard k-epsilon model may be the most well known and widely used method to approximate the effects of turbulence, models with varying degrees of complexity are available and have been successfully used to model various types of room airflow (Nielsen 1998). The simplest of these is the zero equation turbulence model. In these models, a turbulent viscosity component is represented by a simple algebraic function of the fluid density, average velocity, and mixing length. This does not add to the number of equations to be iteratively solved, resulting in very fast simulation times appropriate for a simplified model (Chen et al. 1998).

Large eddy simulation (LES) provides an alternative method of accounting for turbulence. LES seeks to filter out and directly calculate the large-scale turbulent motion, which tends to have the greatest impact on turbulent transport (McGrattan et al. 1994). Smaller-scale turbulent motion (those eddies smaller than the grid cell size chosen) is taken into account with a subgrid scale eddy viscosity model. Because the Navier Stokes equations are not time averaged, this method is inherently time dependent. LES methods are therefore best suited to solving transient flow problems, but results can be averaged over time for comparison with steady-state experimental data. LES has traditionally been more time consuming than RANS methods. However, by limiting the solution to regular geometries, a very fast solver can be used. This technique has been employed to develop a simplified LES model, Fire Dynamics Simulator (FDS), to predict room air motion in fires (McGrattan et al. 2000). This model has also been used to solve some room airflow problems (Emmerich and McGrattan 1998).

2.2. The Fire Dynamics Simulator (FDS)

The Building and Fire Research Laboratory at NIST has recently released version 1.0 of the Fire Dynamics Simulator (FDS). Previous versions of the model were referred to as LES, LES3D and most recently IFS (Industrial Fire Simulator). The name Fire Dynamics Simulator was chosen because model development is heading in a number of different directions; some of which are not necessarily ``industrial" in nature. Below is a brief description of the numerical model. Further details can be found in McGrattan et al. (2000).

Consider a thermally expandable mixture of ideal gases driven by a prescribed heat source. The equations of motion governing the fluid flow can be written in a form suitable for low Mach number applications (Rehm and Baum 1978). Sometimes, this form of the equations is referred to as ``weakly compressible" or

``thermally expandable" to emphasize that the divergence of the gas mixture is governed only by the introduction of heat or a change in the composition of the mixture. High speed compressibility effects are not admitted. The low Mach number approximation is achieved by replacing the spatially and temporally varying pressure in the energy conservation and state equations by an average or background pressure, p_o, that depends only on time. This is done to filter out acoustic waves. The efficiency of the numerical solution of the equations is dramatically increased by this approximation because the speed of sound is assumed infinite and small pressure perturbations need not be tracked in the numerical procedure. The conservation equations are written as follows:

Conservation of Mass

$$\frac{\partial \rho}{\partial t} + \nabla \cdot \rho \mathbf{u} = 0 \tag{1}$$

Conservation of Species

$$\frac{\partial}{\partial t}\left(\rho Y_i\right) + \nabla \cdot \rho Y_i \mathbf{u} = \nabla \cdot \left(\rho D\right)_i \nabla Y_i \tag{2}$$

Conservation of Momentum

$$\rho\left(\frac{\partial \mathbf{u}}{\partial t} + \left(\mathbf{u} \cdot \nabla\right)\mathbf{u}\right) + \nabla p = \rho \mathbf{g} + \nabla \cdot \tau \tag{3}$$

Conservation of Energy

$$\frac{\partial}{\partial t}\left(\rho h\right) + \nabla \cdot \rho h \mathbf{u} - \frac{dp_0}{dt} = \dot{q}''' + \nabla \cdot k \nabla T + \nabla \cdot \sum_i h_i \left(\rho D\right)_i \nabla Y_i \tag{4}$$

Equation of State

$$p_0 = \rho T \Re \sum \left(Y_i / M_i\right) \tag{5}$$

Here, all symbols have their usual fluid dynamical meaning: ρ is the density, $\boldsymbol{u}$ the velocity vector, Y_i and D_i the mass fraction and diffusion coefficient of the ith gas species, p the pressure, $\nabla \cdot \tau$ the viscous stress tensor, $\mathbf{g}$ the gravity vector, h the enthalpy, T the temperature, k the thermal conductivity, t the time, q''' the volumetric heat release rate, and $\Re$ the universal gas constant.

What distinguishes CFD models from one another is how each treats the diffusive terms in the species, momentum and energy equations. Most formulations start with the viscous terms in the momentum equations, and relate other diffusive coefficients to the viscosity.
The components of the viscous stress tensor are given by

$$\tau_{ij} = \mu\left(\frac{\partial u_i}{\partial x_j} + \frac{\partial u_j}{\partial x_i} - \delta_{ij}\frac{2}{3}\frac{\partial u_k}{\partial x_k}\right) \tag{6}$$

For a Large Eddy Simulation (LES) where the grid resolution is not fine enough to capture the mixing processes at all relevant scales, a sub-grid scale model for the viscosity is applied. Following the analysis of Smagorinsky (1963), the viscosity can be modeled as

$$\mu_{LES} = \rho (C_s \Delta)^2 |S| \tag{7}$$

where C_S is an empirical constant, Δ is a length on the order of the size of a grid cell, and $|S|$ is the magnitude of the deformation tensor

$$|S|^2 = 2\left(\frac{\partial u}{\partial x}\right)^2 + 2\left(\frac{\partial v}{\partial y}\right)^2 + 2\left(\frac{\partial w}{\partial z}\right)^2 + \left(\frac{\partial u}{\partial y} + \frac{\partial v}{\partial x}\right)^2 + \left(\frac{\partial u}{\partial z} + \frac{\partial w}{\partial x}\right)^2 + \left(\frac{\partial v}{\partial z} + \frac{\partial w}{\partial y}\right)^2 \tag{8}$$

The thermal conductivity and material diffusivity are related to the turbulent viscosity by

$$k_{LES} = \frac{\mu_{LES} c_p}{Pr} \quad ; \quad (\rho D)_{l,LES} = \frac{\mu_{LES}}{Sc} \tag{9}$$

The Prandtl number Pr and the Schmidt number Sc are assumed to be constant for a given scenario.

There have been numerous refinements of the original Smagorinsky model [Deardorff 1972, Germano et al. 1991, Lilly 1992] but it is difficult to assess the improvements offered by these newer schemes in the context of flow simulations in volumes on the order of hundreds or thousands of cubic meters.

There are two reasons for this. First, the dominant flow features, like a fire plume or ventilation jet, is so dominated by the large scale resolvable eddies that even a constant eddy viscosity gives results almost identical to those obtained using the Smagorinsky (Baum et al. 1997). Second, the lack of precision in most large scale experimental data sets makes it difficult to assess the relative accuracy of each model. The Smagorinsky model with constant C_s produces satisfactory results for most large scale applications where boundary layers are not well resolved.

A second distinguishing feature of CFD models involving fire or combustion is the way it treats the combustion and heat transfer processes. Because the FDS model is intended to be used to evaluate the effect of fires on buildings, the combustion model is extremely simple because in most cases the user prescribes the fire size. The fire is represented by introducing a large number of Lagrangian elements which release heat as they are convected about by the thermally induced motion. Since the fluid motion determines where the heat is actually released, and the heat release determines the motion, the large scale features of the coupling between the fire and the smoke transport are retained. It should be noted, however, that the heat release rate is *not* predicted, but is an input parameter in the computer programs implementing this model. The smoke is simulated by tracking the convected elements after fuel burnout is complete. A specified percentage of the fuel consumed is assumed to be converted to smoke particulate. Thus, knowledge of the spatial distribution of the Lagrangian elements is equivalent to a specification of the smoke particulate density at any instant of time. In short, this method of introducing fire into the calculation ensures that the total heat release rate of the fire is as the user specifies, but it allows the heat of the fire to be released in a way that mimics reality.

2.3. Constructing an FDS Model

The FDS input file is a simple text file that describes the domain, boundary conditions, run control parameters, and output data that are needed. The format of the file is simple enough that a typical room could be described by less than a page of text. Sample problems and a full explanation of the input file are available in a user's manual (McGrattan and Forney 2000). A brief description is presented here.

The first few command lines describe the computational domain, which must be rectangular. Another requirement of the fast solver is that the number of grid cells in each of the coordinate directions must be a multiple of 2, 3, and 5. By default, grid cells are evenly spaced. However, this can be adjusted in up to two of the three coordinate directions using a transformation. Two types of transformations are possible: polynomial and piecewise linear. Transformations using polynomial functions must be monatonic and must

map the endpoints of the domain onto themselves. They are specified by setting values of the polynomial function and its first or second derivatives at various points throughout the domain. Piecewise linear transformations specify the portion of the total number of grid cells belonging to each segment of the coordinate axis. Within each segment, the grid cells are evenly distributed.

Next, various run control quantities are specified. Here, the Smagorinsky constant, ambient temperature, and other default values can be set. The total simulated time and initial time step are also specified. If the initial time step is too large, FDS will automatically reduce it (within limits) until stability constraints are satisfied. If the initial time step is smaller than is needed for stability, the specified time step will be used throughout the simulation. Therefore, it is worthwhile to carefully choose an initial time step so that the simulation time is not increased by imposing a smaller than necessary time step.

Input parameters describing the boundary conditions are also needed. Rectangular obstructions and vents (places where fluid can enter or leave the domain) are specified, and if their dimensions do not automatically match the computational grid, their sizes are altered automatically by FDS. The default surface condition is adiabatic and inert. If velocity, thermal, or species boundary conditions are desired, the surface condition must be described and assigned to the corresponding wall, vent, or obstruction. A fire is also specified as a surface condition.

Other details available to describe the computational domain include sprinklers, heat detectors, particles, species, and chemical reactions. In a fire scenario, particles are emitted from the burning surface and emit heat as they are convected about the room. They can also be used in non-fire scenarios to represent a contaminant, or can simply be inserted into the domain to allow visualization of the airflow pattern. Particles consume considerable computational resources, so a number of options are also available to manage and reduce their impact.

Finally, the format and content of output data may be specified. Files for diagnostic output, sprinkler data, heat release rates, and masses of all species present are automatically generated. Several other optional data files are available. “Thermocouple” data files are comma delimited files that contain a point measurement of temperature, species, velocity, or some other quantity at a regular specified time interval. “Slice” files record data for a specified quantity over a plane or three-dimensional portion of the domain, also at designated time intervals. This data is unformatted and can be time averaged using a companion routine that generates an ASCII output file. Data for two scalar quantities and the three components of velocity can be archived at specified time intervals in plot3d format. Plot3d is a widely used share-ware data analysis program. If particles are used, their information is saved in a separate particle file, which can become quite large. If a boundary quantity is desired, it can be archived in a boundary file.

For post-processing, NIST has developed SMOKEVIEW (Forney and McGrattan 2000) as a companion program to FDS. SMOKEVIEW is able to read all of the various forms of output data generated by FDS, and allows the computational domain and results to be displayed as color graphics and animations. The program is operated through a menu-driven interface.

3. VERIFICATION SIMULATIONS

FDS simulation results were compared with six published experiments. Three of the data sets represent simple test rooms in which forced, natural, and mixed convection were investigated in room-like settings. A fourth case models a more complex room with a real diffuser, furniture, and a pollutant source. All of these data sets were collected under steady state conditions and have been modeled with many other CFD programs. These data sets are intended to test the capability of the program to address room airflow problems in a non-fire setting. This type of verification is needed not only for application of the model to solve problems outside of fire simulation, but also for the modeling of smoldering fires, in which ordinary room airflow phenomena can dominate the initial stages of the fire.

Two additional cases involve fires. These data sets have been used by others for verification of the FDS program, and are included here to provide a side by side comparison with the non-fire results. The effects of fire on execution times and grid refinement required were of particular interest. Since fire is a transient phenomenon, both of these data sets included time series data, allowing the transient capabilities of FDS to be utilized.

FDS is a FORTRAN code that can be compiled for a number of different operating systems. These computations were performed using a personal computer with a 400 MHz Pentium II processor and 128 Mb RAM, using the Windows 98 operating system. FDS was run in a DOS shell from the Windows operating system rather than rebooting the system in DOS. This was done because the traditional DOS operating system is not able to handle the long names of the output files generated by the current version of FDS. The program could be modified to generate appropriate filenames, but it was not expected that such a modification would significantly reduce computing time, so it was not undertaken. No other applications were run on this machine during the timing runs, so that effects of the operating system on timing of the simulations were expected to be minimal, or at least uniform between simulations.

3.1 Forced Convection

Problem Description

The forced convection validation case takes the form of a single, isothermal, three-dimensional room, as shown in Figure 1. Experimental measurements for this configuration were done by Restivo (1979), and have been used in validation of many CFD codes (Davidson and Nielsen 1996, Zhang and Chen 1999), including FDS (Emmerich and McGrattan 1998). The inlet air enters the room along the ceiling with a velocity of 0.455 m/s and a uniform, "top hat" profile. A passive exhaust is located near the floor on the opposite wall, with conditions specified such that there is no buildup of pressure in the enclosure. For the FDS simulation, the initial conditions included no air motion, and a background temperature, density, and pressure throughout the room.

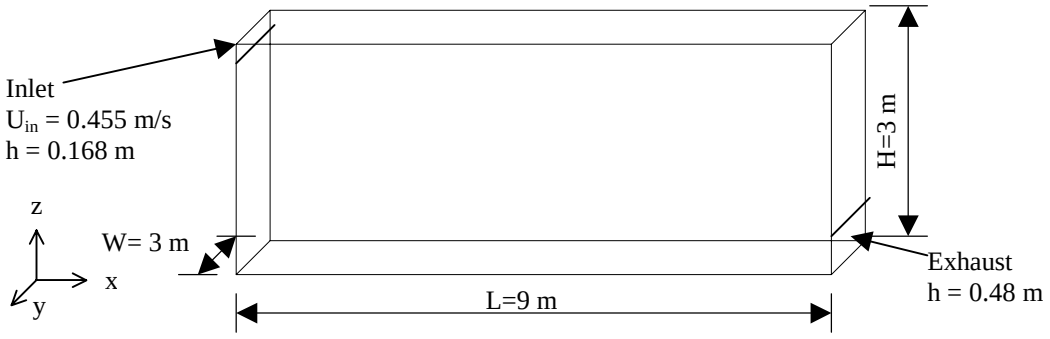

Figure 1. Geometry for the forced convection case.

Grid Selection

To illustrate the effect of grid refinement on both the simulation results and computing time, several grids were investigated. In total, sixteen cases were run, and are shown in Table 1. Cases 1 through 5 were performed without any grid transformation: the domain was divided into evenly spaced cells in the x, y, and z directions. These simulations did not produce good results, however, due to the small inlet height in relation to the overall height of the room. In these cases, the inlet and outlet dimensions had to be adjusted to fit the closest available grid cell. This required at least eighteen total cells in the z direction to represent the inlet by just one cell of the proper height. Therefore, some sort of grid refinement was needed in the z-direction.

Both piecewise linear and polynomial grid transformations were investigated. Because the length of the time step calculated by FDS is related to velocity and the cell size, it was anticipated that the nature of the grid refinement might impact computing time by influencing the number of time steps required. Piecewise linear transformations of the z-axis were used in cases 7, 8, and 13. In case 7, the inlet was represented by six cells of uniform size, the outlet by twelve, and the remaining portion of the room height by fourteen. Case 8 used a similar transformation, with eight cells over the inlet height, sixteen over the outlet height, and forty cells to describe the remainder of the room. Case 13 was also similar, with a somewhat finer grid.

A seventh order polynomial transformation of the z-axis was used for the remaining cases. Cases 6 and 9 were specified with first derivative of 0.5 at the floor and ceiling, second derivative of 0 at the floor and ceiling, with 12 % of the grid cells used to define the inlet, and 25% of the grid cells used to describe the outlet. In cases 10, 11, 12, 14, 15, and 16, 15 % of the grid cells were used to define the inlet, and 30% of the grid cells used to describe the outlet. Note that cases 14 and 15 are identical to cases 12 and 11, except that the initial time step specified was larger. Figure 2 shows the locations of the inlet and outlet vents, the vertical locations in which experimental data were collected, the piecewise linear grid transformations used in cases 7 and 8, and the polynomial transformations with the largest and smallest number of grid cells (cases 6 and 12).

Case	Refinement	Transform type (z-direction)	Smallest cell size (m)	Average time step (s)
1	144 x 50 x 50	none	0.06 x 0.06 x 0.06	>0.1
2	96 x 32 x 32	none	0.09 x 0.09 x 0.09	>0.1
3	64 x 20 x 20	none	0.14 x 0.15 x 0.15	>0.1
4	45 x 15 x 15	none	0.2 x 0.2 x 0.2	>0.1
5	36 x 12 x 12	none	0.25 x 0.25 x 0.25	>0.1
6	96 x 32 x 32	polynomial	0.09 x 0.09 x 0.05	>0.1
7	96 x 32 x 32	piecewise linear	0.09 x 0.09 x 0.03	>0.1
8	96 x 64 x 64	piecewise linear	0.09 x 0.05 x 0.02	0.076
9	60 x 32 x 32	polynomial	0.15 x 0.09 x 0.04	>0.1
10	60 x 20 x 20	polynomial	0.15 x 0.15 x 0.07	>0.1
11	45 x 15 x 20	polynomial	0.2 x 0.2 x 0.07	>0.1
12	36 x 12 x 20	polynomial	0.25 x 0.25 x 0.07	>0.1
13	108 x 45 x 45	piecewise linear	0.08 x 0.07 x 0.03	>0.1
14	36 x 12 x 20	polynomial	0.25 x 0.25 x 0.07	0.329
15	45 x 15 x 20	polynomial	0.2 x 0.2 x 0.07	0.263
16	40 x 15 x 20	polynomial	0.225 x 0.2 x 0.07	0.288

Table 1. Simulations performed for the forced convection case.

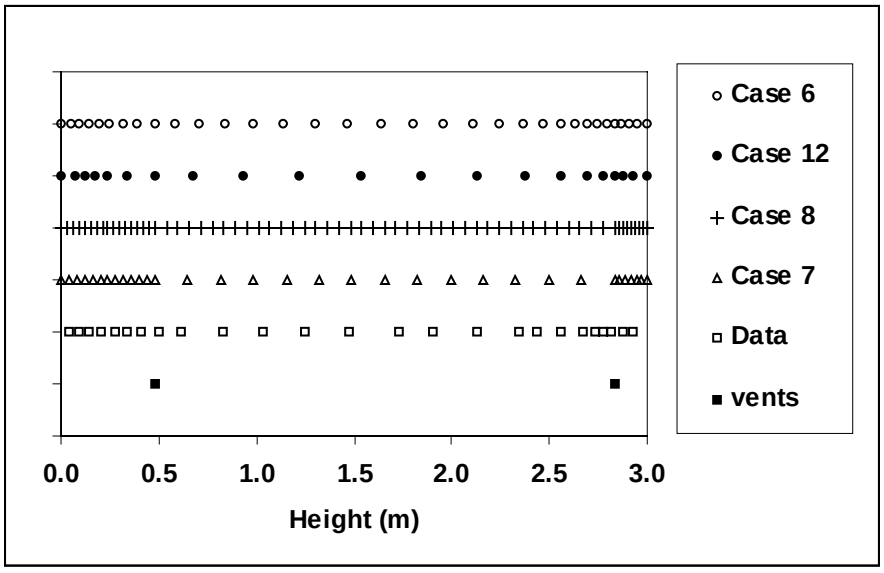

Figure 2. Grid transformations used in the forced convection case.

Computing Times

The ratio of simulated time to computing time was desired as a measure of computational speed. However, this depends on both the time step size and the computing time consumed by the airflow calculation at each time step. The maximum time step is related to the grid refinement, so these effects are not necessarily independent. Obtaining the ratio of simulated to computed time is also complicated by the process that FDS uses to adjust the time step. For each simulation, the user specifies a time step size with which to begin the simulation. If the initial time step is too large, the program will automatically reduce its size until the CFL condition is satisfied. However, if the initial time step is smaller than necessary, the program will not automatically increase the time step. Therefore, it would be possible to double the computing time for a problem simply by cutting the initial time step in half (which would double the number of time steps). Many of the simulations shown in Table 2 were run for a time step somewhat less than that necessary to satisfy the CFL condition, so these computing times do not reflect the minimum time in which the simulation could have been completed. However, another relevant computing time metric can be obtained by dividing the CPU time by the number of grid cells and by the number of time steps in the simulation. The CPU time per cell per time step is shown in Figure 3.

For these simulations, CPU time per cell per time step increased with the number of cells in an approximately linear fashion. This was not expected based on past simulations and others in this report, in which this measure of computing time was nearly constant. The fine grid simulations in this set contained the largest numbers of grid cells and longest computing times in this study. It is likely that inefficiencies related to the operating system developed when memory intensive calculations continued for a long time without rebooting. Therefore, this effect might be reduced with the use of a memory management software package when long simulations with large numbers of grid cells are performed.

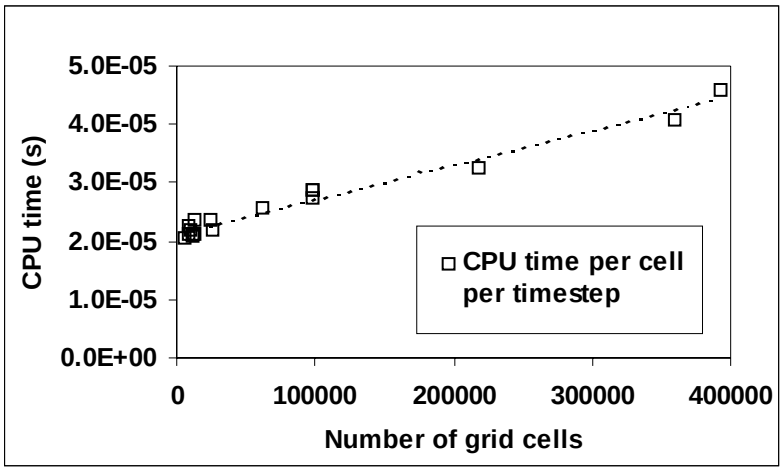

Figure 3. CPU time per cell per time step for the forced convection case.

Four of the simulations listed in Table 1 were given an initial time step larger than was needed to satisfy the CFL condition, and the largest allowable time step was used. An average time step is listed for these cases in Table 1. In general, the average time step tends to increase as the grid cell dimensions get larger. Therefore, not only is the computation at each time step faster for coarse grids, but fewer time steps are needed as well. Figure 4 shows the computing time per cell per second of simulation time for cases 14, 15, and 16. These simulations used coarse grids with polynomial transformation of the z-axis. The dashed line on this plot shows the upper limit for a "real time" simulation, which occurs when the CPU time and simulated times are equal. Points that fall on or below this curve indicate simulations that occur at "real time" or faster. For these cases, a 1:1 ratio between simulated time and CPU time occurs at approximately 13,000 grid cells. Case 14, which uses 8640 grid cells, can be completed in approximately 56% of real time (100 seconds of simulated time can be calculated in about 56 seconds).

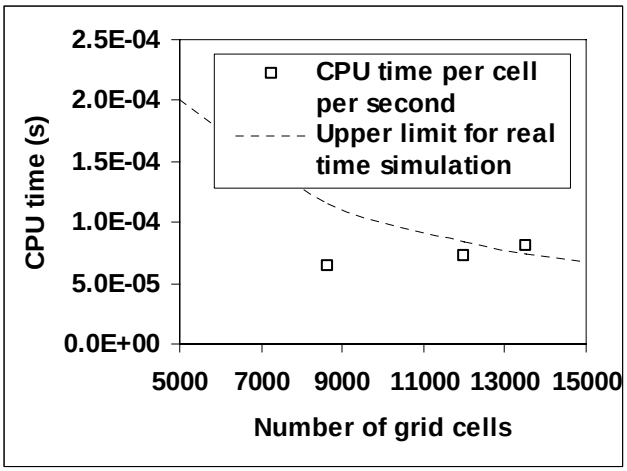

Figure 4. CPU time per cell per second of simulated time for the forced convection case.

Comparison with Experimental Data

The experimental data measured by Restivo (1979) are for a steady-state condition, while the FDS results are inherently transient. Therefore, the FDS simulation must be run long enough to no longer be influenced by the initial condition, and the results averaged over a period long enough to average out time-dependent variations. This is accomplished by comparing various averaging periods until nearly identical results are obtained. The appropriate averaging period was determined by investigating cases 6, 14, and 7. Cases 6 and

14 are the finest and coarsest grids used with polynomial z-axis transformation, and case 7 is the coarsest grid used with the piecewise linear transformation. Dependence on the initial condition no longer influenced the results of these cases after 1000 s of simulated time. Averaging of velocities over successive 500 s time periods produced profiles with slight time-dependent variation, while a 1000 s averaging period produced nearly identical profiles. This finding differs from the experience of Emmerich and McGrattan (1998) with the same simulation, and might be related to changes in the FDS program since that work was completed. Based on the investigation of these three cases, all simulations were run for 2000 s, and results averaged between 1000 s and 2000 s.

Figure 5 shows the airflow vectors generated for a vertical cross section of the room by the 45 x 15 x 20 grid with polynomial transformation. The flow, as recorded in the experiment, consists of a ceiling jet and a clockwise circulation pattern throughout the bulk of the room, with a small area of recirculation in the upper right hand corner. Simulations performed with the standard k-epsilon turbulence model (Chen, Glicksman, and Srebric 1998) have failed to predict this area of recirculation.

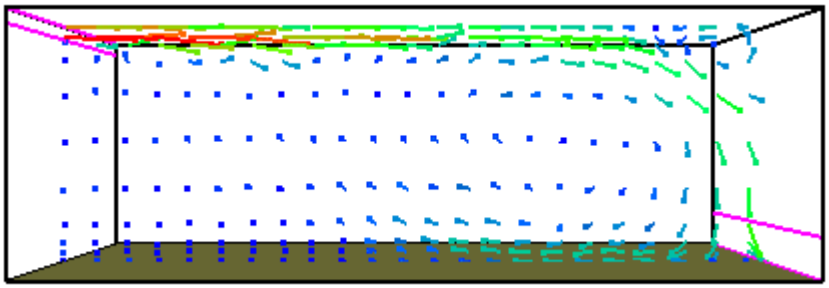

Figure 5. Airflow pattern generated for the forced ventilation case.

Figures 6, 7, and 8 show simulation results plotted with the measured experimental data. The u-component of velocity was measured in four arrays: two vertical arrays located at x=3.0 m and x=6.0 m along the centerline of the room, and two horizontal arrays located near the floor (h=0.084 m) and ceiling (h=2.916 m). These measurements were taken using hot-wire anemometers. While data on the specific instrumentation used are not readily available, hot-wire systems tend to have limitations at low velocities, with typical thresholds of 0.1-0.15 m/s. It is important to keep these limitations in mind when working with experimental data, particularly when low velocities are present.

Figure 6 shows results for the cases in which no transformation was used in the z-direction. The limitation of this approach becomes obvious when the vertical arrays are examined (6a and 6b). Velocities in the inlet region are not well predicted because they are defined by too few grid cells. The data series are plotted with symbolic markers representing the velocity at each grid cell. For the coarsest grid (36x12x12), the inlet is described by only one cell, and since the grid is too coarse, FDS increases the inlet height to fit the grid. To maintain the correct flow rate, the velocity of the flow at the inlet is reduced, and the simulation predicts much lower velocities near the inlet than are measured experimentally. Even for the finest grid used (144x50x50), there are only three grid cells used to describe the inlet, and in all of these cases, the size of the inlet had to be altered to match the computational grid. Therefore, the predicted near-ceiling velocities shown in Figure 6d became a strong function of the grid that was used. Although the outlet is somewhat larger than the inlet, a similar phenomenon can be observed with the outlet and the near-floor flows shown in Figure 6c. These results clearly indicate the need for grid refinement to properly define the inlet and outlet regions, which strongly influence the flow in this room.

Figure 7 shows results obtained for the cases in which a polynomial transformation was used to add grid refinement near the floor and ceiling. These transformations were defined such that the location of the grid cells matched the inlet and outlet locations, so that FDS did not need to adjust the size of the vents. With the exception of the 60x32x32 grid, all of these simulations produce results that reasonably resemble the experimental data. It is interesting to note that the finer grids did not necessarily produce results that more

precisely match the experiment, and that the results generated by the 36x12x20 grid were not significantly less accurate than those generated by the 96x32x32 grid. All of these results produce recirculation in the upper right hand corner of the room, which is best seen in Figure 7d as a negative horizontal velocity component near the wall at x = 9.0 m. The extent of this recirculation seems to be slightly overpredicted by all of the grids, and is much larger for the 60 x 32 x 32 grid. In that case, the inlet jet separates from the ceiling and the secondary recirculation in the upper right corner becomes much larger than was shown in the experiment. There is no obvious reason why this would occur only for the 60x32x32 case. The possible influence of time step was investigated, but identical results were obtained using a much smaller time step. Therefore, the difference must be related to the grid in some way. The most likely cause is the aspect ratio of some of the grid cells, which pushes the rule of thumb limit of three to one. This case illustrates the need to check solutions for grid independence, particularly when grids with high aspect ratios must be used.

In general, the agreement of these results with the experimental data seems to be weakest in the near wall region. This could be attributed to one of two factors. First, more detailed wall functions are available, but they have not been incorporated into the FDS model to preserve its simplicity. Second, the output data from the FDS simulation is given as an average taken at the nearest cell corner to the point specified. The actual measurements were taken very close to the floor and ceiling, and since these locations do not exactly match the computational grid the results are averaged at the nearest cell corner. This dependence on grid cell location may explain why, particularly in Figures 7c and 7d, simulations with coarser grids sometimes more closely match the experimental data. Therefore, the vertical arrays are probably the best indicator of an accurate computational solution.

The piecewise linear transformations shown in Figure 8 also agree reasonably with the experimental data. These transformations were also implemented such that the inlet and outlet match up with the computational grid, and near floor and near ceiling measurement locations (Figures 8c and 8d) averaged at the nearest cell corner. Agreement with the experimental data was generally not better than that which was obtained by polynomial transformations using coarser grids.

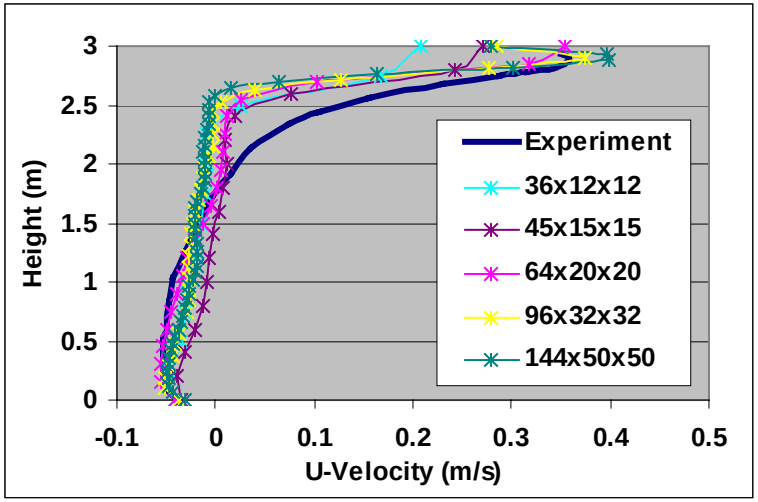

(a) x=3.0 m

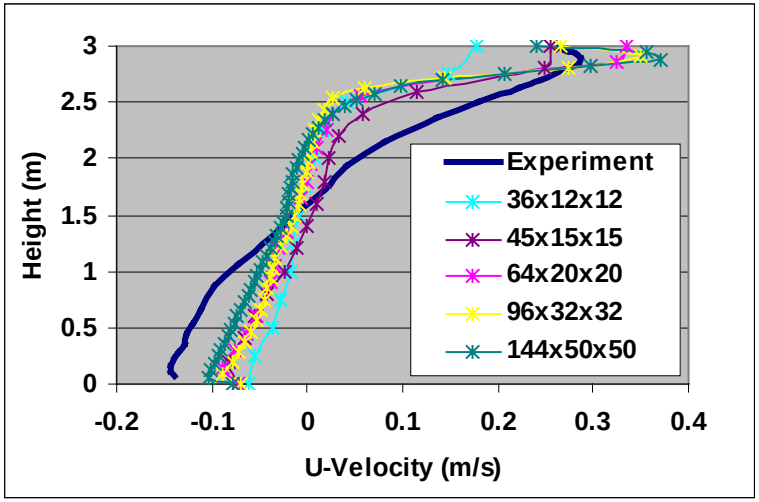

(b) x=6.0 m

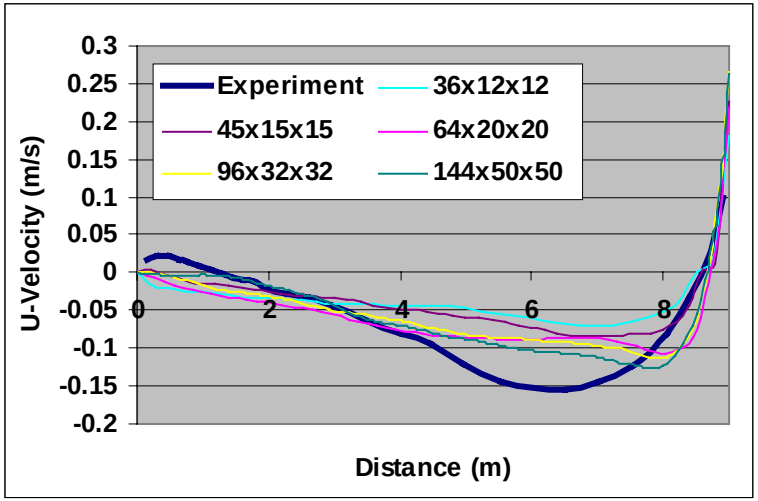

(c) near-floor

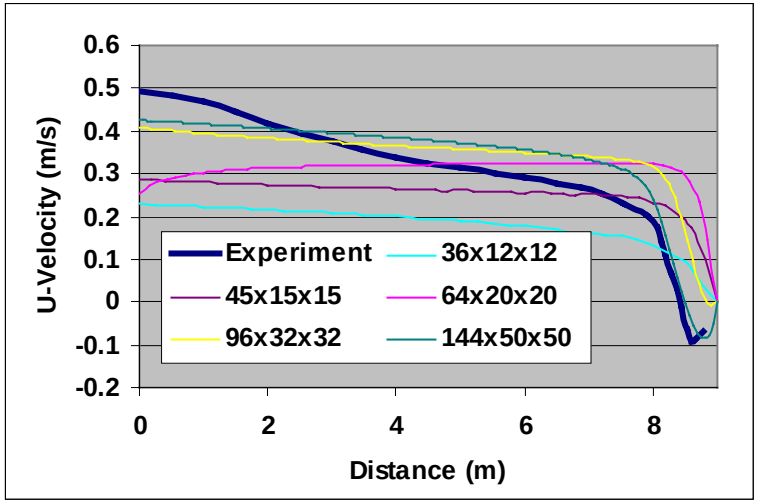

(d) near-ceiling

Figure 6. Forced convection results for non-transformed grids.

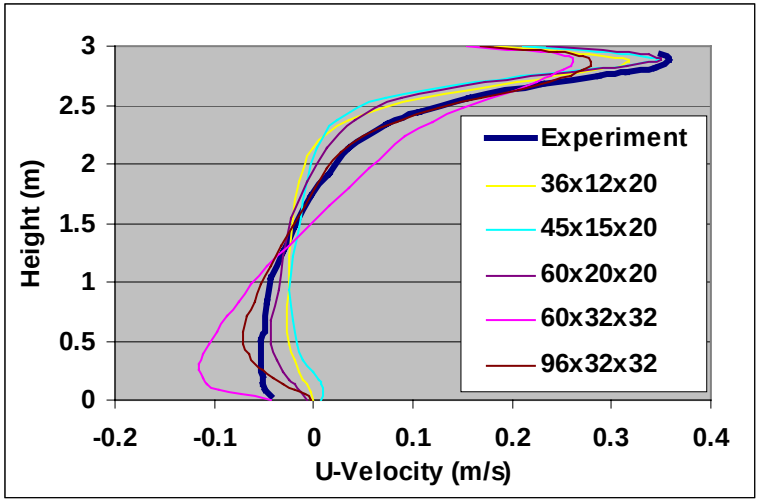

(a) x=3.0 m

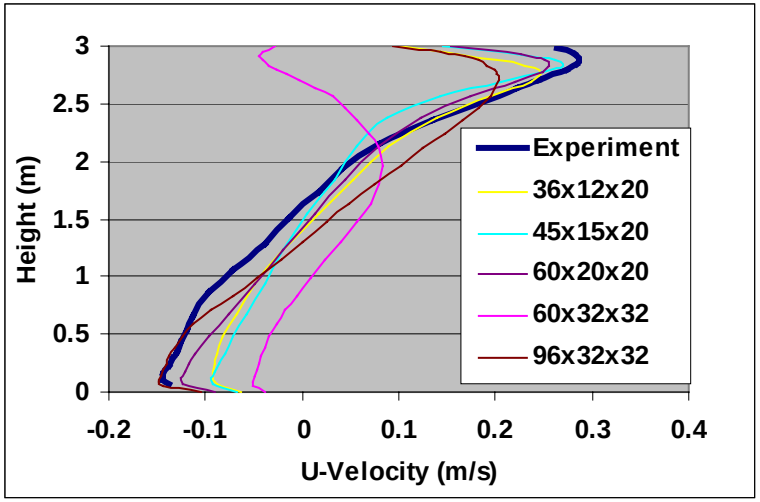

(b) x=6.0 m

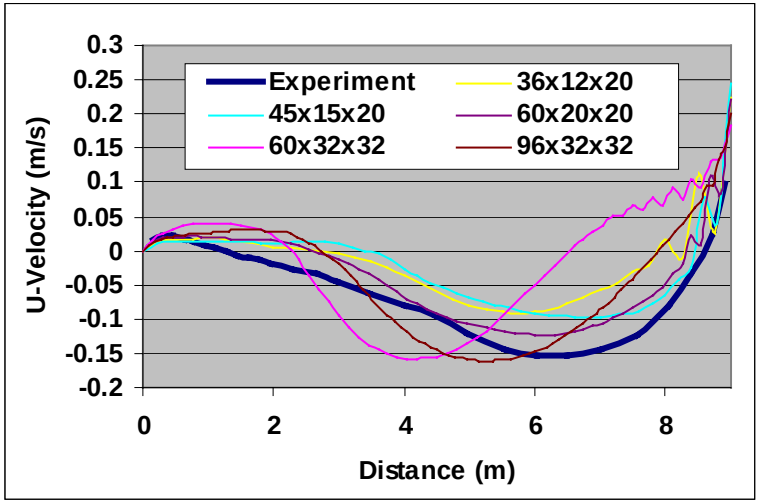

(c) near-floor

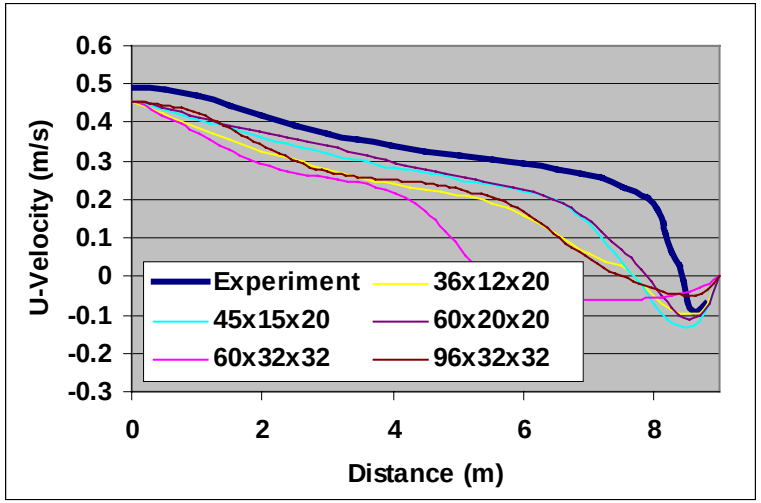

(d) near-ceiling

Figure 7. Forced convection results for cases with polynomial transformation.

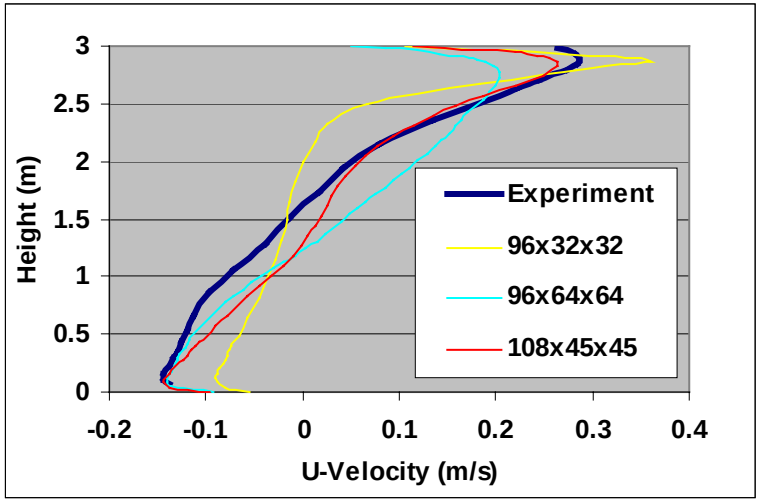

(a)

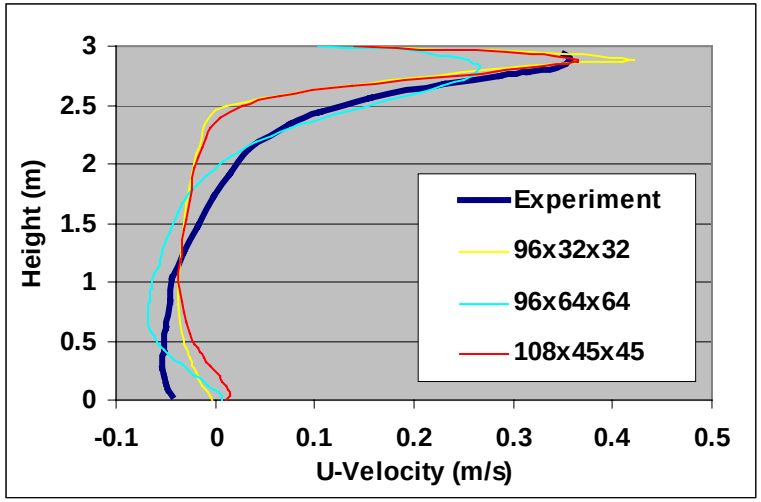

(b)

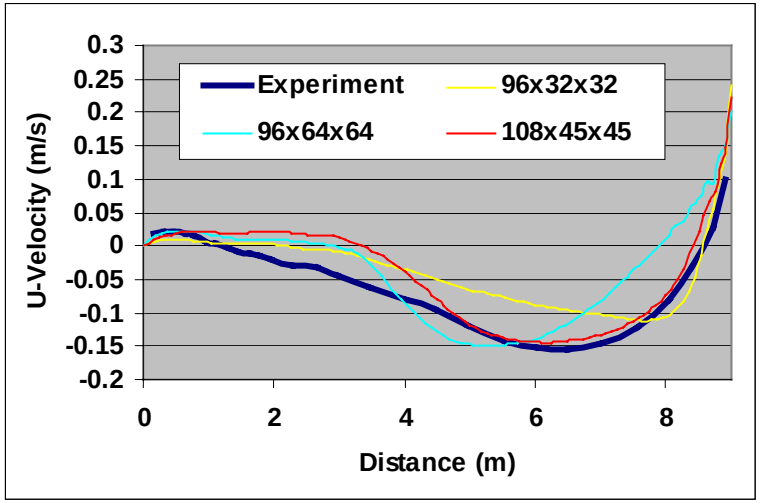

(c)

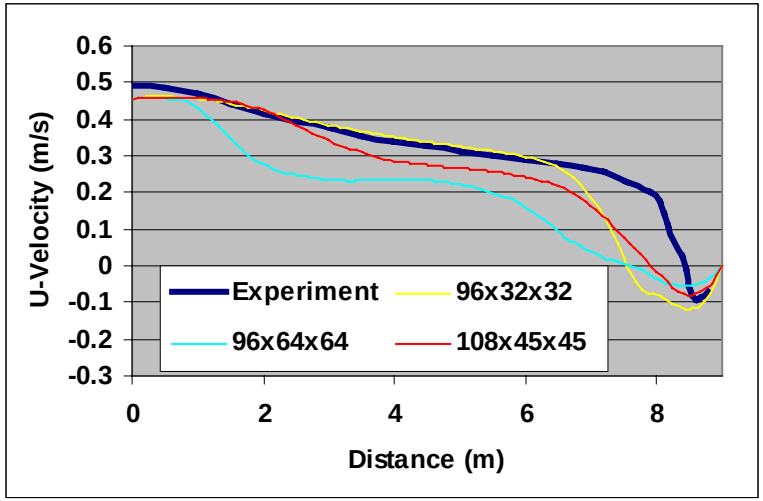

(d)

Figure 8. Forced convection results for piecewise linear transformation.

3.2. Natural Convection

Problem Description

The natural convection case is the least realistic of this study, but is a classic problem used for CFD verification. The test chamber is closed, with no flow inlets or outlets. The left wall is heated to 35.3° C. The right wall is cooled to 19.9° C. All other walls are insulated. This geometry is shown in Figure 9.

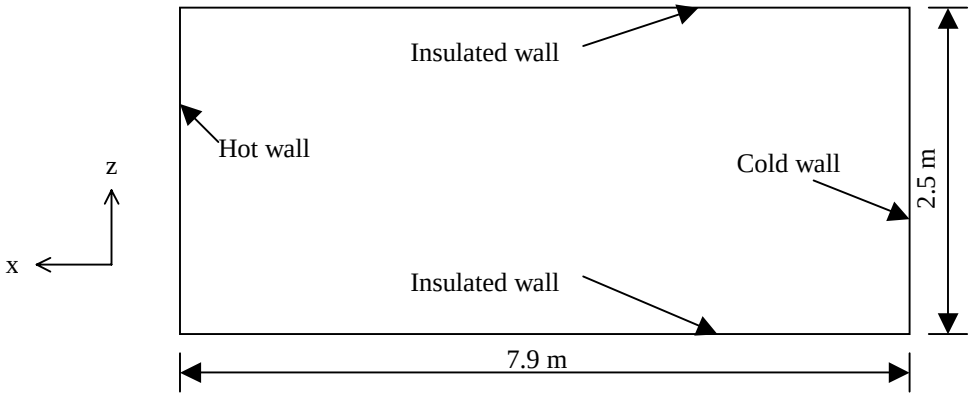

Figure 9. Problem description for the natural convection case.

Problem Representation

This problem is typically solved as a two dimensional case. In FDS, the domain is specified as one cell thick in the y-direction, with a slip boundary condition applied to the front and back walls. FDS does not allow grid transformation with two-dimensional geometries. Therefore, additional cases with a thickness of three cells were run so that grid transformation in the x-direction could be attempted. All of these transformations used polynomials with a first derivative of 0.5 and second derivative of 0.0 at the left and right walls. The seven cases are summarized in Table 2. For each case, a large initial time step was specified, and FDS allowed to determine the largest appropriate time step during the simulation.

Case	Refinement	Transform type	Smallest cell size (m)	Average time step (s)
1	25 x 1 x 8	none	0.32	2.16
2	50 x 1 x 16	none	0.16	0.95
3	81 x 1 x 25	none	0.10	0.51
4	144 x 1 x 50	none	0.05	0.22
5	50 x 3 x 16	polynomial	0.08	0.69
6	81 x 3 x 25	polynomial	0.05	0.37
7	144 x 3 x 50	polynomial	0.03	0.15

Table 2. Simulations performed for the natural convection case.

Computing Time

The CPU time per cell per time step is for these simulations is shown in Figure 10. This measure of computing time was much larger for the 25 x 1 x 8 grid than for any of the other simulations. A breakdown of contribution to computing time from various parts of the program showed that file management and other problem setup tasks make up a much larger percentage of overall computing time for this case. Because only 200 grid cells are present, these "overhead" tasks are spread among fewer grid cells and have a greater impact on overall computing time. The effect of increased computing time for finer grids was not seen for these

cases as it was for the forced convection problem. This may be because the finest grid, with 21,600 cells, was much smaller than the grids used for most of the forced convection cases.

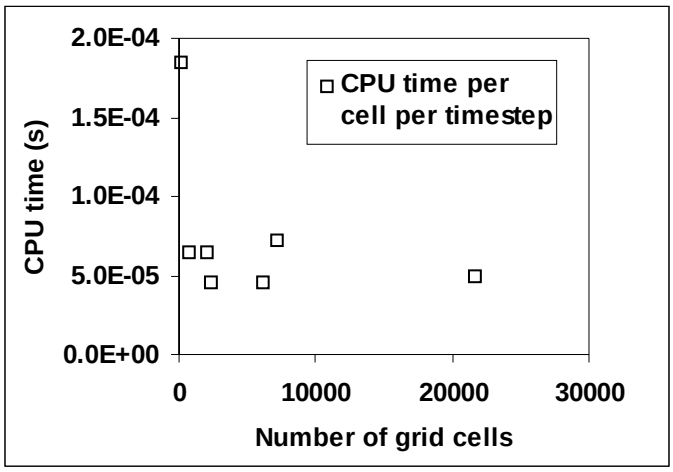

Figure 10. CPU time per cell per time step for the natural convection case.

Figure 11 shows the CPU time per cell per second of simulated time, compared to the upper limit for a "real time" simulation. This shows that the two-dimensional cases with grids of 81 x 1 x 25 and smaller and the three dimensions with grids of 81 x 3 x 25 and smaller can be completed faster than real time. The coarse grid simulations are extremely fast, and can be simulated in as little as 2% of real time. This clearly illustrates the potential time saving benefit of being able to represent room airflow using a two-dimensional geometry.

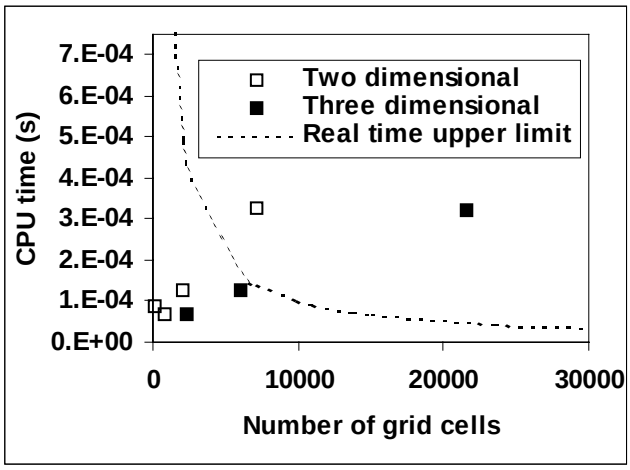

Figure 11. CPU time per cell per second of simulated time for the natural convection case.

Simulation results

The vertical temperature profile in the middle of the chamber (x = 3.95 m) has been measured experimentally by Olson et al. (1990). The measured temperatures are presented in dimensionless form, with dimensionless temperature, Θ, defined as:

$$\Theta = \frac{T - T_c}{T_h - T_c} \tag{10}$$

with T_c = cold wall temperature, T_n = warm wall temperature, and T = Temperature.
Figure 12 shows the results of the two dimensional simulations with no grid refinement, plotted with the experimental data. The FDS simulations are not grid independent, and the temperature stratification in the

room increases as the grid becomes finer. With the Smagorinsky subgrid scale model, the diffusion coefficient is proportional to the grid cell size. When a coarse grid is used, the diffusion may be exaggerated, and the temperature profile can be washed out. On the other hand, when a very fine grid is used, the simulation may not completely transition to a direct numerical simulation (DNS). FDS sets a lower bound on both the viscosity and thermal conductivity so that they cannot go below their actual molecular values. However, the heat transfer correlation does not transition to DNS. In the next release of FDS, there are plans to deal with this issue.

FDS was written as a simplified model and with the intention that relatively coarse grids would be used. As such, it does not include a detailed model of heat transfer at walls. The user may specify convection coefficients for vertical and horizontal surfaces. The heat flux from a constant temperature wall is calculated using this convection coefficient and the temperature difference between the wall and the adjacent fluid cell. This assumption requires that the grid cell size at the wall be larger than the thermal boundary layer thickness. If the grid cell size became too small next to the wall, heat transfer could actually become less efficient. However, this effect does not appear to be strong enough to overcome the diffusion effects in this case.

Results from the simulations with the transformed grids are shown in Figure 13. These simulations show even greater stratification than was obtained with the untransformed grids in Figure 12. The finer grids near the right and left walls lead to less diffusion and a stronger buoyant force near the walls.

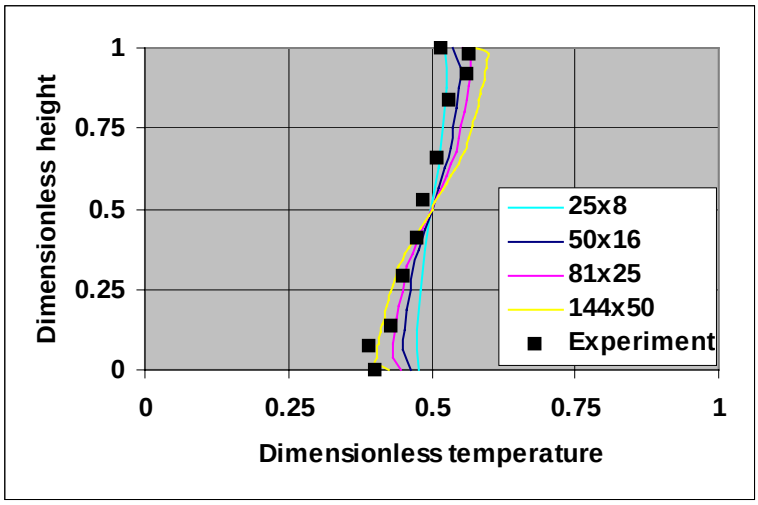

Figure 12. Dimensionless temperatures for two dimensional natural convection cases without grid transformation.

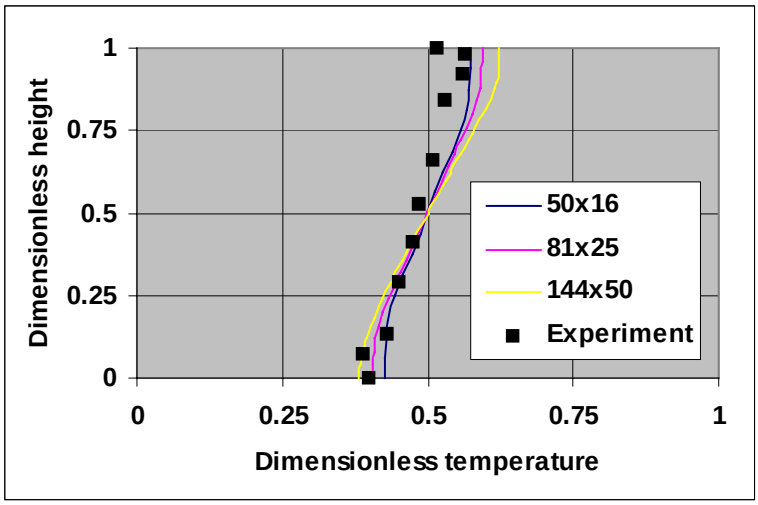

Figure 13. Dimensionless temperatures for three dimensional natural convection cases with polynomial grid transformation.

Since this simulation includes only natural convection created by the heated and cooled walls, these effects are obvious in the results of the simulation. The simulation of cases in which mixed convection effects are present will indicate the extent of these limitations on modeling more realistic room airflows. There are also some steps that the user can take in setting up room airflow problems that might mitigate these effects.

Instead of specifying a wall temperature, the heat flux at the wall could be specified. In FDS, a constant convection coefficient is still used, and the wall temperature is adjusted to provide the correct heat flux. Although the issues with regard to diffusion effects still exist, the user can be certain that the amount of heat transfer is correct. Another good strategy for this type of problem would be to check the approximate boundary layer thickness before choosing the computational grid. In this experiment, the boundary layer on the hot and cold walls was estimated through flow visualization to be between 0.05 and 0.125 m (Olsen, et al. 1990). A rough estimate for the boundary layer thickness can also be obtained from laminar correlations (Incropera and DeWitt 1990). For laminar natural convection over an infinite vertical plate, a thermal boundary layer thickness of 0.05 m can be calculated. Because the flow in this case is turbulent, a somewhat smaller thermal boundary layer would be expected. Using either of these methods to estimate the thermal boundary layer thickness, the user would want to choose a grid cell size greater than 0.05 m. This might suggest the 81 x 1 x 25 two dimensional grid, which reproduces the experimental result reasonably well.

Although velocities were not measured in the original experiment, flow visualization provided some observations that are also useful in evaluating the model. Olson et al. (1990) report that flow from the warm wall reached the ceiling and was observed to move horizontally, slowing down and thickening as it moved toward the cold wall. At the cold wall, this jet reversed direction, and part of it formed a secondary flow moving in the opposite direction beneath the ceiling jet. Some of the flow was also entrained into the cold layer moving downward along the cold wall. Symmetric behavior was observed for the cold jet in the floor of the chamber. The thicknesses of jets along the floor and ceiling were observed to be 10-20% of the room height when they reached the opposing wall. Also, a stagnant region was identified in the central portion of the room; between 40 and 60% of the room height no detectable motion was present.

Figure 14 shows profiles of the horizontal velocity component at the same location as the temperature measurements from Figure 12 for the two-dimensional simulations. All of these simulations show the ceiling and floor jets and the recirculation, although they are too large for the coarsest grid. The remaining three simulations produce ceiling and floor jets that range from about 8-18 % of the room height, consistent with the observation of 10-20% at the far wall. These simulations also show a region of relatively little motion near the center of the room.

This problem has been used to evaluate many CFD models. Xu and Chen (1998) simulated this geometry with a standard k-epsilon turbulence model and two low Reynolds number models. The standard k-epsilon model failed to predict the recirculation, but it was produced by the two low Reynolds number models. Simulations performed by Chen, Glicksman, and Srebric (1998) with a zero-equation turbulence model and a course grid did produce the recirculation, but it was larger than observed in the experiments.

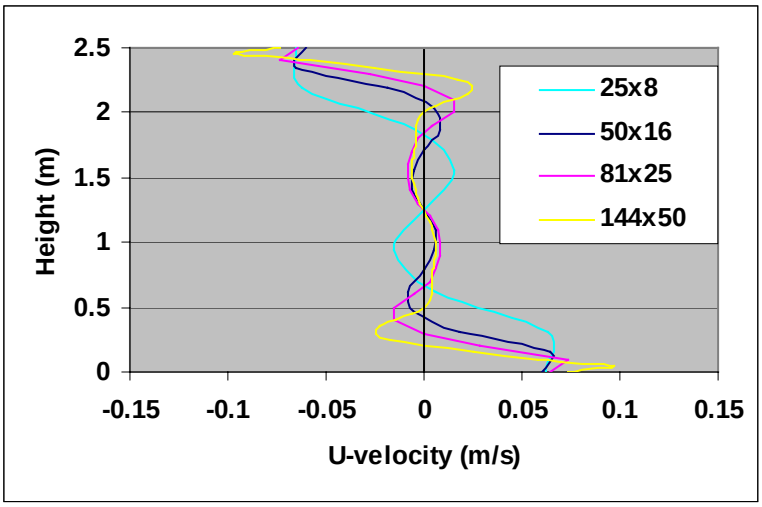

Figure 14. Velocities from two dimensional natural convection cases without grid transformation.

3.3. Mixed Convection

Problem Description

The mixed convection simulations are based on experiments conducted by Blay et. al (1992). This case is similar to another set of mixed convection experiments conducted by Schwenke (1975). Both data sets have been used for verification of CFD results, however, the former was chosen for this study because the data provided is more detailed and the original publication is available in English. The geometry of this case is similar to the forced convection case, except that the chamber is square. Dimensions and boundary conditions are shown in Figure 15. The floor of the chamber is heated to 35.5 ° C, and the supply air enters at a temperature of 15.0 ° C and a velocity of 0.57 m/s. All other walls were maintained at a temperature of 15.0 ° C.

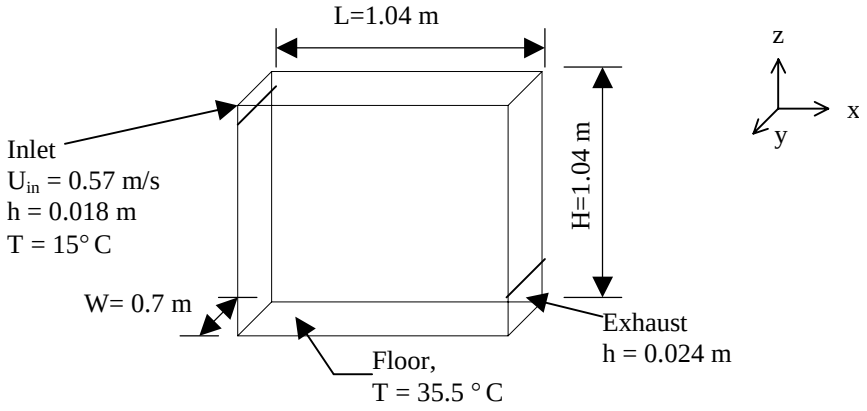

Figure 15. Geometry for the mixed convection case.

Grid Selection

The most influential issue in defining the computational grid for this problem was proper representation of the inlet and outlet. Although their geometry and flow characteristics are relatively simple, the need for grid refinement is dictated by the small height of the inlet and outlet vents relative to the room. If uniform grid spacing in the vertical direction were used, 60 cells would be needed to represent the inlet by just one cell of the proper height. Therefore, transformations were needed. A total of eight cases (shown in Table 3) were investigated. Four of these used piecewise linear transformations, and four used polynomials. In all cases, the grid was specified such that the inlet and outlet were modeled at their exact experimental dimensions (0.018 m and 0.024 m, respectively). Grid refinement of the vertical axis is shown graphically in Figure 16.

The FDS simulations were specified with an initial time step larger than was needed to satisfy the convergence criteria, and the program chose the largest appropriate time step. The average time steps shown in Table 3 are generally much smaller than those obtained for the forced convection case. This is because the time step is related to cell size, which is much smaller for these cases.

This strategy of allowing FDS to find its maximum acceptable time step produced an unstable result for Case 6. This was initially rather puzzling, since stable results were obtained for a similar polynomial grid transformation for both coarser and finer grids. Imposing a smaller time step (0.05 s) for the simulation eliminated the instability, and produced results that were similar to those obtained with the other grids. This was the only simulation in this study that experienced this problem, but it does suggest a potential pitfall of this strategy. One possible explanation is that the stability constraint $\delta t << \delta x^2/\nu$ may not have been satisfied. FDS only checks this constraint for DNS simulations, but it could become important for LES simulations with small grid cells, such as those that were needed to correctly model the inlet and outlet in this problem. This is yet another reason why checking results against those generated with different grids and smaller time steps is essential when experimental data are not available.

Case	Refinement	Transform type (z-direction)	Cells representing inlet, outlet	Smallest cell size (m)	Average time step (s)
1	10 x 8 x 10	piecewise linear	1, 1	0.10 x 0.09 x 0.018	0.16
2	20 x 15 x 20	piecewise linear	2, 2	0.05 x 0.05 x 0.009	0.04
3	40 x 30 x 40	piecewise linear	2, 2	0.03 x 0.02 x 0.009	0.04
4	40 x 30 x 40	piecewise linear	4, 4	0.03 x 0.02 x 0.004	0.02
5	10 x 8 x 10	polynomial	1, 1	0.10 x 0.09 x 0.018	0.19
6	15 x 10 x 15	polynomial	1, 1	0.07 x 0.07 x 0.018	>0.05*
7	20 x 15 x 20	polynomial	2, 2	0.05 x 0.05 x 0.008	0.04
8	40 x 30 x 40	polynomial	4, 4	0.03 x 0.02 x 0.004	0.02

*Unstable solution with code-determined time step

Table 3. Simulations performed for the mixed convection case.

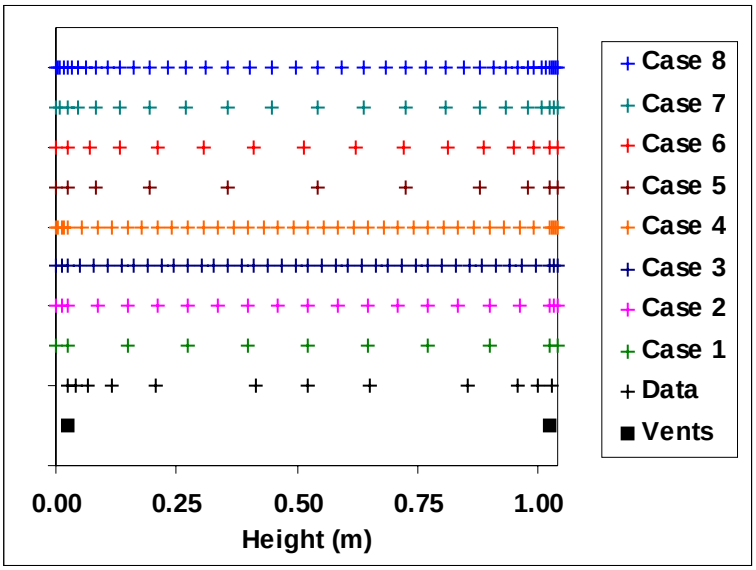

Figure 16. Grids transformations used in the mixed convection case.

Computing Times

Figure 17 shows computing time per cell per time step for the mixed convection case. For these simulations, this measure of computing time only varied only by about 10%, and showed very little relationship to the number of grid cells.

In Figure 18, the computing time per cell per second is plotted for the coarse grid cases. Cases 1 and 5, with the 10 x 8 x 10 grids, can be simulated in approximately 20% of real time. Case 6 appears to be much slower, consuming about 150% of real time. This is partially because the time step for this simulation had to be reduced to produce a stable solution. The original solution was obtained at a speed that was faster than real time, and it might be possible to "fine tune" the time step to obtain a faster, stable solution. Since the results obtained did not seem significantly better than those generated by the 10 x 8 x 10 grids, this was not pursued.

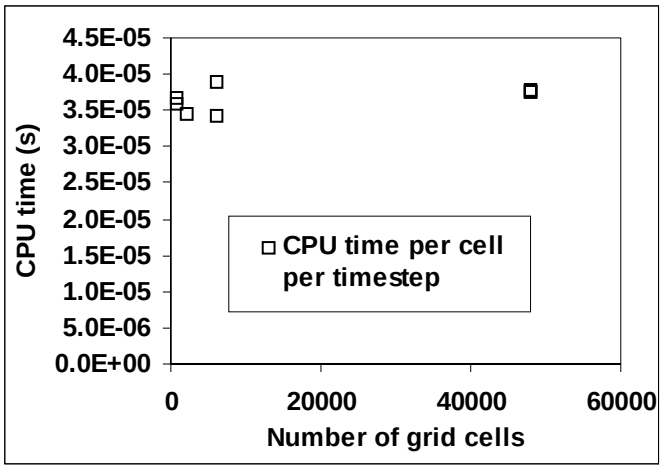

Figure 17. CPU time per cell per time step for the mixed convection case.

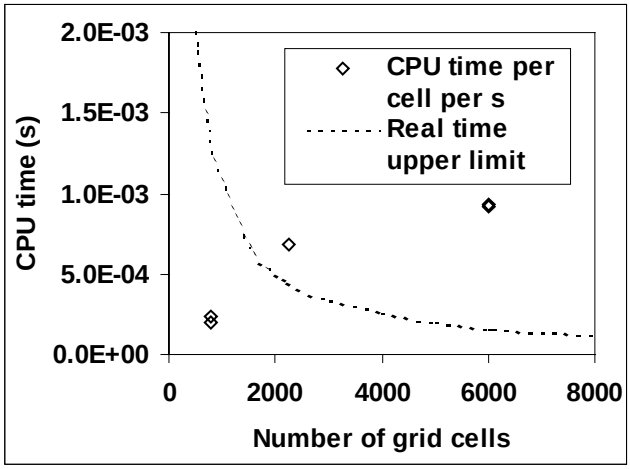

Figure 18. CPU time per cell per second for the mixed convection case.

Comparison With Experimental Data

The experiments included several cases in which the floor temperature and inlet velocity were varied. They documented two different flow patterns that were related to the Froude number of the flow: at high Froude numbers, a counterclockwise flow pattern developed, while at lower Froude numbers the inlet jet separated from the ceiling and a clockwise flow pattern formed. This was a result of reduced inlet jet momentum in relation to the buoyancy force caused by the heated floor. In decreasing and increasing the Froude number until the flow switched between flow regimes, a significant hysteresis effect was noted. However, in all cases the counterclockwise flows were produced below Fr=1.92 and clockwise flows were produced above Fr=3.41.

The Froude number for the data set that is presented here is 5.31, well above the threshold at which a counterclockwise flow pattern is expected. Blay et al.(1992) present computational results obtained for this data set using two different low Reynolds number k-epsilon turbulence models. The Jones and Launder model incorrectly produced a counterclockwise flow because it overestimated heat transfer from the floor. The Lam and Bremhorst model with modifications by Davidson produced the correct clockwise flow pattern. Likewise, all of the FDS simulations performed for this study correctly produced a clockwise flow pattern with the exception of the original case 6 simulation. The problem with that simulation was corrected by reducing the time step.

Figures 19 and 20 show the simulation results compared with velocity and temperature data collected from poles located at x=0.502 and z=0.502 m. The x-component of velocity was measured at the pole located at x=0.502 m, and the z-component measured at z=0.502 m.

The velocities predicted by FDS resemble the experimental data reasonably well, although the predicted temperature profile is slightly more linear than the measured one. It is interesting to note that there is little difference between the results obtained with piecewise linear and polynomial grid transformation, nor is there a clear improvement related to number of grid cells. Cases 3 and 4 differed only in the number of cells used to define the inlet and outlet, and the additional detail in that region does not appear to improve the result significantly.

There does seem to be more variation in the temperature profiles generated using different levels of grid refinement. Again, the heat transfer in this problem is not independent of the grid. The bulk temperature in the room tends to decrease as the number of grid cells increases. Cases 3 and 4 had the same total number of grid cells, but the size of grid cells adjacent to the floor and ceiling was smaller in case 4 than in case 3, and the bulk temperature was lower in case 4 as well. Therefore, it seems that making the grid cells near the floor smaller reduces the heat transfer from the floor. Given the small size of the grid cells in this case, this is most likely due to violation of the assumption that the boundary layer is smaller than the first grid cell. FDS, a coarse grid model, calculates the heat transfer based on a constant heat transfer coefficient and the temperature difference between the wall and the first grid cell. This means that the conventional expectation of improved results with a finer grid may be incorrect. In this case, the wall heat transfer would be better modeled using a coarse grid. Unfortunately, a fine grid was needed to adequately define the inlet and outlet flows for this problem.

Choice of convection coefficient is another factor that strongly influences the heat transfer from constant temperature walls. Additional tests with these data showed that the results were very sensitive to the choice of these coefficients. Since the experimental data was available, it would have been possible to "tune" the CFD model to more closely reproduce the measured temperatures. However, this was not done since it was felt that the results would not be representative of the kinds of predictions that could be produced by a practitioner using the model in a situation for which experimental data were not available.

Choosing a convection coefficient to represent room airflows is not an easy task, but it can have a significant impact on the results generated by the simulation. In FDS, convection coefficients are expressed in the form,

$$h=C(\Delta T)^{1/3} \qquad (11)$$

where h is the heat transfer, ΔT is the temperature difference, and C is an empirical convection coefficient. The default values used in FDS are taken from Holman (1989), which gives a simplified relationship for air in which C_v=0.95 W/m^{2}K$^{4/3}$ and C_h=1.43 W/m^{2}K$^{4/3}$ for idealized, infinite vertical and horizontal surfaces. However, FDS allows the user to specify horizontal and vertical convection coefficients that are applied to all heated or cooled surfaces in the enclosure.

Convection coefficients published elsewhere can be quite different from these values, and may be more appropriate for indoor air situations. Incropera and Dewitt (1990) give relationships, also for idealized situations, that produce C_v=1.18 W/m^{2}K$^{4/3}$ and C_h=1.78 W/m^{2}K$^{4/3}$ using properties of air at 27° C. The heat transfer section of the 1997 ASHRAE Handbook of Fundamentals gives C_v=1.31 W/m^{2}K$^{4/3}$ and C_h=1.52 W/m^{2}K$^{4/3}$, however, it is noted that these relationships may not be entirely appropriate for convection in rooms, citing experiments conducted by Bauman et. al (1993) that suggest even higher coefficients may often be appropriate.

The thermal transmission section of the ASHRAE Handbook of Fundamentals and a number of HVAC texts give overall constant heat transfer coefficients of 8.29 W/m^{2}K (vertical) and 9.26 W/m^{2}K (horizontal) for still air next to a wall. These include radiation: once it is subtracted out, they become 3.08 and 4.05 W/m^{2}K, respectively. It is noted that these values were calculated for ΔT=5.56 ° C and an ambient temperature of 21° C. This temperature difference is higher than usually occurs in indoor situations.

Bauman et. al (1993) conducted experiments to calculate heat transfer coefficients in room-like situations. However, the tests themselves were actually done in water and similarity relationships used. They found that

the flows did not transition to turbulence as soon as was expected, so the relationship that they developed for vertical walls takes the form of a correlation for laminar flow.

In reality, the convection in real rooms is probably influenced by both forced and natural convection. Especially near the diffuser, the flow may not be well approximated by the idealized situation of still, cool air exposed to an infinite, heated plate. In this type of situation, it may be appropriate to use a higher convection coefficient.

Table 4 summarizes the published convection coefficients relevant to room airflow problems. For this problem horizontal and vertical coefficients of C_h=4.05 and C_V=2.03 were selected based on experience and judgement. This selection produced very good results when used with a coarse grid. If a fine grid were needed for some reason, one might attempt to increase the convection coefficient in an attempt to obtain the same heat transfer rate. This would be a rather un-scientific approach: it would be better in such a case to simply specify the desired heat flux at the wall.

Source	correlation	C_v	C_h	For $\Delta T=2^\circ$ C	
				Q_v	Q_h
Holman	$h=C(\Delta T)^{1/3}$	0.95	1.43	2.39	3.60
Incorpera & Dewitt	$h=C(\Delta T)^{1/3}$	1.18	1.78	2.97	4.49
ASHRAE Fundamentals (Sec. 3)	$h=C(\Delta T)^{1/3}$	1.31	1.52	3.30	3.83
ASHRAE Fundamentals (Sec. 22)	h=C	3.08	4.05	6.16	8.10
Bauman, et.al	$h=C(\Delta T/H)^{0.22}$	2.03	na	3.80	na

Table 4. Surface Convection Coefficients Relevant to Room Airflow.

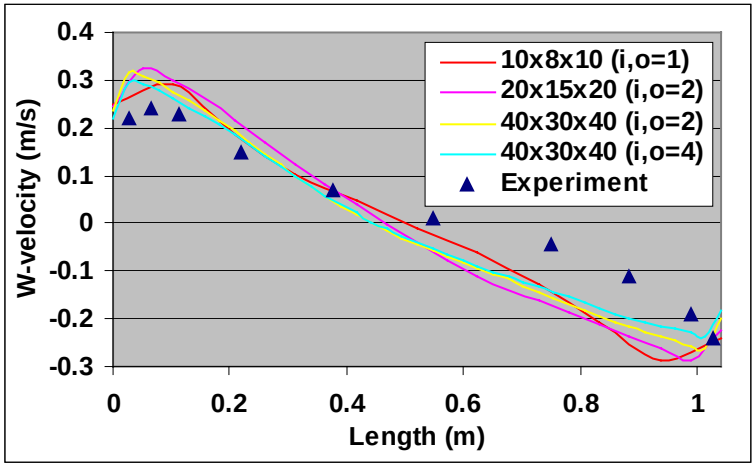

(a) W-velocity at z=0.502

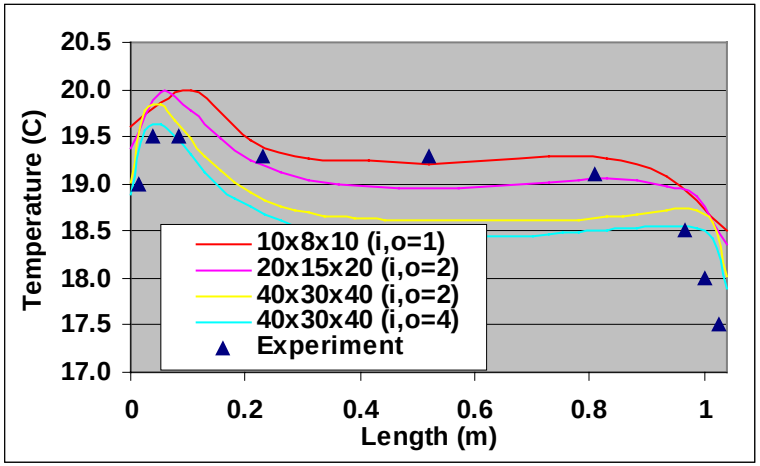

(b) Temperature at z=0.502

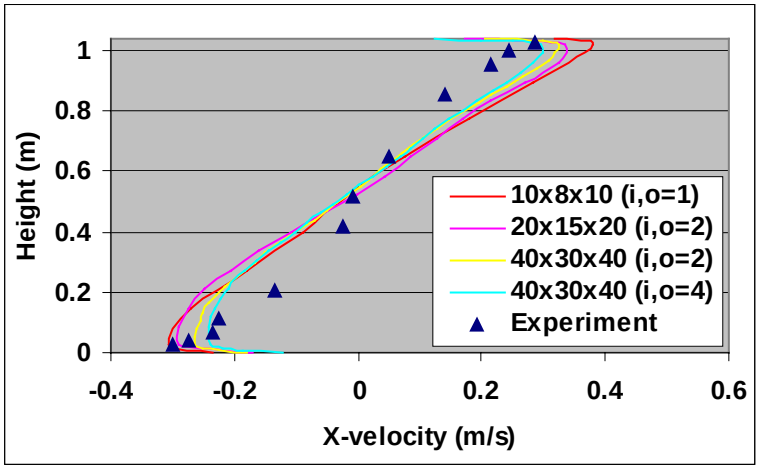

(c) X-Velocity at x=0.502

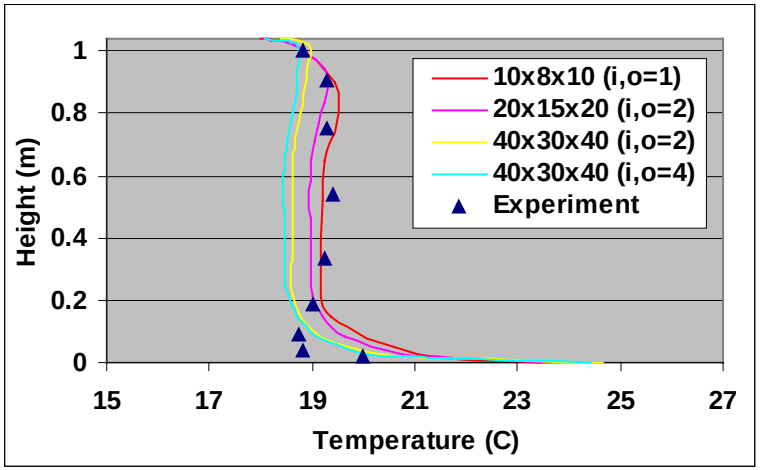

(d) Temperature at x=0.502

Figure 19. Mixed convection results for the piecewise linear transformations.

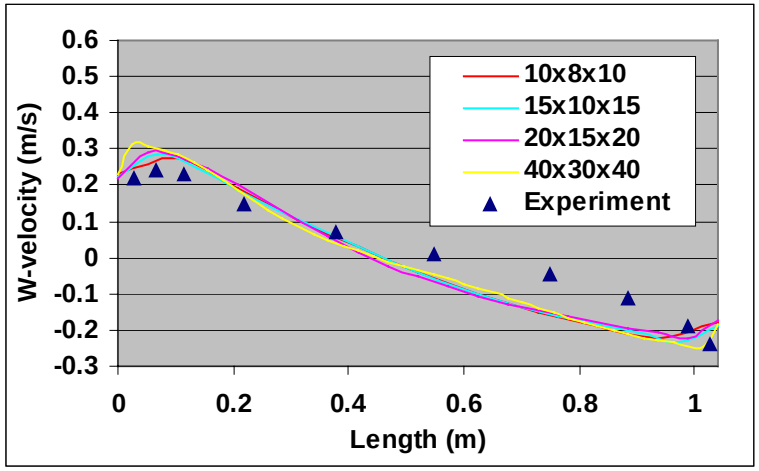

(a) W-velocity at z=0.502

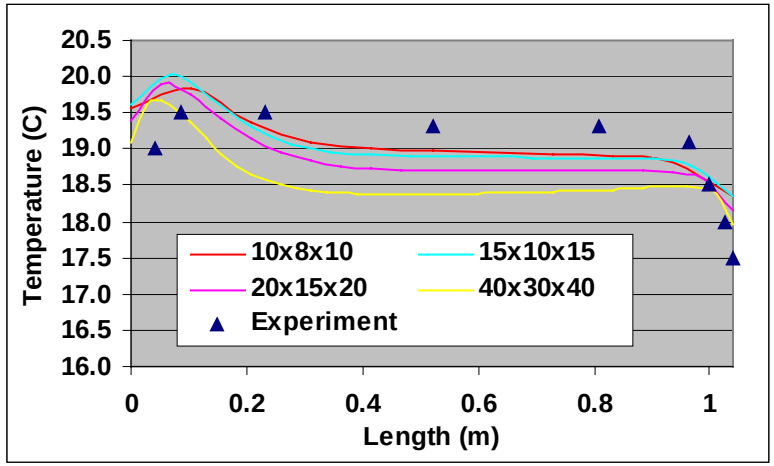

(b) Temperature at z=0.502

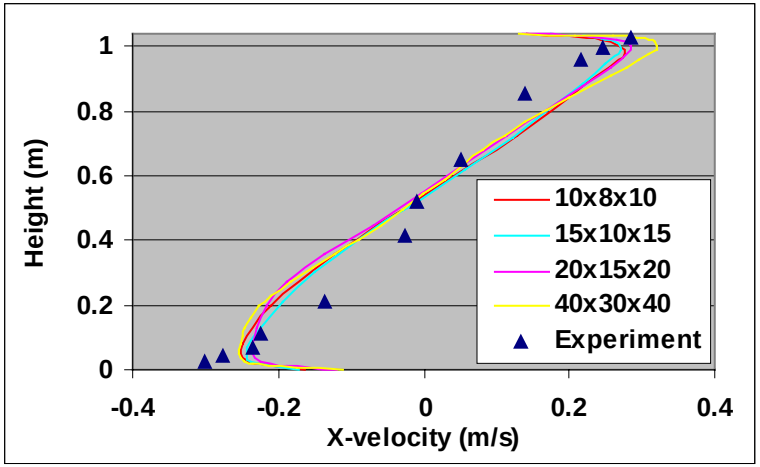

(c) X-Velocity at x=0.502

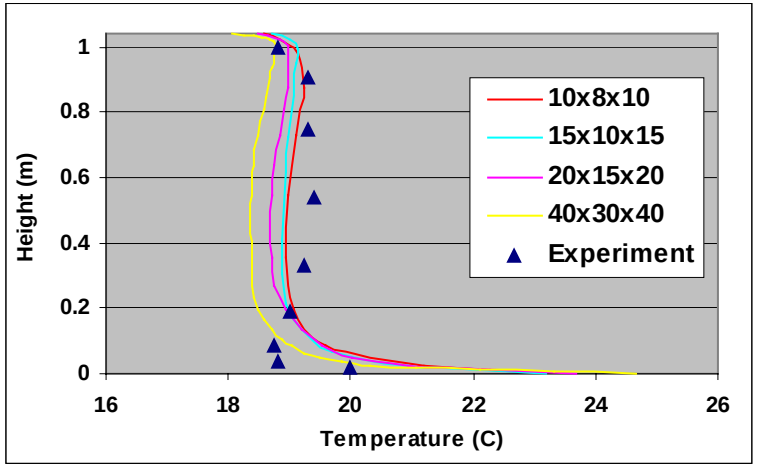

(d) Temperature at x=0.502

Figure 20. Mixed convection results for the polynomial transformations.

3.4. Displacement Ventilation

Problem Description

The most complex and realistic non-fire validation case is modeled after a displacement ventilation test room described by Yuan et al. (1998). This three dimensional room, shown in Figure 21, contains computers, furniture, and lighting fixtures as well as heated rectangular boxes intended to represent occupants. The room is ventilated with cool supply air introduced via a diffuser that is mounted on a side wall, near the floor. Displacement ventilation systems distribute cool supply air in the lower portion of the room. This air rises as it is warmed by heat sources and exits through a return located in the upper part of the room. The flow pattern is intended to remove contaminants by sweeping them upward at the source and removing them from the room.

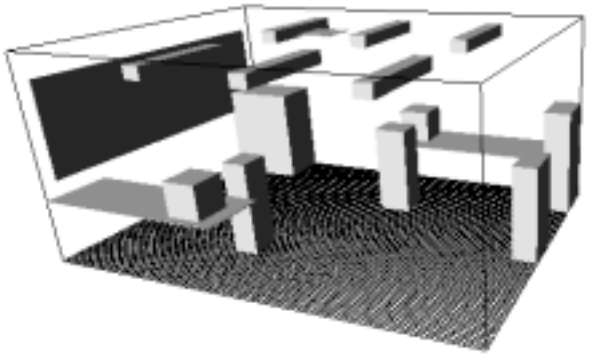

Figure 21. Geometry for the displacement ventilation case.

Computational results are compared with a steady-state experimental result obtained with a ventilation rate of 4 air changes per hour and a supply air temperature of 17.0° C. The total heat load introduced by six lamps, two computers, and two occupants (represented using boxes heated by incandescent lamps) was 636 W. Sulphur hexafluoride (SF_6) was introduced as a tracer gas near the breathing zone of the occupants at a rate of 0.00023 kg/hr each. Wall, floor, and ceiling temperatures were measured during the experiment, and these values were used to specify boundary conditions for the CFD simulation. Temperature, SF_6 concentration, and velocity were measured using vertical sensor arrays mounted on nine poles with locations shown in Figure 22.

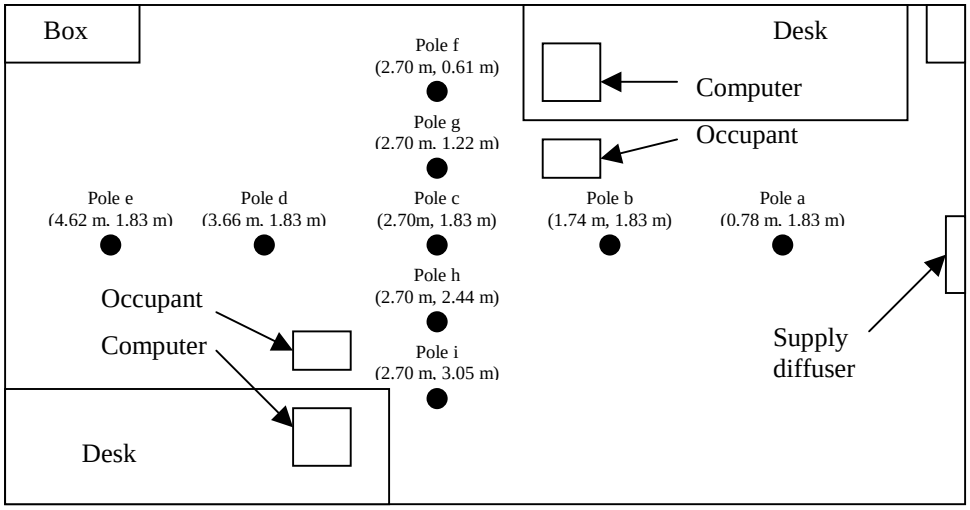

Figure 22. Measurement locations for the displacement ventilation case.

Problem representation

When the problem definition begins to include objects and obstacles in the room, a finer grid is often needed to properly define these objects. To represent this geometry using relatively coarse grids, there were two options. The first would be to specify a grid transformation that would allow each object to be defined at its proper dimensions. This would have required grid transformation in all three directions, and would have been mathematically complicated due to the number of objects present. This strategy was ultimately rejected because undesirable aspect ratios would be needed to maintain a coarse grid while properly representing objects such as the desks, which are very thin in the vertical direction. Instead, a regular grid was specified and the size of obstacles adjusted to fit the grid. This resulted in significant changes in the dimensions of some objects for the cases with coarse grids.

Heated objects were defined using an FDS feature that allows the user to specify a uniform heat release rate per unit surface area. For example, the heat release associated with each occupant was 75 W. For the computational model, 75 W was divided by the surface area of the occupant, and this rate specified for all of its surfaces. When FDS adjusts the dimensions of an object to accommodate the grid, the heat release rate per unit area is adjusted by the program as well, so that the intended quantity of heat is released.

The tracer gas sources were defined in much the same way. FDS requires contaminants to be introduced either at a vent or at the surface of an object that is at least two cells thick. In the actual experiment, the tracer gas was introduced through a small tube, just in front of the occupants. This had to be simulated in FDS as a contaminant release from the surface of an object defined by at least two grid cells. In the coarsest grid case, the occupants were defined by only four cells; therefore, the best strategy was to specify a uniform mass release flowing from the surface that represented the top of the occupants' heads. A mass flux per unit surface area was specified, and was adjusted as necessary by FDS for each case to provide the correct influx of SF_6 based on the surface area of the grid-adjusted occupants.

Real diffusers present another difficulty when modeling realistic situations. The velocity profile of flow leaving an inlet diffuser typically has a major influence on the flow pattern in the room, so it is important to model the diffuser appropriately. Since their geometry is often complicated, diffusers may require rather detailed specifications and grid refinement. For this case, the flow leaving the diffuser was evenly distributed over the face area of the diffuser, and modeled as a unidirectional, "top hat" profile. This method was chosen after comparing results obtained using a few slightly more sophisticated methods, without obtaining superior results.

Four levels of grid refinement were investigated, as shown in Table 5. The coarsest grid represented the room by only 1,728 cubic cells of approximately 0.3 m x 0.3 m x 0.3 m. This required significant adjustments to the size of most objects within the room, as a single grid cell was approximately the same size as one of the computers. The largest adjustment was made to the thickness of the desks, which increased by a factor of 30 from an actual thickness of 0.01 m. Significant adjustments were also made to larger objects such as the occupants, with actual dimensions of 0.4 m x 0.35 m x 1.1 m modeled as 0.3 m x 0.3 m x 1.2 m. The finest grid represented the room by 86,400 cells with dimensions 0.08 m x 0.08 m x 0.08 m. This representation allowed the occupants to be modeled as 0.40 m x 0.32 m x 1.13 m, very close to their actual size. Even with this much finer grid, however, the thickness of the desk was multiplied by a factor of eight so that it could be represented using one grid cell.

Case	Refinement	Transform type	Approximate cell dimension (m)	Average time step (s)
1	18 x 12 x 8	none	0.3 x 0.3 x 0.3	1.02
2	25 x 18 x 12	none	0.2 x 0.2 x 0.2	0.64
3	50 x 36 x 24	none	0.1 x 0.1 x 0.1	0.22
4	64 x 45 x 30	none	0.08 x 0.08 x 0.08	0.17

Table 5. Simulations performed for the displacement ventilation case.

In all four cases the time step was specified so that FDS could determine the largest time step appropriate for each case based on stability requirements. Table 5 shows a reduction in average time step size from 1.02 s to 0.17 s that occurs as the grid becomes finer. This gives the coarse grid a dual advantage with regard to computing time, since the larger time steps reduce the total number of calculations that are performed while fewer cells also means that each calculation is faster. Figure 23 shows the CPU time consumed per cell per time step, which is relatively constant for these cases. The two simulations with the coarsest grids are slightly slower on a per cell per time step basis, but the output files again show that this is because "fixed costs" associated with file management, prep time, and generation of output files consume a greater percentage of the overall computational resources and are spread over a smaller number of time steps.

It should be noted here that FDS offers the user a variety of ways to report and visualize results, and that indiscriminate use can consume substantial computing time. The approach taken for all of the simulations in this study was to obtain the results necessary for diagnostics and comparison with experimental data, and to omit most of the more time-intensive visualization files. There are four file formats for visualizing and reporting output data. The thermocouple file is a comma delimited file that reports time series flow data at specified points. For this problem ten points were specified for diagnostic purposes. Slice files record time series flow data at specified "slices" through the domain. In this case, 27 slice files were specified to record temperature, velocity, and SF_6 concentration at each of the nine instrumentation pole locations. These results were then time averaged for comparison to the experimental data. Two additional slice files were used to record temperature and SF_6 concentration for an xz-plane centered on the y-axis of the room. These results were used for visualization and diagnostics. Data files formatted for the shareware visualization program plot3d were also generated every 1000 s, for a total of five plot3d output files. Each of these files archive five flow quantities for the entire flow domain at a single time, and can be a useful diagnostic tool. A fourth type of output, the particle file, allows the user to visualize Lagrangian particles that are carried by the flow. In the case of a fire, these particles may also continue to burn and release heat as they are distributed throughout the room. These particles influence the calculation, and have the potential to consume considerable computing time and disk space. Their impact can be reduced by saving only a fraction of the particles or by setting an age limit, so that particles that have been in the domain for a specified length of time are deleted. To reduce computing time, particles were not used in this simulation. For coarse grids, the time required to model particles, even with age limitations in place, can be on the order of that required for the rest of the simulation. Therefore, the need for output data is something that must be considered when computing time is of concern.

The CPU time consumed per cell per second of simulated time is shown in Figure 24. For this case, the two coarsest grids can be simulated at speeds faster than real time. The 18 x 12 x 8 grid can be simulated in about 13% of real time, while the 25 x 18 x 12 grid consumes about 61% of real time.

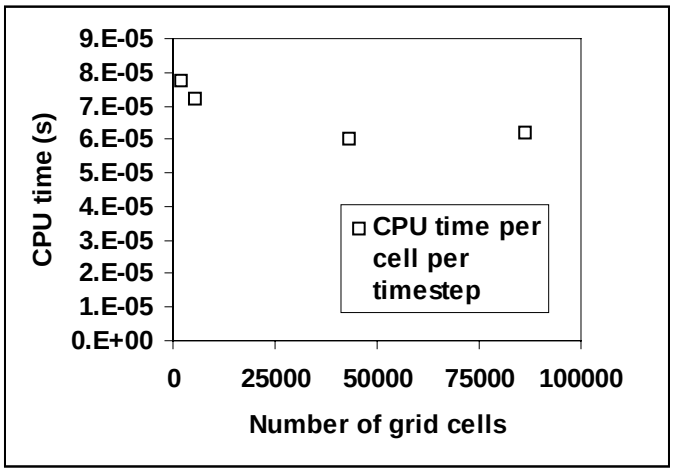

Figure 23. CPU time per cell per time step for the displacement ventilation case.

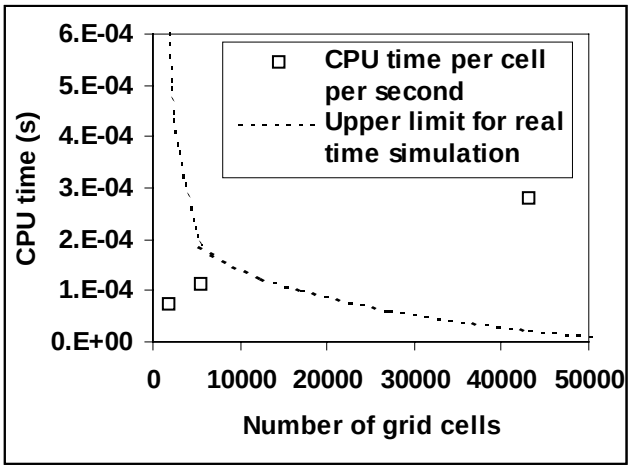

Figure 24. CPU time per cell per second of simulated time for the displacement ventilation case.

Each simulation was run for 5,000 s of simulated time. This was done based on investigations of the coarsest and finest grid cases (cases 1 and 4), which showed that 5,000 s of simulation was needed to obtain steady state velocity, temperature, and species profiles that were independent of the averaging period used. These investigations showed significant differences among these three parameters in the averaging period needed to obtain a uniform result and in the length of time needed until the result was no longer affected by the initial condition. For example, uniform steady state temperature profiles could be generated by averaging data over periods of at least 500 s, after the first 1500 s of the simulation. However, an averaging period of 1500 s was needed to generate uniform velocity profiles, and an initial period of 3500 s was needed before species concentration no longer depended on the initial condition. The efficiency of the data reduction process was maximized by using the same averaging period for temperature, velocity, and species concentration. To obtain steady state results, all flow variables were averaged between 3500 s and 5000 s.

Comparison With Experimental Data

Figures 25, 26, and 27 compare the predictions of the four FDS simulations with measured temperature, SF_6 concentration and average velocity. Comparisons are shown for three of the nine instrumentation poles at locations d, f, and h. These were chosen as a representative sampling of the measurement locations.

Figure 25 shows temperatures predicted by four FDS simulations. As the computational grid becomes finer, the results of the simulations can be seen to converge until the predictions of the two finest grids are very similar to one another. This suggests that the flow solution is approaching grid independence. In addition, the locations of the heated objects are becoming better defined. For the coarse grids, object and measurement locations were modified to fit the grid. Therefore, heat sources may be slightly closer to or further away from the measurement location than intended. In all cases, however, the general trend predicted by the model matches the experimental data. For the two fine grids, the agreement is quite good. The coarse grid results, while not quite as good a match, might be acceptable in exchange for computing speed.

The results for SF_6 concentration, shown in Figure 26, are not quite as good. At all three measurement points, the coarse grids tend to predict much higher concentrations near the floor than were measured experimentally. This seems to be related to poor grid refinement, and the results obtained using the finer grids are in much closer agreement with the experimental data. Still, a 50x36x24 grid is needed to capture the general trends of the concentration profile in the lower half of the room, and the 64x45x30 grid gives an even better result. In the upper half of the room, the model gives good results at pole h and over-predicts the concentration at poles d and f, particularly near the height of the source. The way in which the tracer gas sources were defined in the computational model has a significant impact on this result. Instead of a point source, the SF_6 release is modeled as being spread over a larger area, part of which is closer to poles d and f than the original source. Concentrations at these poles are also likely to be more influenced by this change in

source location since the local velocities tend to move air from the area of the source toward the pole. The flow pattern in the vicinity of pole h tends to move air from the nearest source away from the pole, so localized variations would have less effect on the contaminant concentration there. It is likely that the results of the fine grid simulations could have been improved by defining a small object adjacent to the occupant from which the tracer gas is introduced. While this would not have been possible for the coarser grids, a fine grid would allow it. Overall, the results in Figure 26 indicate a need for fine grids to properly represent both contaminant diffusion and to approximate point sources.

The velocity profiles in Figure 27 also appear to be converging to a uniform solution for the two finer grids. While the comparison to the experimental data may not be striking, it is certainly reasonable given the limitations of velocity measurement instrumentation at these low velocities. These results also tend to follow general trends observed through flow visualization and generated by other CFD programs. The most notable of these is the reversal of flow direction that happens in the lower portion of the room. Cool air entering the room at the diffuser forms a gravity wave that travels across the lower portion of the room. Above this layer, an area of recirculation exists. This reversal in flow direction can be seen in the computational results as the velocity dips at about 0.2 m above the floor. This effect is captured throughout most of the room with the coarse grid used in Case 1, however, it is best seen in the results of the cases with the finer grids.

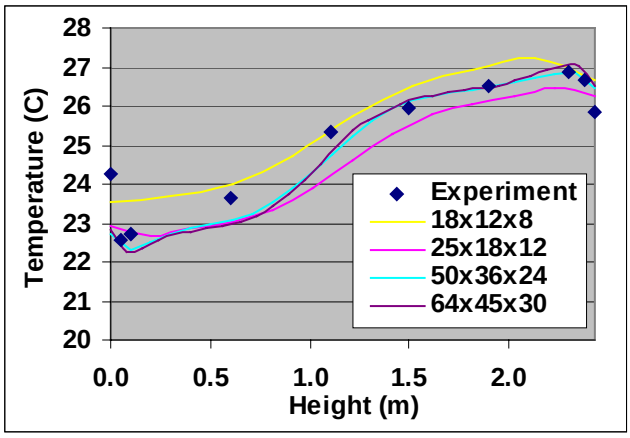

(a)

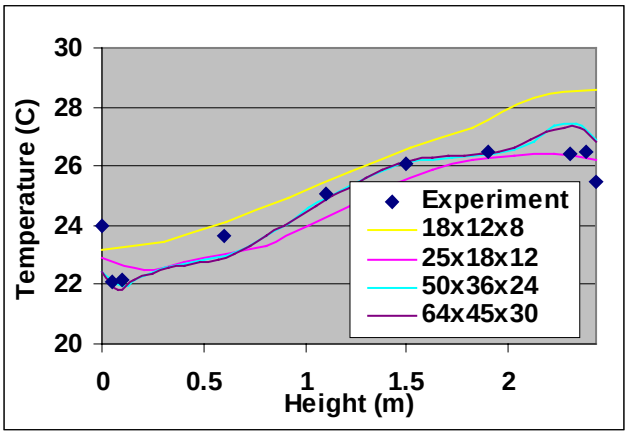

(b)

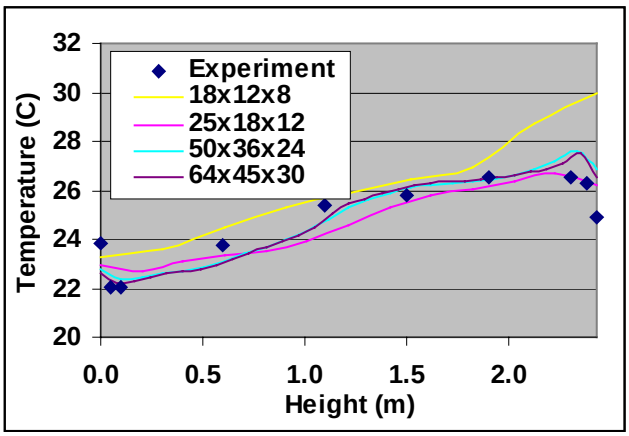

(c)

Figure 25. Temperatures predicted for the displacement ventilation case.
(a) Pole d (x=3.66 m, y=1.83 m) (b) Pole h (x=2.70 m, y=2.44 m) (c) Pole f (x=2.70 m, y=0.61 m)

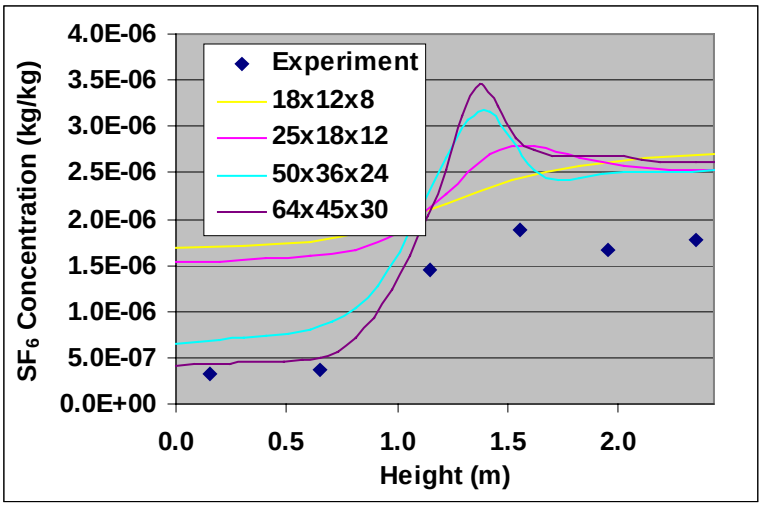

(a)

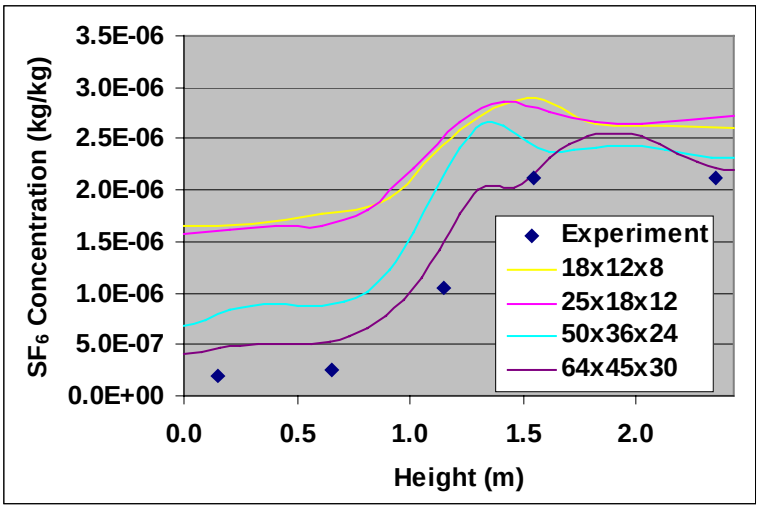

(b)

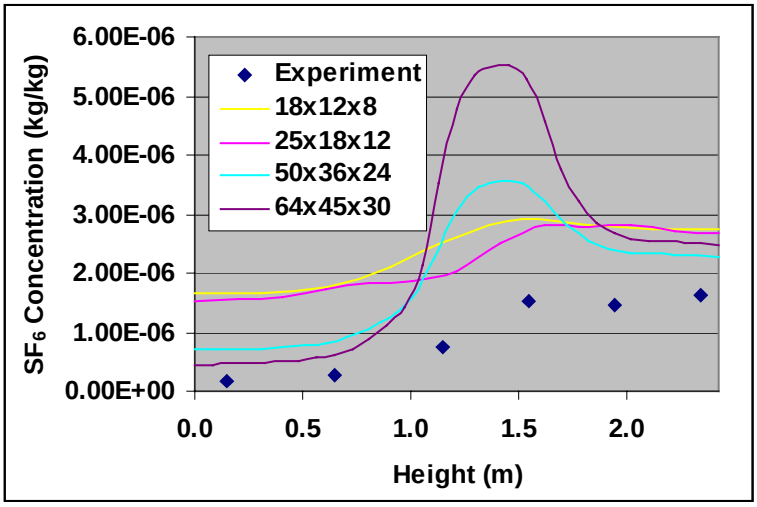

(c)

Figure 26. SF_6 concentration predicted for the displacement ventilation case.
(a) Pole d (x=3.66 m, y=1.83 m) (b) Pole h (x=2.70 m, y=2.44 m) (c) Pole f (x=2.70 m, y=0.61 m)

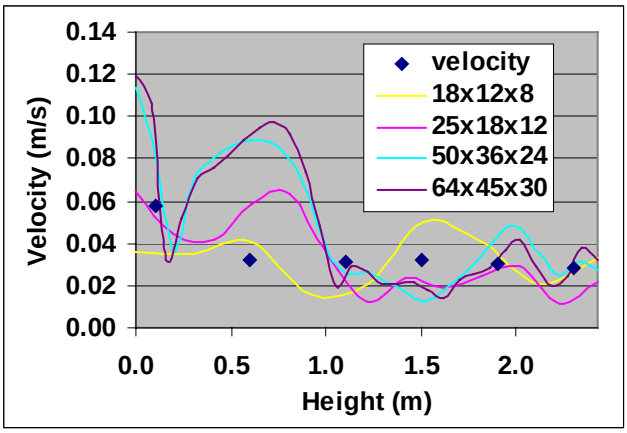

(a)

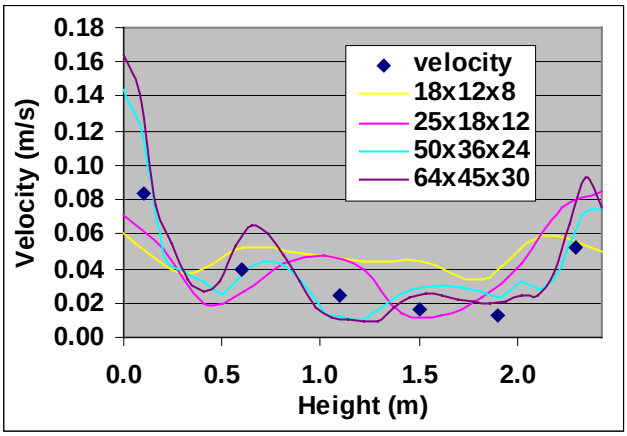

(b)

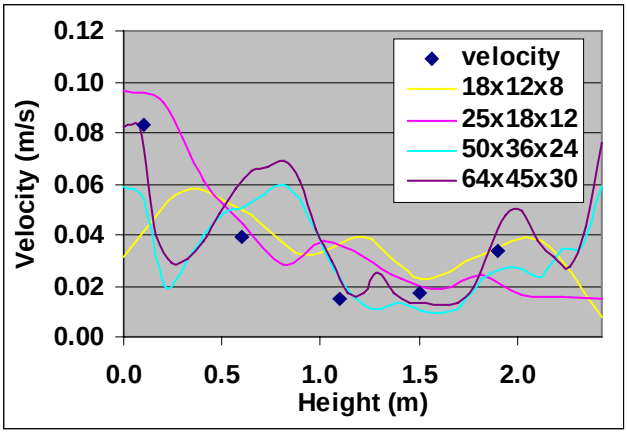

(c)

Figure 27. Velocities predicted for the displacement ventilation case.
(a) Pole d (x=3.66 m, y=1.83 m) (b) Pole h (x=2.70 m, y=2.44 m) (c) Pole f (x=2.70 m, y=0.61 m)

3.5 Ventilated Fire

Problem Description

These simulations were based on full scale fire tests directed by The Sandia National Laboratory (SNL), sponsored by the US Nuclear Regulatory Commission (USNRC), and performed by the Factory Mutual Research Corporation (FMRC). The ventilated room modeled here is based on their Test #5, described in detail by Nowlen (1991). A schematic drawing of the test chamber is shown in Figure 28.
Friday and Mowrer (2000) first simulated these tests with the Fire Dynamics Simulator (FDS). Their paper reported basic information comparing results for a few grid dimensions and comparing computing times on various platforms. They illustrated the importance of selecting an appropriate grid to balance result accuracy and computational time. This study considers the issues of computing time and grid refinement in more depth using a single platform.

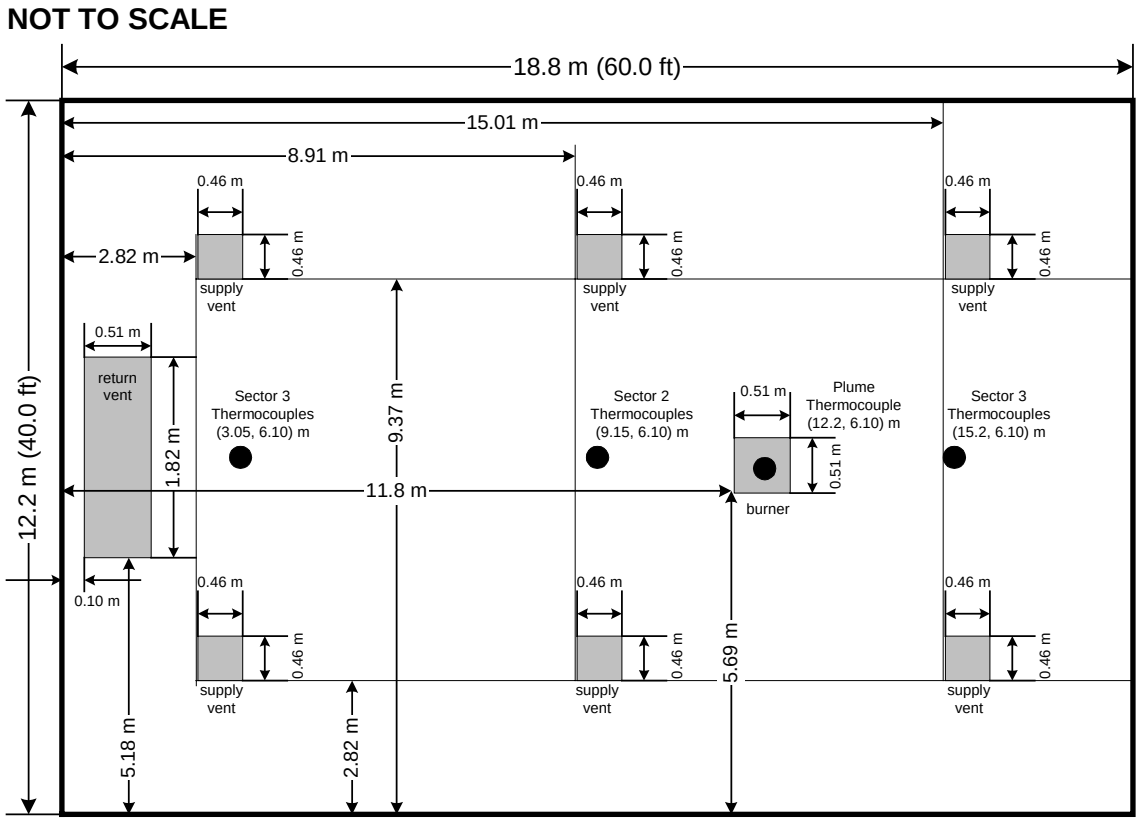

Figure 28 Geometry for the Ventilated Fire.

The test chamber was 18.3 m by 12.2 m by 6.1 m, with a concrete floor. Wall and ceiling panels were constructed of 25.4 mm heat-treated, inorganic calcium silicate board supported by an external wood frame. Forced ventilation entered the chamber via six 0.61 m square inlet ducts extending 1.2 m below the ceiling. Four-way air deflector caps partially blocked the flow below the ducts. One 0.61 m by 1.83 m exhaust vent was located on the ceiling Figure 29 shows this arrangement in a wireframe view generated by Smokeview. Some additional unintended air leakage was also observed during the test, but was not accounted for by the model.

Over 200 data channels recorded temperature, velocity, and species concentration at five second intervals during the 10-minute fire test. Figure 28 shows the measurement locations. Gas quantities were not modeled in this study, since this adds an extra equation and increases the computational time. Friday and Mowrer noted difficulty comparing their results with the experimental velocity measurements. Therefore, this report

considers only the measured temperatures. Since this report draws from the original simulations run by Friday and Mowrer (2000), the reader may wish to refer to that report for more extensive details of the simulation setup.

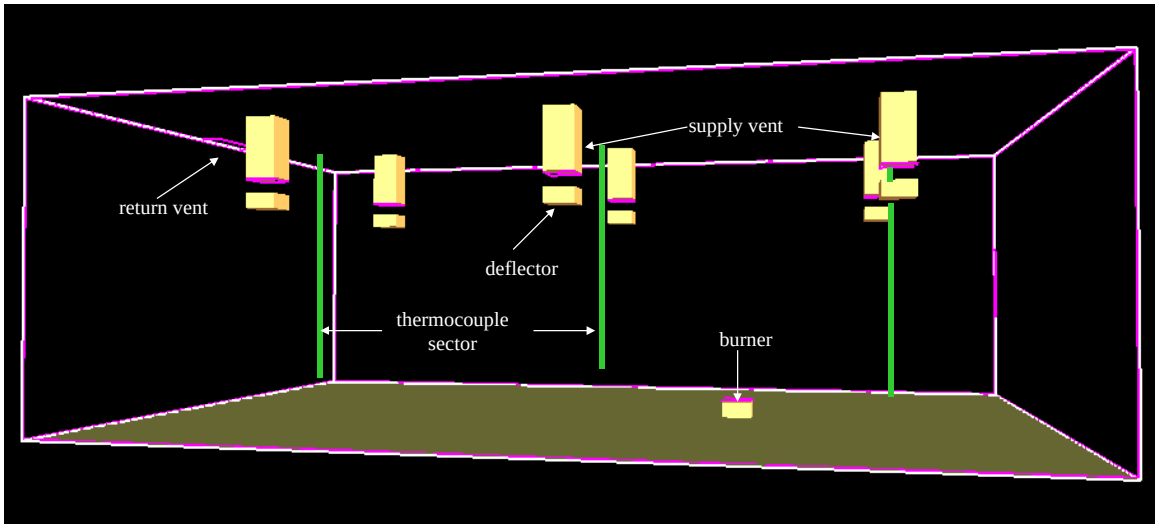

Figure 29. Smokeview Wire Frame of the Ventilated Fire.

Friday and Mowrer noted a 60 second lag between the start of the fire and detection of the temperature rise by the centerline plume thermocouple. They also noted that shifting the data by 60 seconds improved early predictions but deteriorated later predictions, although no reason for this shift was apparent. Therefore, the timing of the experiment may be uncertain. The analysis in this report presents the data as it was reported by Nowlen (1991) and does not attempt any data correction techniques.

Grid Selection

The computational grid must be specified to properly define the features of the room. This test chamber did not contain many objects, however, the supply vents are 0.46 m square. This suggests a maximum grid cell size. The fire source is roughly this size, and the return vent is larger. The supply and return vents are scattered throughout the room, in locations that do not suggest an obvious grid transformation. It might be beneficial to create a transformed grid that is smaller near a fire event. The fire will be the largest driving force to the flow, and finer grid cells might give better results in the vicinity of the fire.

The computational domains for both of the fire experiments are full-size rooms with fires in them. Therefore, the grid cells are much larger than used in many of the indoor air quality cases. The smallest cell dimension used for this case was 0.15 m, an order of magnitude larger than the finest grid used for the indoor air quality cases. Despite the larger grid cells, the fire cases required a much shorter time step. This happens because the time step is determined in part by how quickly a particle travels across a grid cell. A particle cannot move more than one grid cell per time step. If the particles are moved by a strong convective force, as with a large fire, the allowable time step is greatly reduced. This increases overall computing time since more steps are needed for the simulation.

Table 6 shows the 11 cases simulated. Four cases were modeled with no grid transformation. A very coarse grid with dimensions 1.5 m x 1.2 m x 0.61 m was chosen for very fast computational time. The size of the 0.46 m square supply vents was distorted significantly, and FDS reduced the supply velocity to achieve the correct volume flux. The fire source size was also increased to accommodate the grid, and its properties adjusted to obtain the correct heat release rate. Very coarse grids would have required significant distortion of the deflector plates as well. Therefore, some of the simulations were run without modeling the deflector plates at all. These cases are shown in Table 6 with an asterisk.

Case	Refinement	Transformation type (*x*- and *y*- directions)	Radiation modeled?	Smallest cell size (m)	Average time step (s)
1*	12 x 10 x 10	none	no	1.50 x 1.20 x 0.61	0.21
2*	30 x 20 x 20	none	no	0.61 x 0.61 x 0.61	0.064
3	60 x 40 x 20	none	no	0.30 x 0.30 x 0.30	0.044
4	60 x 40 x 20	piecewise linear	no	0.15 x 0.15 x 0.30	0.036
5*	30 x 20 x 20	piecewise linear	no	0.30 x 0.30 x 0.30	0.044
6	60 x 40 x 20	polynomial	no	0.13 x 0.15 x 0.30	0.035
7*	30 x 20 x 20	polynomial	no	0.25 x 0.30 x 0.30	0.044
8*	30 x 20 x 20	none	yes	0.61 x 0.61 x 0.61	0.063
9*	30 x 20 x 20	piecewise linear	yes	0.30 x 0.30 x 0.30	0.045
10*	30 x 20 x 20	polynomial	yes	0.25 x 0.30 x 0.30	0.044
11	90 x 60 x 30	none	no	0.15 x 0.15 x 0.15	0.025

* Deflector plates on supply vents not modeled.

Table 6 Simulations Performed for Ventilated Fire

Grid transformations were also investigated. The number of cells near the fire source was increased in both the *x*- and *y*-directions to better capture the fire effects. In the case of piecewise linear transformation, twice as many grid cells were used in the vicinity of the fire. The polynomial transformations specified a first derivative equal to zero and second derivative equal to one at the mid-point of the fire in both the *x*- and *y*-directions. The *x*-direction transformation is shown in Figure 30, along with the supply and return vent locations and the fire position.

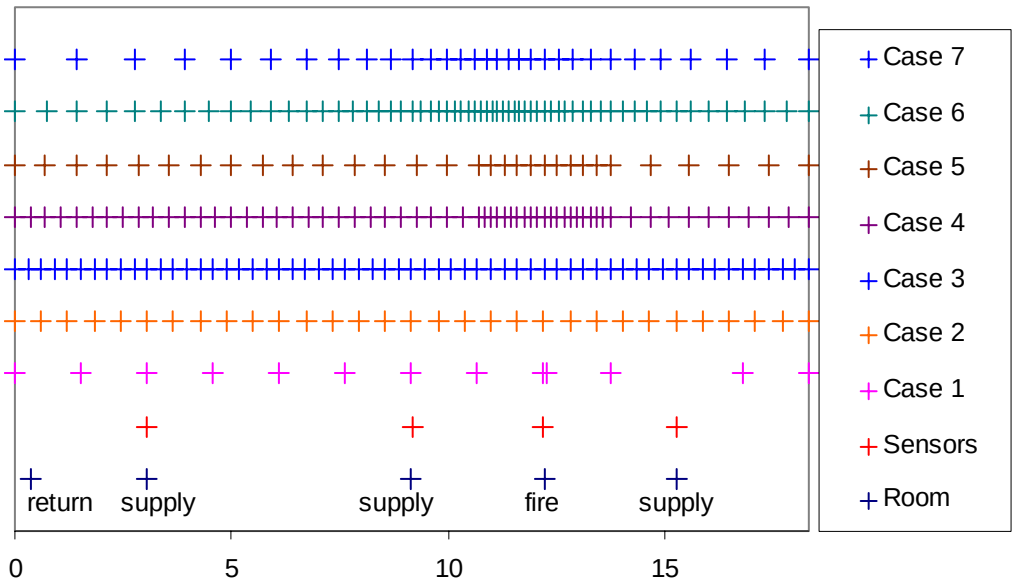

Figure 30 Grid transformations used in the ventilated fire (x- direction)

Three additional cases included radiation calculations. In most cases, the user does not activate the radiation calculations because they consume considerable computational time. Since this study focused on results versus computational time, the radiation calculations were run for three coarse grids to study their effect on both timing and results.

Computing Times

As with the indoor air quality simulations, these simulations were structured to run quickly. The record data was narrowed to only those parameters needed for comparison with the experiment. A large starting time step was specified to allow FDS to choose its own time step.

Figure 31 shows the CPU time per cell per time step, plotted against number of grid cells. In this case, there was no relationship between number of grid cells and this measure of computing time. A total of six cases were run with 12,000 grid cells. The three in which radiation were modeled consume up to five times as much CPU time per timestep than the cases in which radiation effects were neglected. Since the radiation calculation adds considerable computing time, its effect on the results of the simulation should be carefully considered.

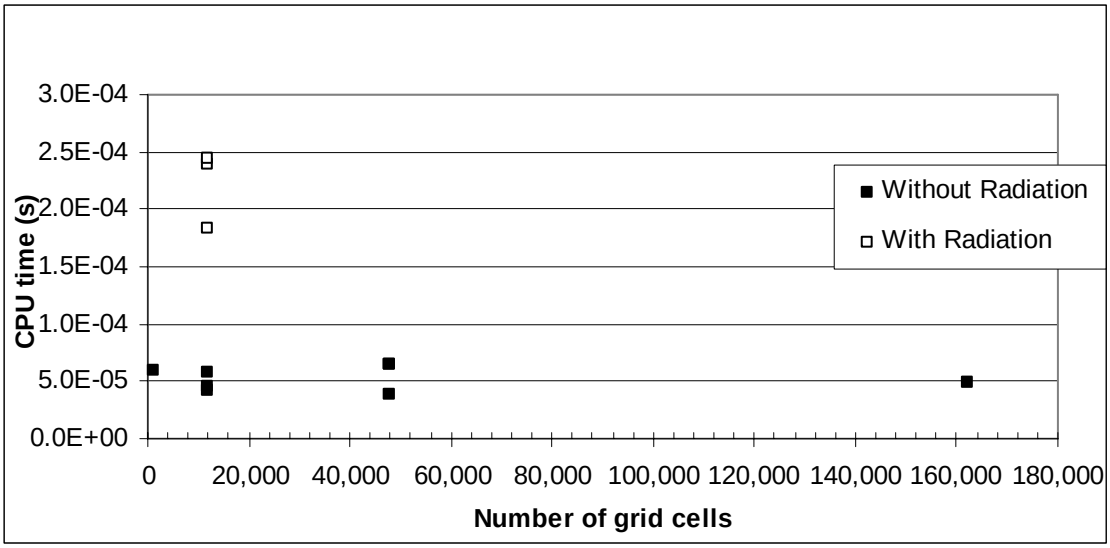

Figure 31 CPU time per cell per time step for ventilated fire

CPU time per cell per second of simulated time is shown in Figure 32. The only case that fell below the real time threshold was the extremely coarse grid (12 x 10 x 10). The 30x20x20 grid simulations where slightly above the threshold and show promise for achieving real time on a faster computing platform, as long as radiation is neglected.

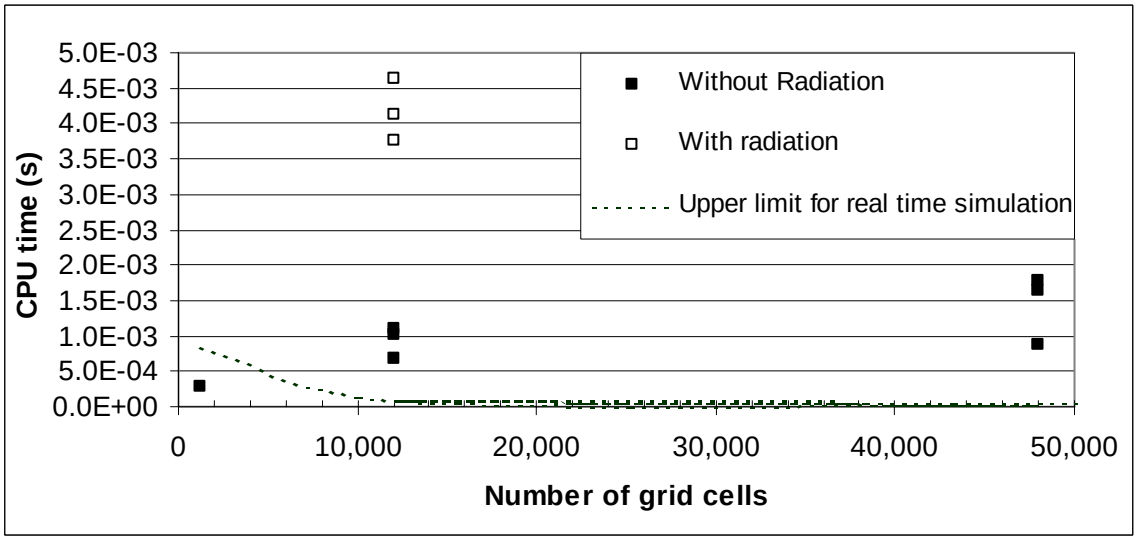

Figure 32 CPU time per cell per second of simulated time for the ventilated fire

Comparison with Experimental Data

The fire experiments provide transient results. No time averaging was necessary, and the FDS results are reported directly. This report compares average normalized temperatures by grid selection and vertical location.

Tempatures are compared using a Normalized Error Fraction (NEF) that was used by Friday and Mowrer (2000). The NEF is defined by the equation:

$$\mathrm{NEF} = \frac{\mathrm{T}_{\mathrm{predicted}} - T_{measured}}{T_{\max,measured} - T_{ambient}} \tag{2}$$

where $T_{predicted}$ is the temperature predicted by FDS, $T_{measured}$ is the temperature from the experiment, $T_{max,measured}$ is the maximum measured temperature during that test, and $T_{ambient}$ is the ambient temperature. An NEF of zero indicates that the predicted and measured temperatures agree exactly.

Figures 33 - 35 show Normalized Error Fraction. The closer the results are to zero, the better the agreement between the experiment and FDS results. The plume temperature is measured using a single thermocouple at 0.98 H directly above the burner. The other five data sets represent the average NEF for three thermocouples at the given location on the vertical arrays.

The first set of graphs show results for the non-transformed grids. Graph (a) shows the coarsest grid, with NEF between –0.2 and 0.2 for the entire duration of the test. The most notable aspect of this result is the underprediction of the plume temperature by FDS. Because the grid is so coarse, temperatures are averaged over a larger area, and plume temperature is underpredicted. Although the results for this case may not be significantly worse in absolute terms as those from the simulations in which finer grids were used, this underprediction could pose a safety threat. The results of these simulations seem to reach grid independence with the two finest grids.

Figure 34 shows the NEF for the cases with grid transformation. The results are only slightly better than the equivalent non-transformed grids. For both cases, the plume temperature rises slightly for the finer grid. Therefore, the 60 x 40 x 20 grid seems to be needed to resolve the plume behavior.

The last set of NEF graphs in Figure 35 show the results for the simulations run with the radiation calculations. These graphs demonstrate roughly the same degree of agreement between the simulated and experimental results as was present in the cases in which radiation was not considered. Given the experimental uncertainty associated with the experiments and the complexity of the process being modeled, the agreement may be considered reasonable for all cases. The most significant difference between the calculations with and without radiation is the dramatic increase in simulation time.

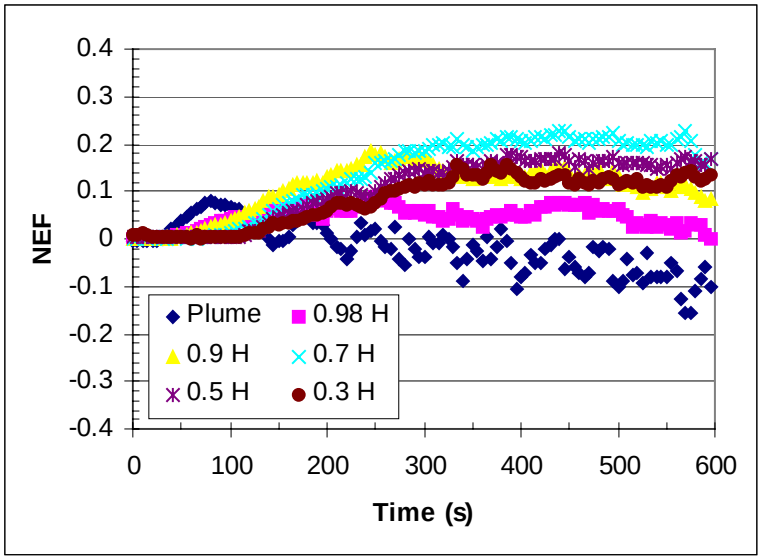

(a) Case 1, 12 x 10 x 10 grid

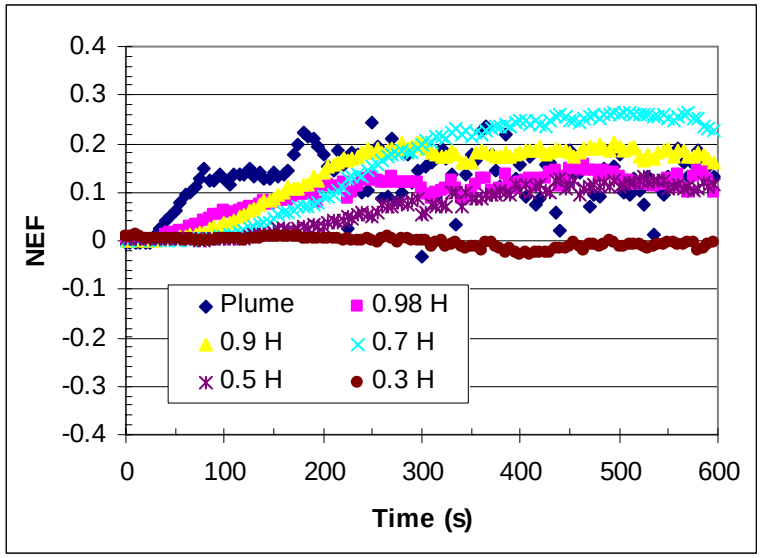

(b) Case 2, 30 x 20 x 20 grid

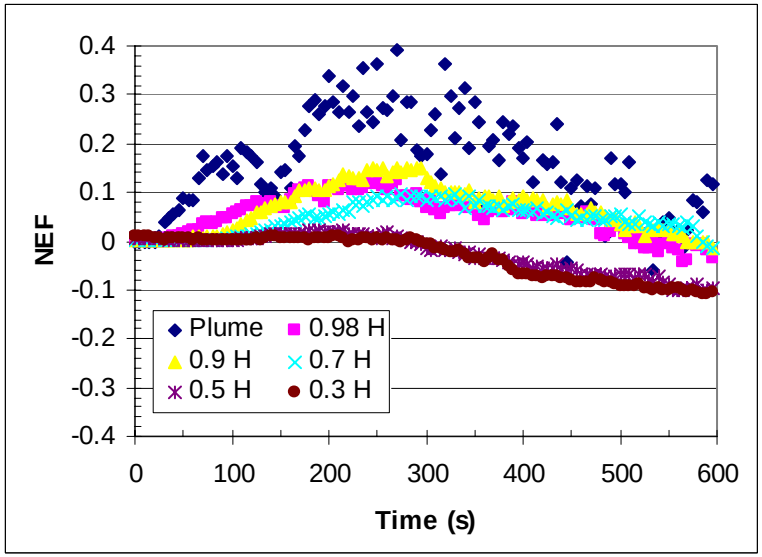

(c) Case 3, 60 x 40 x 20 grid

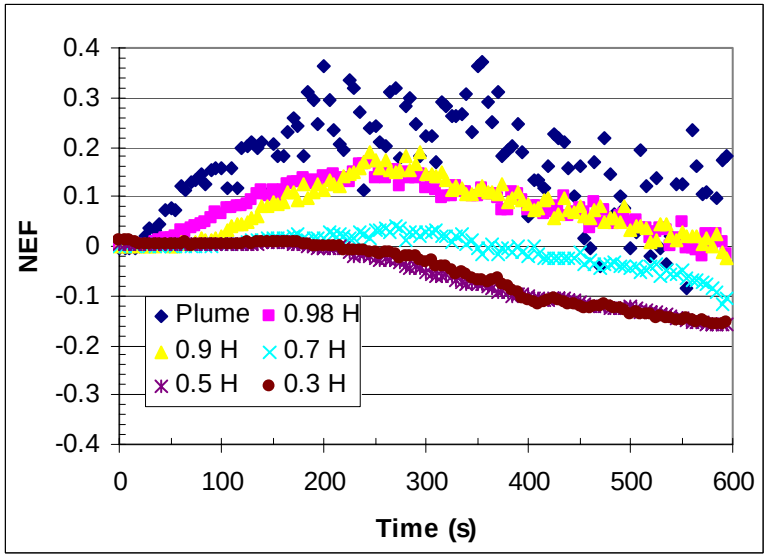

(d) Case 11, 90 x 60 x 30 grid

Figure 33: Normalized Error Fraction for the ventilated fire with no grid transformation

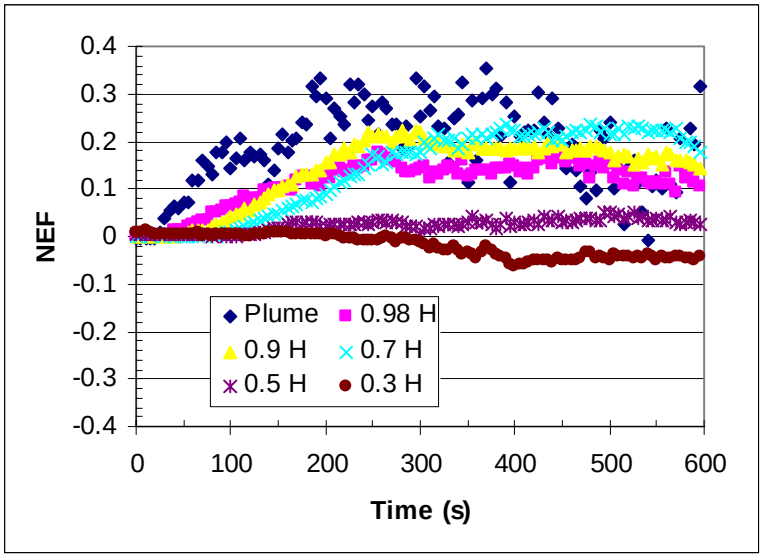

(a) Case 5, 30 x 20 x 20 piecewise linear

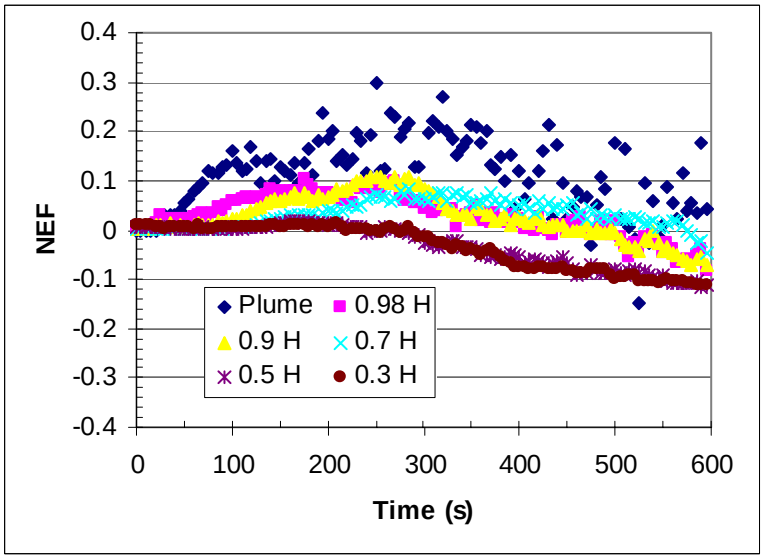

(b) Case 4, 60 x 40 x 20 piecewise linear

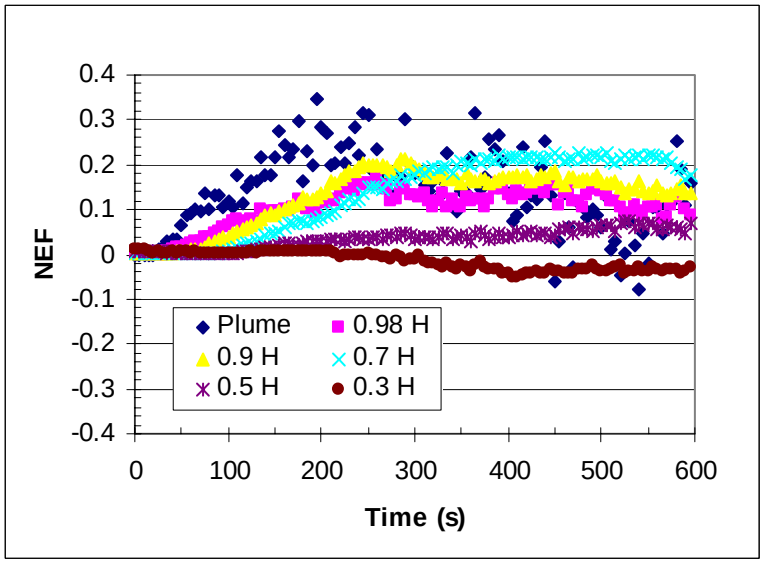

(c) Case 7, 30 x 20 x 20 polynomial

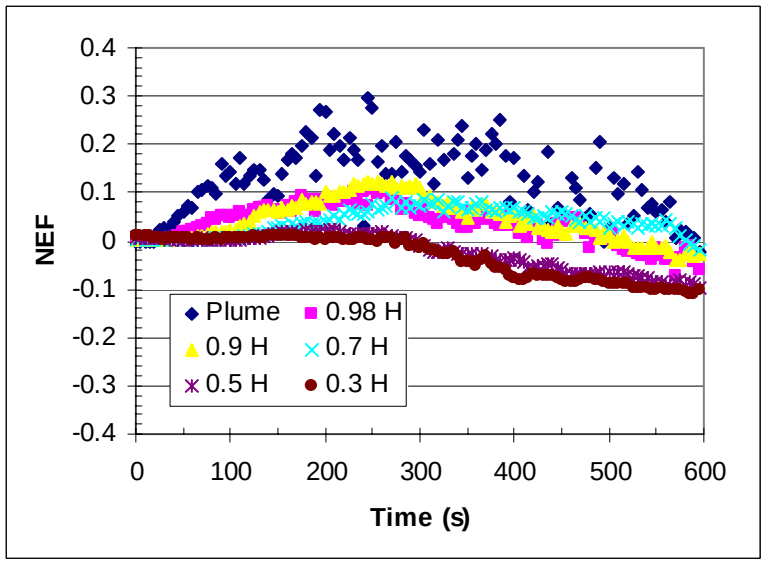

(d) Case 6, 60 x 40 x 20 polynomial

Figure 34: Normalized Error Fraction for the ventilated fire with grid transformation

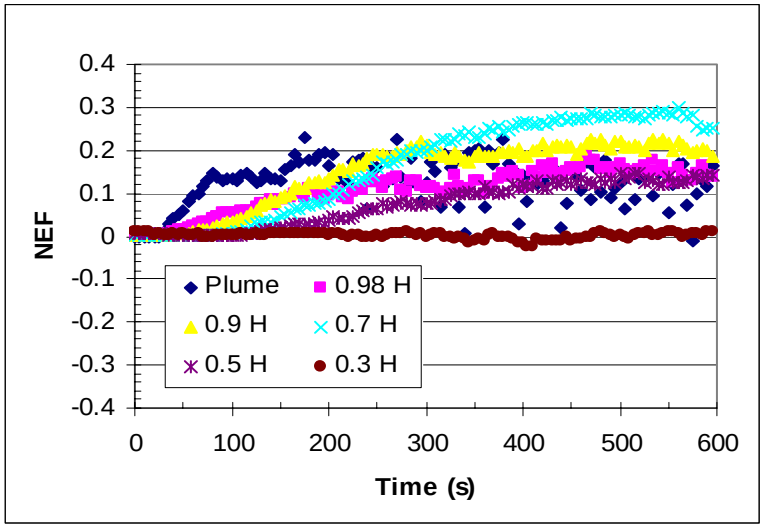

(a) Case 8, untransformed grid

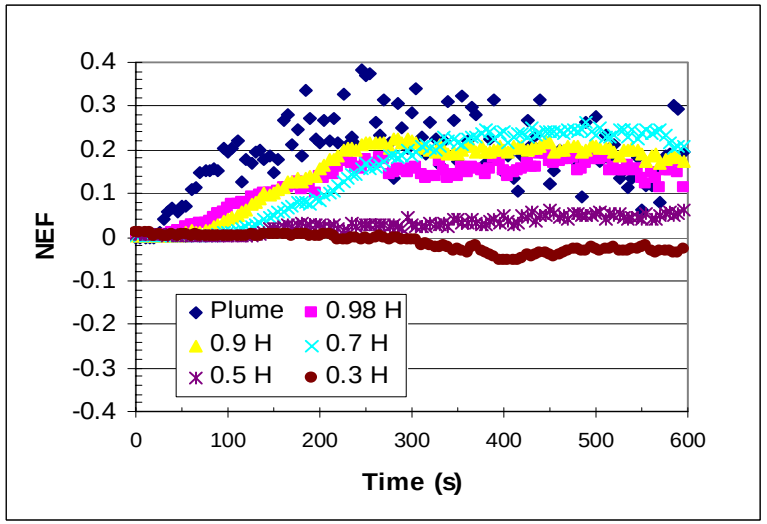

(b) Case 9, piecewise linear grid transformation

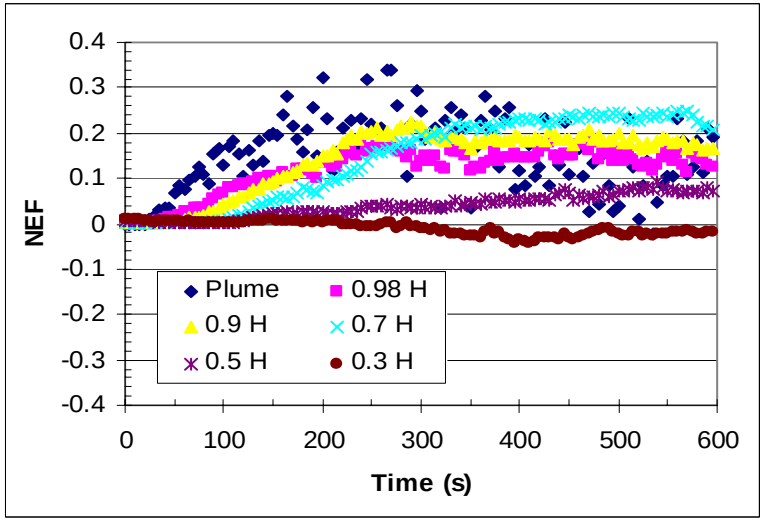

(c) Case 10, polynomial grid transformation

Figure 35: Normalized Error Fraction for the ventilated fire, radiation calculations enabled

3.6. Corner Fire

Vettori (1999) first modeled this set of experiments with the Fire Dynamics Simulator (FDS) and another simulation tool. That work compared the output from the two simulations against a large number of experiments, including slow and fast burning fires. Here, FDS simulation results are compared with experimental data from two of those experimental tests with grid size altered to observe the impact on computational time and simulation results.

Problem Description

Figure 36 shows a plan view of the test chamber, burner, and instrumentation for the experimental setup. The rectangular chamber was 9.2 x 5.6 m x 2.4 m with a hollow steel door to the outside that remained closed during testing. An open wooden stairway led to an upper floor with the same dimensions as the fire compartment. Wooden joists measuring 0.038 m x 0.24 m were spaced at 0.41 m intervals across the ceiling and were supported by a single steel beam that spanned the width of the room. A rectangular methane gas burner measuring 0.7 m x 1.0 m x 0.31 m was placed in the corner of the chamber. Slow and fast burning fires that reached 1055 kW in 600 and 150 s respectively were monitored. Figure 37 shows a wireframe view of the room setup that was generated using Smokeview.

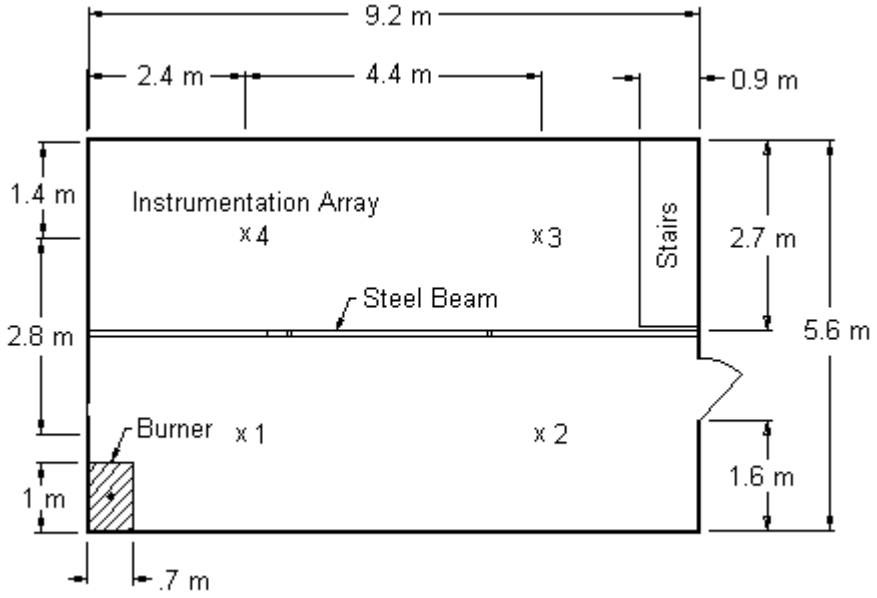

Figure 36. Plan view of experimental layout for the corner fire.

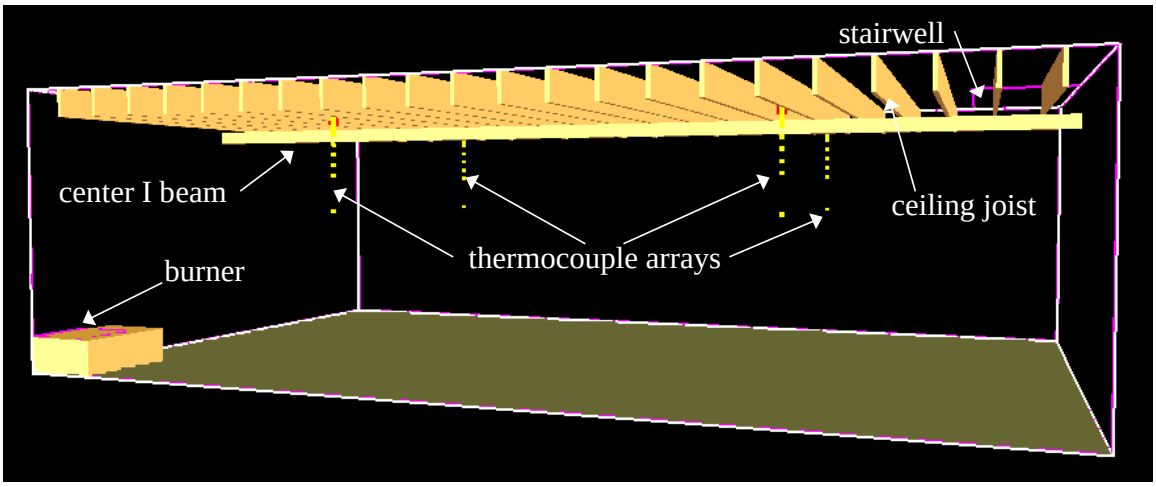

Figure 37 Wire frame view of corner fire experiment.

All temperature measurements were made using Type K thermocouples with a 0.51 mm nominal diameter, with a standard uncertainty of ±2.2 °C based on manufacturer's data. These were arranged in four vertical arrays shown in Figures 36 and 37. For each array, measurements were taken at locations of 0, 25, 50, 75, 100, 125, 150, 250, 350, 450, 550, and 900 mm below the ceiling.

Grid Selection

Defining the computational grid for this case was less straightforward than for the ventilated fire experiments. In Vettori's simulations, individual ceiling joists were modeled with four grid cells between them, for a total of 113 grid cells in the *x*-direction. This level of grid refinement requires nearly 300,000 grid cells for a three dimensional simulation, so it was the finest grid that was investigated for this study. Four different grids were used to model the slow and fast burning fires, for a total of eight simulation cases. The two finest grids defined the ceiling joists at their proper dimensions via piecewise linear transformation of the x-axis. The ceiling joists were not modeled with the two coarsest grids, and no transformation was used. Omitting the ceiling joists allowed a significant reduction in the number of grid cells needed; however, this would not be a viable option if the flow near the ceiling joists were important, as it might be in a study of ceiling mounted detector activation. The eight simulations are summarized in Table 7. Figure 38 shows the location of grid cells on the x-axis for the four grids, as well as the locations of joists, vents, and sensor arrays.

Case	Refinement	Transform type (*x*-direction)	Smallest cell size (m)	Average time step (s)	Fire Speed
1	113 x 64 x 40	piecewise linear	0.092 x 0.088 x 0.066	0.0044	fast
2	72 x 32 x 20	piecewise linear	0.11 x 0.18 x 0.13	0.0102	fast
3	45 x 24 x 16	none	0.20 x 0.23 x 0.16	0.0140	fast
4	12 x 10 x 10	none	0.77 x 0.56 x 0.26	0.0458	fast
5	113 x 64 x 40	piecewise linear	0.092 x 0.088 x 0.066	0.0096	slow
6	72 x 32 x 20	piecewise linear	0.11 x 0.18 x 0.13	0.0254	slow
7	45 x 24 x 16	none	0.20 x 0.23 x 0.16	0.0367	slow
8	12 x 10 x 10	none	0.77 x 0.56 x 0.26	0.129	slow

Table 7. Simulations performed for the corner fire.

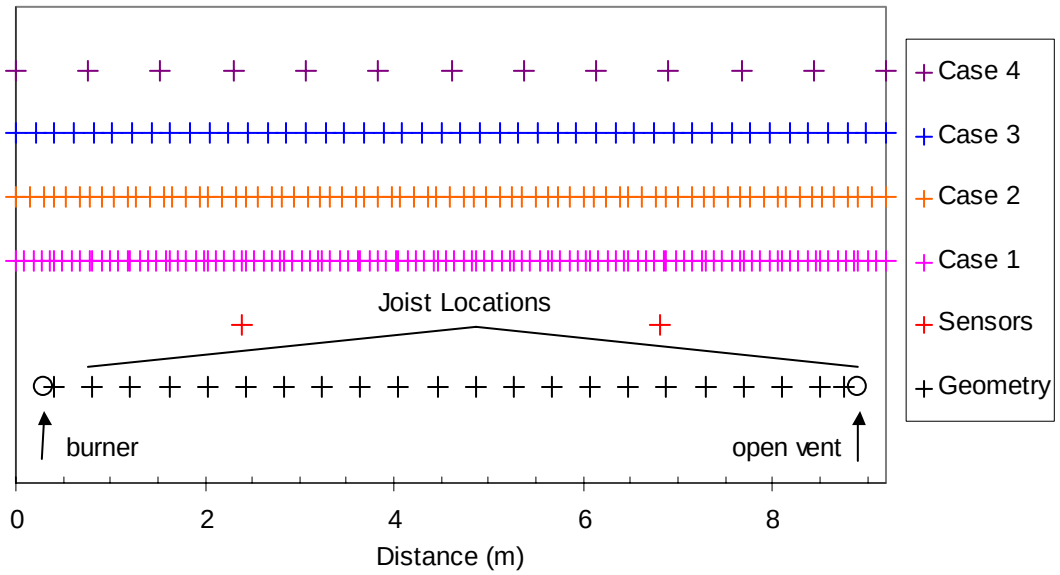

Figure 38. Grid spacing for the corner fire (x- direction).

Computing Times

The output information collected for this simulation was again kept to a minimum to reduce effects on simulation time, and FDS was again allowed to calculate the maximum permissible time step. Figure 39 shows the CPU time per cell per time step. Generally, computing times for the fast and slow burning fires are very close to one another, except in the case of the coarsest grid. For that case, the fast fire simulation was much slower on a per time step basis. Examination of computing time usage broken down by task showed that the primary difference between the two simulations was that the sprinklers were activated for the fast burning fire, but not for the slow burning fire. This was actually true of all of the fast fire simulations, but the additional computing time consumed was much larger on a per grid cell basis for the coarse grid case. In the other cases, the penalty associated with sprinkler activation was spread out over many more time steps and grid cells.

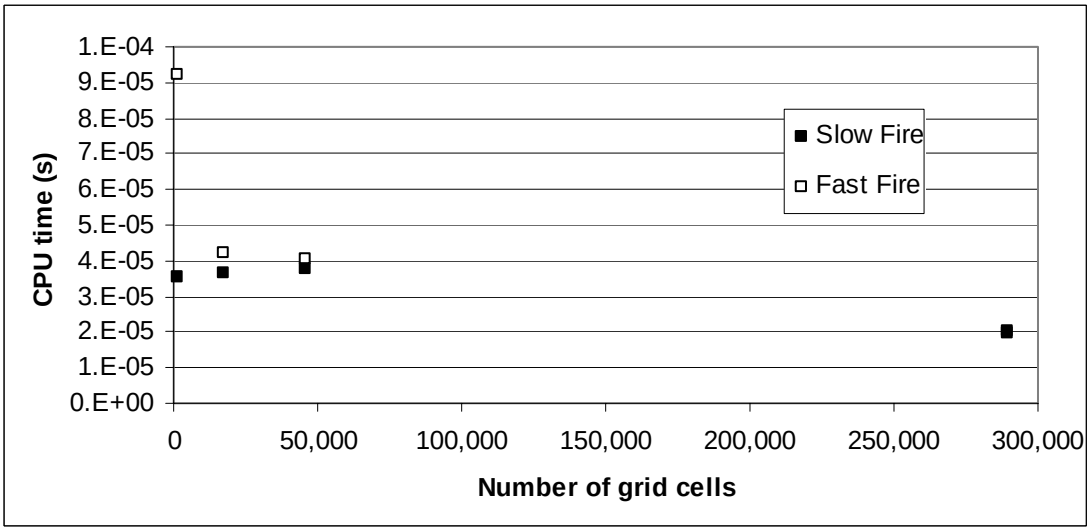

Figure 39. CPU time per cell per time step for corner fire.

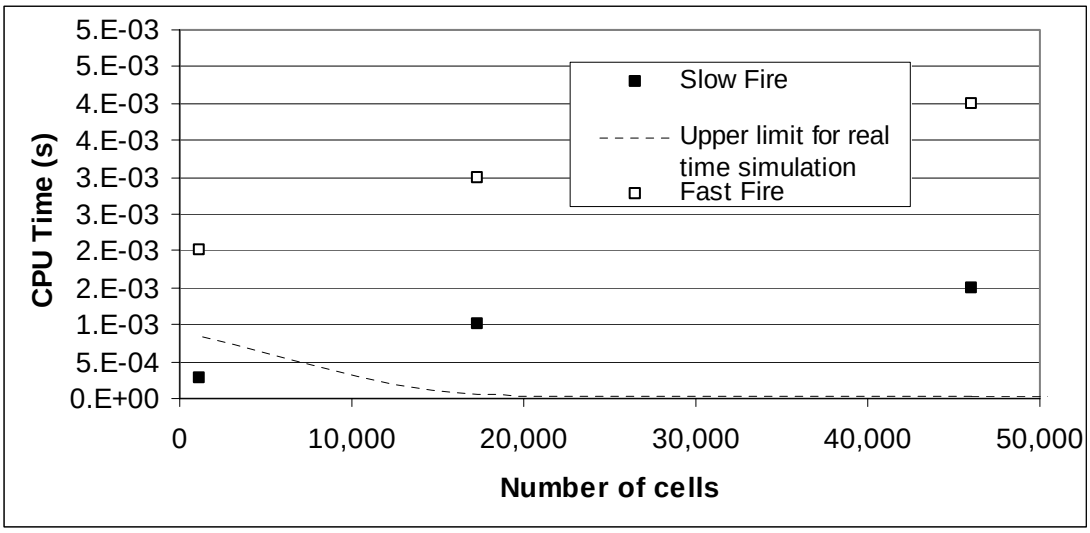

Figure 40. CPU time per cell per second of simulated time for corner fire.

Figure 40 shows the computing time in comparison to real time. Only Case 8 with the coarsest grid and slow fire was simulated in less than real time. Since the time step is limited by the time required for a particle to travel the length of one grid cell, shorter time steps were needed to model the fast burning fire. For the same reason, shorter time steps are required for both fire types as the grid becomes finer. As Table 8 shows, the average time step for the slow burning fire is roughly twice that required for the fast fire.

Comparison with Experimental Data

As with the ventilated fire, the NEF is again used to compare the experimental and simulated temperature profiles. A NEF of zero indicates that the predicted and measured temperatures agree exactly. Results for the fast and slow burning fires are shown in Figures 41 and 42 respectively.

In Figure 41, all of the simulations show the temperatures as overpredicted by the model, particularly as time progresses. This may be attributable to the actual experimental conditions not matching precisely with the model inputs. This is suggested by the trend at all of the thermocouple locations to follow a similar pattern. Some differences between the coarse and fine grids are apparent, however. When the coarse grid is used, temperatures in the lower portion of the room tend to be higher while temperatures in the upper portion of the room tend to be lower than those predicted by the finer grids. This is a result of artificial diffusion created by the large grid cells. Also, because the ceiling joists are not modeled, the patterns predicted by the simulation at points close to the ceiling are sometimes different.

The agreement between simulation and experiment is much closer in Figure 42, which shows the slow burning fire. In these cases, the predictions tend to be within about 10% of the experiment. Again, for the coarse grid cases, temperatures at the lower thermocouples tend to be higher than expected, and those at upper thermocouples tend to be slightly lower. In general, the finer grids give a narrower range of NEF for the various measurement heights.

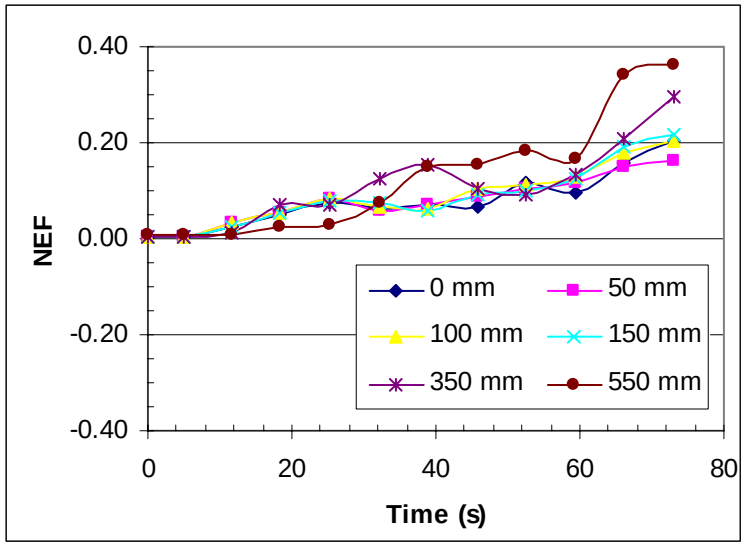

(a) Case 1, 113 x 64 x 40 grid

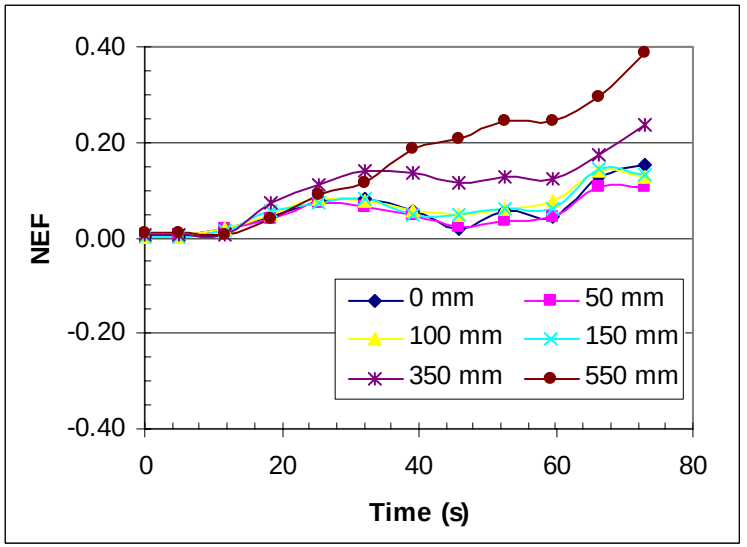

(b) Case 2, 72 x 30 x 20 grid

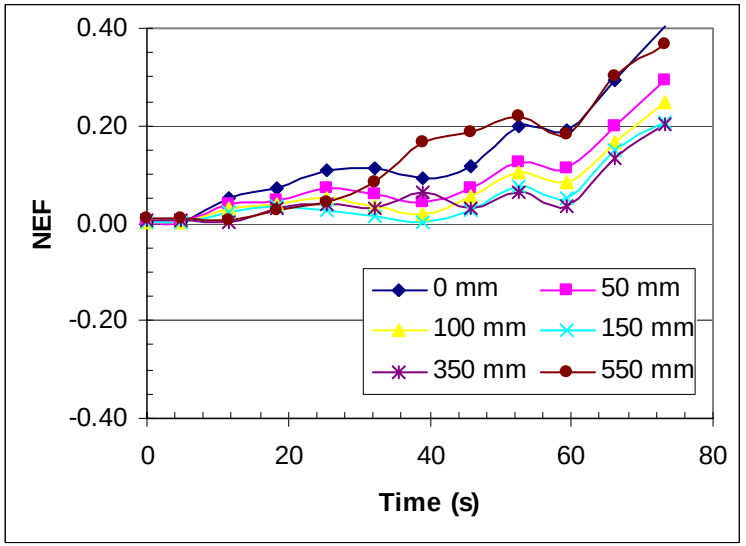

(c) Case 3, 45 x 24 x 16 grid

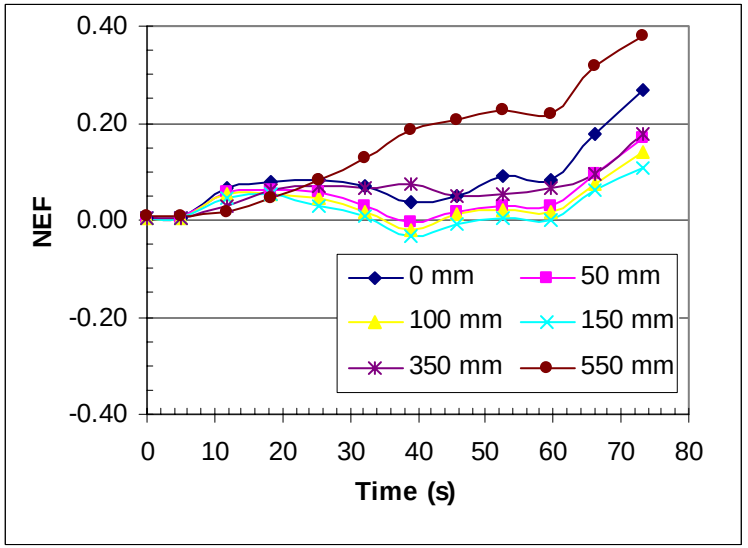

(d) Case 4, 12 x 10 x 10 grid

Figure 41: Fast corner fire normalized error fraction

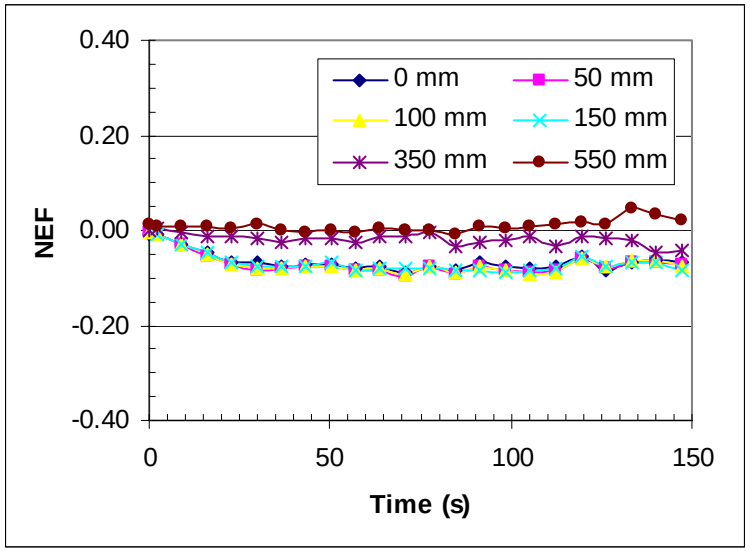

(a) Case 5, 113 x 65 x 40 grid

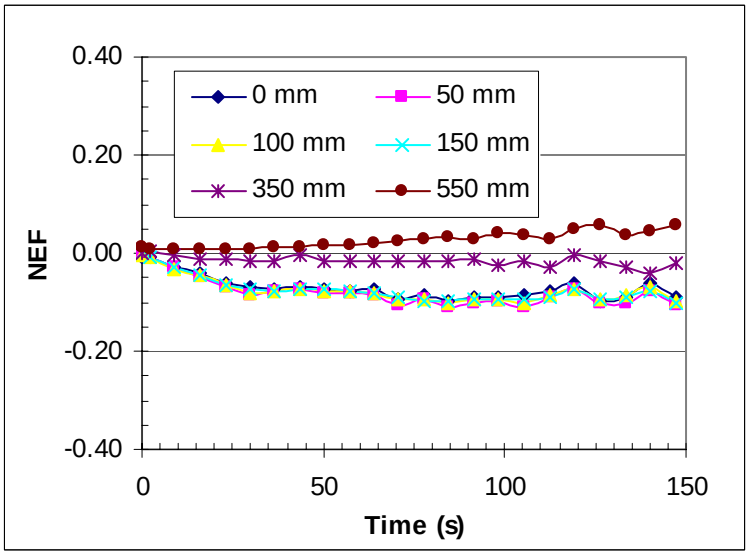

(b) Case 6, 72 x 32 x 20 grid

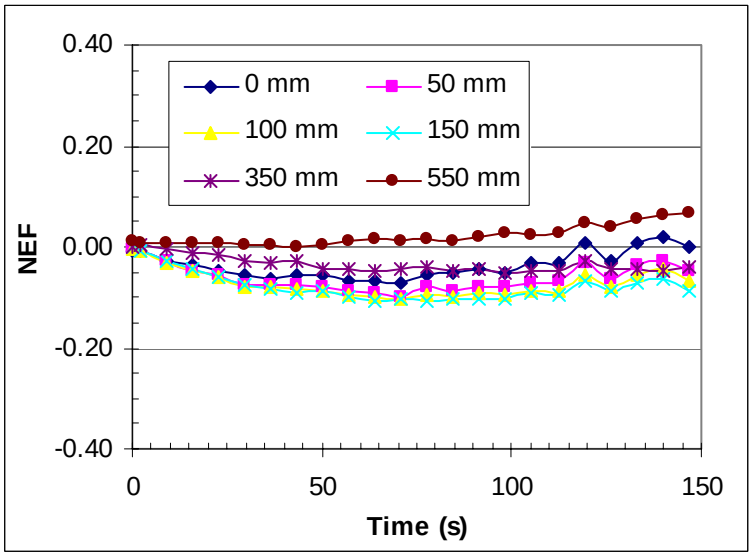

(c) Case 7, 45 x 24 x 16 grid

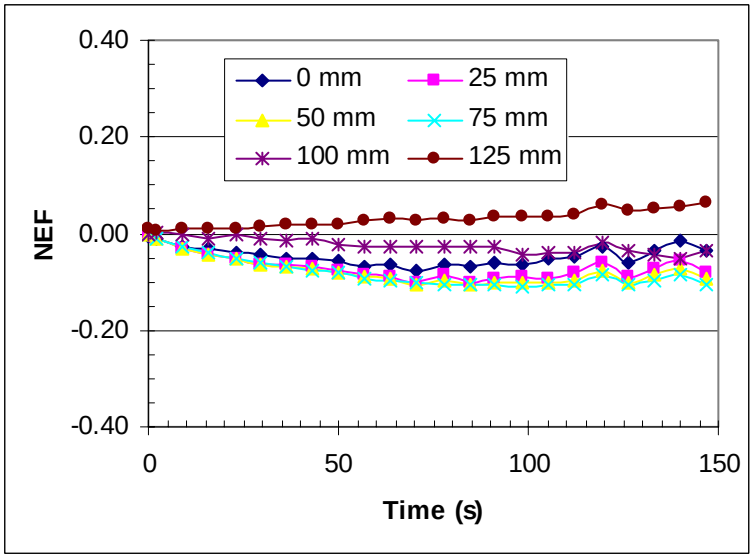

(d) Case 8, 12 x 10 x 10 grid

Figure 42: Slow corner fire normalized error fraction.

4. DISCUSSION

4.1. Computing Time

The computing time required for each of these simulations depends on both the average time step length and the computing time consumed per time step. Figure 43 shows the average time step for all of the simulations. In general, time step length is limited to the time required for a particle to travel the length of one grid cell. Therefore, for each of the six validation problems, time step increases with the cell dimension. Also, much smaller time steps can be used for problems with strong convective motion, such as the fires. This effect is also apparent within the corner fire results: for each grid dimension the larger time step represents the slow burning fire and the smaller time step represents the fast burning fire. However, both of these fires require significantly smaller time steps than the non-fire scenarios. To obtain similar computing times, the fires were simulated with coarser grids to partially offset this difference.

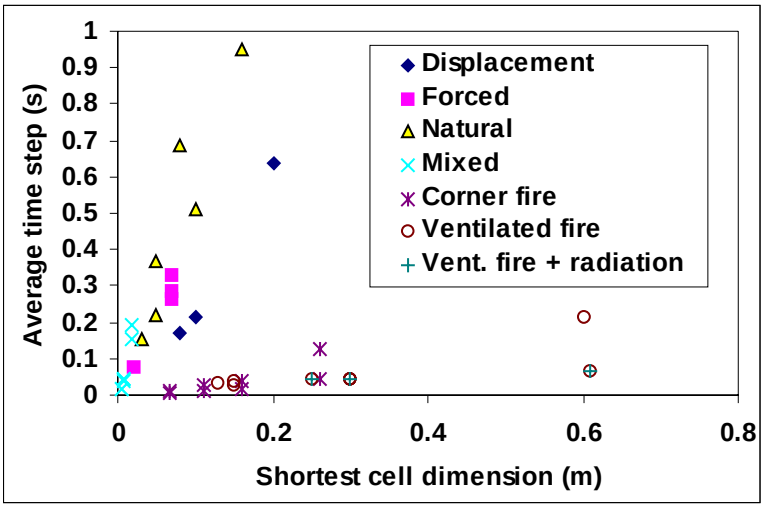

Figure 43. Average time step.

Clearly, shorter time steps increase overall simulation time because more time steps are needed. A second factor affecting overall simulation speed is the CPU time required for each timestep. This quantity, shown in Figure 44, generally does not depend on number of grid cells, and is instead related to the equations that must be solved. It is possibile that large simulations may be less efficient if system resources are strained. Also simulations with a very small number of grid cells sometimes appear to consume more computing time simply because there are fewer cells and time steps for "overhead" tasks such as results reporting and sprinkler activation to be spread among. Of the scenarios shown, the most CPU time is consumed by the radiation cases. This would be expected because of the additional equations involved. The next most time consuming simulations are the very coarse mixed convection case and the very coarse fast corner fire case, again because of these "overhead" tasks. The shortest CPU time is needed for the forced ventilation scenario, which would be expected since this case does not require the energy or species equations to be solved.

Putting both of these factors together, Figure 45 shows the CPU time required per cell per second of simulated time for each of the scenarios. This measure of CPU time is referenced against a "real time upper limit", in which the simulated and simulation times would be equal. Three of the four non-fire scenarios were simulated in less than real time with reasonable results. A somewhat longer simulation time was needed to properly model species diffusion for the displacement ventilation scenario. Using a very coarse grid, it was possible to obtain reasonable predictions of temperatures generated by the slow corner fire. This may not have been the case, however, if species were also tracked. The stronger convective forces in the fast corner fire required longer computing times, however, these are still quite reasonable and could be improved even further with a more powerful computer. Likewise, one of the ventilated fire cases is faster than real

time, but the predicted plume temperature is too low. A finer grid is needed to reduce the numerical diffusion.

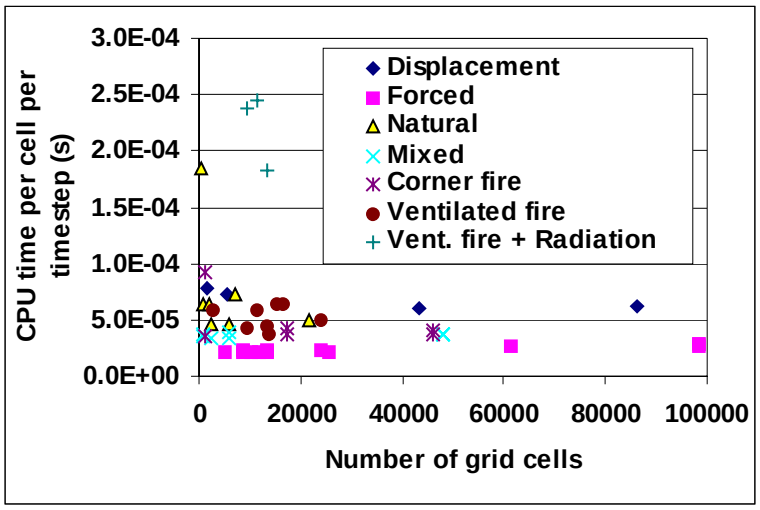

Figure 44. CPU time per cell per timestep.

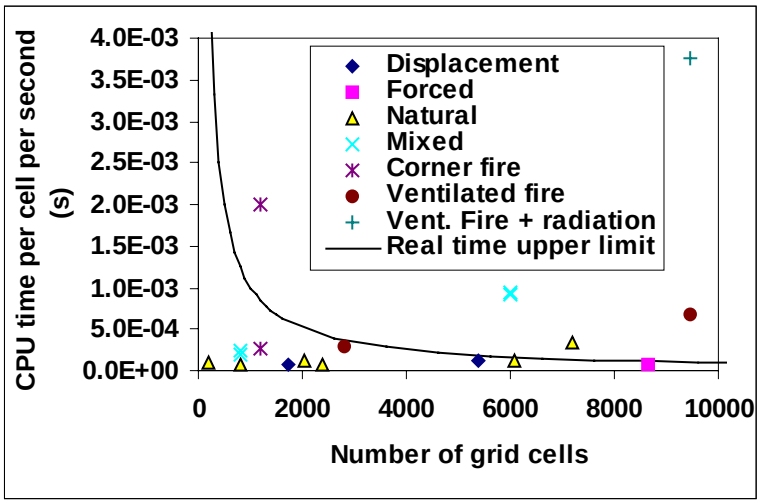

Figure 45. CPU time per cell per second.

4.2. Results Comparison

Comparison with experimental results has identified a number of issues important to building simulations and developing expectations for the computational results. Development of the computational model should include an investigation of the influence of number of grid cells, grid refinement technique, and time step on the results. The need to properly specify obstructions, heat transfer boundary conditions, inlet diffusers, and contaminant releases is also clear. In a design situation, it is likely that certain boundary conditions, such as surface temperatures or inlet velocity profiles, would not be as well defined. This might require additional simulations to assess the sensitivity of the solution to fluctuations in these input parameters.

It would also have been possible to improve the agreement of the CFD models with the experimental results by "fine-tuning" the inputs. For example, the temperature profiles predicted for the displacement ventilation case might have better matched the experimental results if another convection coefficient had been used in the model. It would have been possible to continually adjust the convection coefficients until the best possible result was obtained. However, this would not be possible when modeling a new situation. The approach taken here was to choose convection coefficients based on past experience and published studies and not adjust them. With a new situation, the modeler should give careful thought to selecting convection

coefficients. Fire simulations tend to be dominated by the fire behavior, so that the convection from other surfaces is often less important. However, surface convection can be an important aspect of non-fire flows, and the choice of coefficient can become critical. If the heat flux from a surface is known, it should be specified directly; otherwise care should be taken to select coefficients from published sources that best describe the situation to be modeled.

The way in which FDS treats surface convection also leads to a departure from the accepted wisdom that a finer grid will produce better results. This convection model requires that the grid cell adjacent to a fixed-temperature wall be larger than the thermal boundary layer. Smaller grid cells could lead to under-prediction of heat transfer. In certain cases, there could be a trade-off between keeping grid cells large enough to get the correct heat transfer and small enough to properly define the room geometry or to predict diffusion correctly. Empirical correlations can be used to approximate boundary layer thickness to determine whether a conflict might arise. If this is the case, it would be worthwhile to try to specify a surface heat flux instead of a fixed temperature.

In general, the results obtained for these simulations were accurate enough to be useful. However, even though the experimental results were generated and measured under controlled conditions, the agreement between model and experiment was not always precise and is sometimes best compared qualitatively. The results pattern for the fast corner fire suggests that perhaps the original experimental conditions are not understood as well as one might want them to be, and that the results are systematically affected. These experiences should be used to calibrate expectations of the model.

5. CONCLUSIONS

The collective experience of the many simulations performed to model these six flow problems highlights several issues relevant to the use of the code for modeling a wider variety of scenarios. The inclusion of both fire and non-fire scenarios allows issues specific to each type of modeling to be identified. In general, the FDS code was able to produce results that agree reasonably with the experimental data. However, a systematic modeling approach that considers the problem solving technique employed by the code is essential to obtaining the best results.

For a single problem, at least a few simulations should be performed to check the influence of the number of grid cells, grid refinement technique, and time step on the solution. In particular, grid cell size should be checked to verify that it is large enough to properly model heat transfer from constant temperature surfaces, and small enough to properly represent diffusion conditions. This should be done in addition to any investigation of possible variation in boundary conditions that may also be necessary.

Some care is also needed to define the model in a way that is appropriate for the program and for the problem to be solved. For non-fire scenarios, heat transfer coefficients should be carefully selected and defined in a manner that is consistent with a coarse grid model. This may be less important for fire-dominated flows.

The true power of a simplified model is its ability to produce very fast solutions. Most of the non-fire problems cold be solved at faster than real time speeds on a mid-level personal computer. With the exception of the displacement ventilation problem, the results obtained at these speeds were nearly as good as those obtained with the finer grids at slower computing times. In the displacement ventilation case, a finer grid was required to properly capture diffusion of the tracer gas.

Because the stronger convective forces present in the fire cases required much shorter time steps, these simulations tended to consume slightly more computing time. However, these simulations were still quite fast, and reasonable results were obtained with coarse grids. These simulations were slower than real time, but still fast enough to be convenient and useful in a design environment. With a more powerful computer, many of these simulations might be conducted in real time as well.

REFERENCES

ASHRAE 1997. *Handbook of Fundamentals – SI Edition*. American Society of Heating, Refrigerating, and Air-Conditioning Engineers, Inc. Atlanta, GA.

Baum, H., K. McGrattan, and R. Rehm. 1997. Three Dimensional Simulations of Fire Plume Dynamics. *Journal of the Heat Transfer Society of Japan*. 35:455-52.

Bauman, F., A. Gadgil, R. Kammerud, E. Altmayer, and M. Nansteel. 1983. "Convective Heat Transfer in Buildings: Recent Research Results." *ASHRAE Transactions*. 89(1A)215-33.

Blay, D. S. Mergui, ad C. Niculae. 1992. "Confined Turbulent Mixed Convection in the Presence of a Horizoneal Buoyant Wall Jet." HTD-Vol. 213. *Fundamentals of Mixed Convection*. ASME . p.65-72.

Chen, Q. 1997. "Computational Fluid Dynamics for HVAC: Successes and Failures." ASHRAE Transactions. Vol. 103(1): 178-187.

Chen, Q., L. Glicksman, and J. Srebric. 1998. "Simplified Methodology to Factor Room Air Movement and the Impact on Thermal Comfort into Design of Radiative, Convective, and Hybrid Heating and Cooling Systems." Final report ASHRAE RP-927.

Davidson, L. and P. Nielsen. 1996. Large "Eddy simulation of the Flow in a Three-Dimensional Ventilated Room." *Roomvent '96*. Vol. 2.

Deardorff, J. 1972. "Numerical Investigation of Neutral and Unstable Planetary Boundary Layers." *Journal of Atmospheric Sciences*. 29:91-115.

Emmerich, S. and K. McGrattan. 1998. "Application of a Large Eddy Simulation Model to Study Room Airflow." *ASHRAE Transactions*. Vol. 104(1B):1128-1140.

Forney, G. and K. McGrattan 2000. *User's Guide for Smokeview Version 1.0 – A Tool for Visualizing Fire Dynamics Simulation Data*. Technical Report NISTIR 6513. National Institute of Technology. Gaithersburg, Maryland. May.

Friday, P. and Mowrer, F. 2000. *Comparison of FDS Model Predictions with FM/SNL Fire Test Data*. Masters Thesis. University of Maryland.

Germano, M., U. Piomelli, P. Moin, and W. Cabot. 1991. A Dynamic Subgrid-Scale Eddy Viscosity Model. *Physics of Fluids A*, 3:1760-1765.

Holman, J. 1989. *Heat Transfer*. McGraw-Hill. New York. 5th Ed.

Incropera, F. and D. DeWitt 1990. *Fundamentals of Heat and Mass Transfer. Third ed.* Wiley and Sons.

Lilly, D. 1992. "A Proposed Modification of the Germano Subgird-Scale Closure Method." *Physics of Fluids A*, 4:633-635.

McGrattan, K., R. Rehm, and H. Baum. 1994. "Fire-driven Flows in Enclosures." *Journal of Computational Physics*. 110:285-291.

McGrattan, K., H. Baum, R. Rehm, A. Hamins, and G. Forney. 2000. *Fire Dynamics Simulator, Technical Reference Guide*. Technical Report NISTIR 6467, National Institute of Technology. Gaithersburg, Maryland. January.

McGrattan, K. and G. Forney 2000. *Fire Dynamics Simulator - User's Manual*. Technical Report NISTIR 6469, National Institute of Technology, Gaithersburg, Maryland, January.

Nielsen, P. 1998. "The Selection of Turbulence Models for Prediction of Room Airflow." *ASHRAE Transactions*. 104(1B)963-970.

Nowlen, S.P. 1991. Survivor's Guide for Users of the Baseline Validation Test Data, Revision 1. Sandia National Laboratories. June.

Olsen, D., L. Glicksman, and H. Ferm. 1990. "Steady-State Natural Convection in Empty and Partitioned Enclosures at High Rayleigh Numbers." *Transactions of ASME*. Vol. 112. August.

Rehm, R. and H. Baum. 1978. "The Equations of Motion for Thermally Driven, Buoyant Flows." *Journal of Research of the NBS*. 83:297-308.

Restivo, A. 1979. *Turbulent Flow in Ventilated Rooms*. University of London, Mechanical Engineering Department.

Schwenke, H. 1975. "Ueber das Verhalten elener horizontaler Zuluftstrahlen im begrenzten Raum," Luft- und Kaltetechnik, 5, 241-246.

Smagorinsky, J. 1963. General Circulation Experiments with Primitive Equations. I. The Basic Experiment. *Monthly Weather Review*. 91:99-164.

Vettori, Robert. 1999. *Response of Automatic Sprinklers and Heat Detectors beneath smooth and obstructed ceilings: Comparison of fire model predictions with large scale experimental data*. Masters Thesis. University of Maryland.

Xu and Chen. 1998. "Numerical Simulation of Air Flow in a Room with Differentially Heated Vertical Walls." *ASHRAE Transactions*. 104(1A):168-175.

Yuan, X., Chen, Q., Glicksman, L.R., Hu, Y., and X. Yang. 1998. "Measurements and computations of room airflow with displacement ventilation," *ASHRAE Transactions*. 105(1):340-352.

Zhang, W. and Q. Chen. 1999. "Large Eddy Simulation of Natural Convection Flow in a Room with a Filtered Dynamic Subgrid Scale Model. *International Symposium on Computational Technologies for Fluid/Thermal/Structural/Chemical Systems with Industrial Applications*. pp. 263-268. PVP-Vol. 297-1. Edited by Klein C.R. and Kawano, S., August 1-5, Boston, Massachusetts.

APPENDIX A: Sample input files

A.1. Forced convection (case 14)

```
 &HEAD CHID='forced14', TITLE='Davidson study, 36X12X20, grid xform' /
 &GRID IBAR=36,JBAR=12,KBAR=20 /
 &PDIM XBAR=9.0, YBAR=3.0, ZBAR=3.0 /
 &TRNZ IDERIV=1, CC=0.0, PC=0.5 /
 &TRNZ IDERIV=1, CC=3.0, PC=0.5 /
 &TRNZ IDERIV=2, CC=0.0, PC=0.0 /
 &TRNZ IDERIV=2, CC=3.0, PC=0.0 /
 &TRNZ IDERIV=0, CC=2.55, PC=2.832 /
 &TRNZ IDERIV=0, CC=0.90, PC=0.480 /
 &TIME DT=0.4,TWFIN=2500. /
 &MISC TMPA=20., ISOTHERMAL=.TRUE., CSMAG=0.14 /
 &PL3D DTSAM=200, QUANTITIES='VELOCITY', 'U-VELOCITY', 'V-VELOCITY' ,'W-VELOCITY',
'PRESSURE' /
 &SURF ID='INLET', VOLUME_FLUX=-0.22932 /
 &VENT XB=0.0, 0.0, 0.0, 3.0, 2.832, 3.0, SURF_ID='INLET' /
 &VENT XB=9.0, 9.0, 0.0, 3.0, 0.0, 0.48, SURF_ID='OPEN' /
 &SLCF XB=3., 3., 1.5, 1.5, 0., 3., QUANTITY='U-VELOCITY', DTSAM=1.0 /
 &SLCF XB=6., 6., 1.5, 1.5, 0., 3., QUANTITY='U-VELOCITY' /
 &SLCF XB=0., 9., 1.5, 1.5, 2.916, 2.916, QUANTITY='U-VELOCITY' /
 &SLCF XB=0., 9., 1.5, 1.5, 0.084, 0.084, QUANTITY='U-VELOCITY' /
```

A.2. Natural convection (case 2)

```
&HEAD CHID='natural2',TITLE='Sample fire in multiple room layout' /
&GRID IBAR=50, JBAR=1, KBAR=16 /
&PDIM XBAR=7.9,YBAR=.16,ZBAR=2.5 /
&TIME DT=1.0,TWFIN=5000. /
&MISC TMPA=27.6 /
&SURF ID='hot' ,TMPWAL=35.3 /
&SURF ID='cold',TMPWAL=19.9 /
&SURF ID='slip',VBC=1. /
&VENT CB='XBAR' ,SURF_ID='hot'  /
&VENT CB='XBAR0',SURF_ID='cold' /
&VENT CB='YBAR' ,SURF_ID='slip' /
&VENT CB='YBAR0',SURF_ID='slip' /
&SLCF XB=0.00,7.90,0.08,0.08,0.00,2.50, QUANTITY='TEMPERATURE' /
&SLCF XB=0.00,7.90,0.08,0.08,0.00,2.50, QUANTITY='U-VELOCITY' /
&SLCF XB=0.00,7.90,0.08,0.08,0.00,2.50, QUANTITY='W-VELOCITY' /
&SLCF XB=0.00,7.90,0.08,0.08,0.00,2.50, QUANTITY='VELOCITY' /
&SLCF XB=3.95,3.95,0.08,0.08,0.00,2.50, QUANTITY='TEMPERATURE' /
&SLCF XB=3.95,3.95,0.08,0.08,0.00,2.50, QUANTITY='U-VELOCITY' /
```

A.3. Mixed convection (case 1)

```
 &HEAD CHID='mixed1', TITLE='mixed convection, blay case, grid 10x8x10' /
 &GRID IBAR=10, JBAR=8, KBAR=10 /
 &PDIM XBAR=1.04, YBAR=0.7, ZBAR=1.04 /
 &TRNZ CC=0.104, PC=0.024 /
 &TRNZ CC=0.936, PC=1.022 /
 &TIME DT=0.3, TWFIN=1000. /
 &MISC TMPA=15., CSMAG=0.14, SURF_DEFAULT='WALL', C_HORIZONTAL=4.0,
C_VERTICAL=2.03 /
```

```
 &PL3D DTSAM=200, QUANTITIES='TEMPERATURE', 'U-VELOCITY', 'V-VELOCITY', 'W-
VELOCITY', 'PRESSURE' /
 &SURF ID='INLET', VOLUME_FLUX=-0.007182 /
 &SURF ID='FLOOR', TMPWAL=35.5 /
 &SURF ID='WALL', TMPWAL=15.0 /
 &VENT XB=0.0, 0.0, 0.0, 0.7, 1.0022, 1.04, SURF_ID='INLET' /
 &VENT XB=1.04, 1.04, 0.0, 0.7, 0.0, 0.024, SURF_ID='OPEN' /
 &VENT CB='ZBAR0', SURF_ID='FLOOR' /
 &SLCF XB=0., 1.04, 0.35, 0.35, 0.52, 0.52, QUANTITY='W-VELOCITY', DTSAM=1.0 /
 &SLCF XB=0., 1.04, 0.35, 0.35, 0.52, 0.52, QUANTITY='TEMPERATURE' /
 &SLCF XB=0.52, 0.52, 0.35, 0.35, 0., 1.04, QUANTITY='U-VELOCITY' /
 &SLCF XB=0.52, 0.52, 0.35, 0.35, 0., 1.04, QUANTITY='TEMPERATURE' /
 &SLCF XB=0., 1.04, 0.35, 0.35, 0., 1.04, QUANTITY='TEMPERATURE' /
 &SLCF XB=0., 1.04, 0.35, 0.35, 0., 1.04, QUANTITY='VELOCITY' /
```

A.4. Displacement ventilation (case 2)

```
 &HEAD CHID='disp2', TITLE= 'Data for Chen validation, case 1' /
 &GRID IBAR=18, JBAR=12, KBAR=8 /
 &PDIM XBAR=5.16, YBAR=3.65, ZBAR=2.43 /
 &TIME DT=1.5,TWFIN=5000. /
 &MISC TMPA=26.7, C_HORIZONTAL=4.05, C_VERTICAL=3.08 /
 &PL3D DTSAM=1000., QUANTITIES='SF6','U-VELOCITY','V-VELOCITY','W-
VELOCITY','TEMPERATURE' /
 &PART NPSAM=500, QUANTITY='SF6', AGE=1, DTSAM=100 /
 &SPEC ID='SF6', MW=146. /
 &SURF ID='PERSON', HEAT_FLUX=0.0419 /
 &SURF ID='COMP1', HEAT_FLUX =0.13563 /
 &SURF ID='COMP2', HEAT_FLUX =0.2168 /
 &SURF ID='LAMP', HEAT_FLUX =0.051515 /
 &SURF ID='CEILING', TMPWAL=25.61 /
 &SURF ID='FLOOR', TMPWAL=23.56 /
 &SURF ID='WINDOW', TMPWAL=27.68 /
 &SURF ID='LOWALL', TMPWAL=24.21 /
 &SURF ID='UPWALL', TMPWAL=25.72 /
 &SURF ID='INLET', TMPWAL=17.0, VOLUME_FLUX=-0.05085, MASS_FRACTION(1)=0.0 /
 &SURF ID='TRACER', HEAT_FLUX=0.0419, VEL=-0.001, MASS_FLUX(1)=7.33E-7 /
 &OBST XB=2.01,2.29,0.9125,1.21,0.0,1.215,SURF_IDS='TRACER','PERSON','PERSON' /
 &OBST XB=3.15,3.44,2.43,2.73,0.0,1.215,SURF_IDS='TRACER','PERSON','PERSON' /
 &OBST XB=1.98, 2.38, 0.1, 0.5, 0.75, 1.15, SURF_ID='COMP1' /
 &OBST XB=3.13, 3.53, 3.15, 3.55, 0.75, 1.15, SURF_ID='COMP2' /
 &OBST XB=0.35, 2.58, 0.0, 0.75, 0.74, 0.75 /
 &OBST XB=2.93, 5.16, 2.90, 3.65, 0.74, 0.75 /
 &OBST XB=0., 0.33, 0., 0.58, 0., 1.32 /
 &OBST XB=4.21, 5.16, 0., 0.58, 0., 1.24 /
 &OBST XB=1.03, 1.23, 0.16, 1.36, 2.18, 2.33, SURF_ID='LAMP' /
 &OBST XB=2.33, 2.53, 0.16, 1.36, 2.18, 2.33, SURF_ID='LAMP' /
 &OBST XB=3.61, 3.81, 0.16, 1.36, 2.18, 2.33, SURF_ID='LAMP' /
 &OBST XB=1.03, 1.23, 2.29, 3.49, 2.18, 2.33, SURF_ID='LAMP' /
 &OBST XB=2.33, 2.53, 2.29, 3.49, 2.18, 2.33, SURF_ID='LAMP' /
 &OBST XB=3.61, 3.81, 2.29, 3.49, 2.18, 2.33, SURF_ID='LAMP' /
 &OBST XB=0.0, 0.28, 1.51, 2.04, 0.03, 1.14 /
 &VENT XB=0.28, 0.28, 1.51, 2.04, 0.03, 1.14, SURF_ID='INLET' /
 &VENT XB=2.365, 2.795, 1.61, 2.04, 2.43, 2.43, SURF_ID='OPEN' /
 &VENT CB='ZBAR0', SURF_ID='FLOOR' /
 &VENT XB=4.14, 5.16, 0.00, 3.65, 2.43, 2.43, SURF_ID='CEILING' /
```

```
&VENT XB=3.18, 4.14, 0.00, 3.65, 2.43, 2.43, SURF_ID='CEILING' /
&VENT XB=2.365, 3.18, 0.0, 1.61, 2.43, 2.43, SURF_ID='CEILING' /
&VENT XB=2.795, 3.18, 1.61, 2.04, 2.43, 2.43, SURF_ID='CEILING' /
&VENT XB=2.365, 3.18, 2.04, 2.745, 2.43, 2.43, SURF_ID='CEILING' /
&VENT XB=2.365, 3.18, 2.745, 3.65, 2.43, 2.43, SURF_ID='CEILING' /
&VENT XB=1.26, 2.365, 0.0, 3.65, 2.43, 2.43, SURF_ID='CEILING' /
&VENT XB=0.00, 1.26, 0.00, 3.65, 2.43, 2.43, SURF_ID='CEILING' /
&VENT XB=5.16, 5.16, 0.15, 3.5, 1.24, 2.10, SURF_ID='WINDOW' /
&VENT XB=5.16, 5.16, 0.58, 3.5, 0.94, 1.24, SURF_ID='WINDOW' /
&VENT XB=0.0, 0.0, 0.58, 1.51, 0.0, 0.85, SURF_ID='LOWALL' /
&VENT XB=0.0, 0.0, 2.04, 3.65, 0.0, 0.85, SURF_ID='LOWALL' /
&VENT XB=5.16, 5.16, 0.58, 3.65, 0.0, 0.85, SURF_ID='LOWALL' /
&VENT XB=2.58, 4.21, 0.0, 0.0, 0.0, 0.85, SURF_ID='LOWALL' /
&VENT XB=0.35, 2.58, 0.0, 0.0, 0.0, 0.74, SURF_ID='LOWALL' /
&VENT XB=0.35, 2.58, 0.0, 0.0, 0.81, 0.85, SURF_ID='LOWALL' /
&VENT XB=0.33, 0.35, 0.0, 0.0, 0.0, 0.85, SURF_ID='LOWALL' /
&VENT XB=0.0, 2.93, 3.65, 3.65, 0.0, 0.85, SURF_ID='LOWALL' /
&VENT XB=2.93, 5.16, 3.65, 3.65, 0.81, 0.85, SURF_ID='LOWALL' /
&VENT XB=2.93, 5.16, 3.65, 3.65, 0.0, 0.74, SURF_ID='LOWALL' /
&VENT XB=0.0, 0.0, 0.0, 0.58, 1.32, 2.43, SURF_ID='UPWALL' /
&VENT XB=0.0, 0.0, 0.58, 1.51, 0.85, 2.43, SURF_ID='UPWALL' /
&VENT XB=0.0, 0.0, 1.51, 2.04, 1.14, 2.43, SURF_ID='UPWALL' /
&VENT XB=0.0, 0.0, 2.04, 3.65, 0.85, 2.43, SURF_ID='UPWALL' /
&VENT XB=5.16, 5.16, 3.5, 3.65, 0.85, 2.1, SURF_ID='UPWALL' /
&VENT XB=5.16, 5.16, 0.58, 3.5, 0.85, 0.94, SURF_ID='UPWALL' /
&VENT XB=5.16, 5.16, 0.15, 3.65, 2.1, 2.43, SURF_ID='UPWALL' /
&VENT XB=5.16, 5.16, 0.0, 0.15, 1.24, 2.43, SURF_ID='UPWALL' /
&VENT XB=0.33, 4.21, 0.0, 0.0, 0.85, 1.24, SURF_ID='UPWALL' /
&VENT XB=0.33, 5.16, 0.0, 0.0, 1.24, 1.32, SURF_ID='UPWALL' /
&VENT XB=0.0, 5.16, 0.0, 0.0, 1.32, 2.43, SURF_ID='UPWALL' /
&VENT XB=0.0, 5.16, 3.65, 3.65, 0.85, 2.43, SURF_ID='UPWALL' /
&THCP XYZ=4.0, 1.0, 0.6, QUANTITY='SF6', DTSAM=1.0 /
&THCP XYZ=1.5, 2.65, 0.6, QUANTITY='SF6' /
&THCP XYZ=1.5, 1.0, 2.0, QUANTITY='SF6' /
&THCP XYZ=4.5, 3.0, 2.0, QUANTITY='SF6' /
&THCP XYZ=2.58, 1.825, 2.40, QUANTITY='SF6' /
&THCP XYZ=4.0, 1.0, 0.6, QUANTITY='TEMPERATURE' /
&THCP XYZ=1.5, 2.65, 0.6, QUANTITY='TEMPERATURE' /
&THCP XYZ=1.5, 1.0, 2.0, QUANTITY='TEMPERATURE' /
&THCP XYZ=4.5, 3.0, 2.0, QUANTITY='TEMPERATURE' /
&THCP XYZ=2.58, 1.825, 2.40, QUANTITY='TEMPERATURE' /
&SLCF XB=0.78, 0.78, 1.83, 1.83, 0.0,2.43, QUANTITY='TEMPERATURE', DTSAM=1.0 /
&SLCF XB=1.74, 1.74, 1.83, 1.83, 0.0,2.43, QUANTITY='TEMPERATURE' /
&SLCF XB=2.7, 2.7, 1.83, 1.83, 0.0,2.43, QUANTITY='TEMPERATURE' /
&SLCF XB=3.66, 3.66, 1.83, 1.83, 0.0,2.43, QUANTITY='TEMPERATURE' /
&SLCF XB=4.62, 4.62, 1.83, 1.83, 0.0,2.43, QUANTITY='TEMPERATURE' /
&SLCF XB=2.7, 2.7, 0.61, 0.61, 0.0,2.43, QUANTITY='TEMPERATURE' /
&SLCF XB=2.7, 2.7, 1.22, 1.22, 0.0,2.43, QUANTITY='TEMPERATURE' /
&SLCF XB=2.7, 2.7, 2.44, 2.44, 0.0,2.43, QUANTITY='TEMPERATURE' /
&SLCF XB=2.7, 2.7, 3.05, 3.05, 0.0,2.43, QUANTITY='TEMPERATURE' /
&SLCF XB=0.78, 0.78, 1.83, 1.83, 0.0,2.43, QUANTITY='SF6' /
&SLCF XB=1.74, 1.74, 1.83, 1.83, 0.0,2.43, QUANTITY='SF6' /
&SLCF XB=2.7, 2.7, 1.83, 1.83, 0.0,2.43, QUANTITY='SF6' /
&SLCF XB=3.66, 3.66, 1.83, 1.83, 0.0,2.43, QUANTITY='SF6' /
&SLCF XB=4.62, 4.62, 1.83, 1.83, 0.0,2.43, QUANTITY='SF6' /
&SLCF XB=2.7, 2.7, 0.61, 0.61, 0.0,2.43, QUANTITY='SF6' /
```

```
&SLCF XB=2.7, 2.7, 1.22, 1.22, 0.0,2.43, QUANTITY='SF6' /
&SLCF XB=2.7, 2.7, 2.44, 2.44, 0.0,2.43, QUANTITY='SF6' /
&SLCF XB=2.7, 2.7, 3.05, 3.05, 0.0,2.43, QUANTITY='SF6' /
&SLCF XB=0.78, 0.78, 1.83, 1.83, 0.0,2.43, QUANTITY='VELOCITY' /
&SLCF XB=1.74, 1.74, 1.83, 1.83, 0.0,2.43, QUANTITY='VELOCITY' /
&SLCF XB=2.7, 2.7, 1.83, 1.83, 0.0,2.43, QUANTITY='VELOCITY' /
&SLCF XB=3.66, 3.66, 1.83, 1.83, 0.0,2.43, QUANTITY='VELOCITY' /
&SLCF XB=4.62, 4.62, 1.83, 1.83, 0.0,2.43, QUANTITY='VELOCITY' /
&SLCF XB=2.7, 2.7, 0.61, 0.61, 0.0,2.43, QUANTITY='VELOCITY' /
&SLCF XB=2.7, 2.7, 1.22, 1.22, 0.0,2.43, QUANTITY='VELOCITY' /
&SLCF XB=2.7, 2.7, 2.44, 2.44, 0.0,2.43, QUANTITY='VELOCITY' /
&SLCF XB=2.7, 2.7, 3.05, 3.05, 0.0,2.43, QUANTITY='VELOCITY' /
&SLCF XB=0.0, 5.16, 1.61, 1.58, 1.58, 2.43, QUANTITY='TEMPERATURE' /
&SLCF XB=0.0, 5.16, 1.61, 1.58, 1.58, 2.43, QUANTITY='SF6' /
```

A.5 Ventilated Fire (case 4)

```
&HEAD CHID='FMSNL4',TITLE='FMSNL Test #5- 1ft grid with piecewise linear transformation' /
&GRID IBAR=60,JBAR=40,KBAR=20 /
&PDIM XBAR=18.29,YBAR=12.19,ZBAR=6.10 /
&TRNX CC=9.14,PC=10.67 /
&TRNX CC=15.24, PC=13.72 /
&TRNY CC=3.05,PC=4.57 /
&TRNY CC=9.15, PC=7.62 /
&TIME DT=0.5,TWFIN=600. /
&PART QUANTITY='TEMPERATURE',DTPAR=0.05 /
&MISC TMPA=21.0  /
&SURF ID='burner',HRRPUA=787.,TBO=0.5,TAU_Q=-240. /
&SURF ID='wall',ALPHA=1.55E-7,KS=0.1035,DELTA=0.0254, RADIATION=.FALSE. /
&SURF ID='port',TMPWAL=21,VOLUME_FLUX=-0.63 /
&OBST XB=2.82,3.28,2.82,3.28,4.88,6.10 /#1 injection port
&OBST XB=2.82,3.28,2.82,3.28,4.57,4.57 /deflector plate
&OBST XB=8.91,9.37,2.82,3.28,4.88,6.10 /#2 injection port
&OBST XB=8.91,9.37,2.82,3.28,4.57,4.57 /deflector plate
&OBST XB=15.01,15.47,2.82,3.28,4.88,6.10 /#3 injection port
&OBST XB=15.01,15.47,2.82,3.28,4.57,4.57 /deflector plate
&OBST XB=2.82,3.28,8.91,9.37,4.88,6.10 /#4 injection port
&OBST XB=2.82,3.28,8.91,9.37,4.57,4.57 /deflector plate
&OBST XB=8.91,9.37,8.91,9.37,4.88,6.10 /#5 injection port
&OBST XB=8.91,9.37,8.91,9.37,4.57,4.57 /deflector plate
&OBST XB=15.01,15.47,8.91,9.37,4.88,6.10 /#6 injection port
&OBST XB=15.01,15.47,8.91,9.37,4.57,4.57 /deflector plate
&OBST XB=11.79,12.60,5.69,6.50,0.00,0.30 /sand burner
&VENT CB='EAST',SURF_ID='wall' /
&VENT CB='WEST',SURF_ID='wall' /
&VENT CB='NORTH',SURF_ID='wall' /
&VENT CB='SOUTH',SURF_ID='wall' /
&VENT CB='TOP',SURF_ID='wall' /
&VENT XB=2.82,3.28,2.82,3.28,4.88,4.88,SURF_ID='port' /
&VENT XB=8.91,9.37,2.82,3.28,4.88,4.88,SURF_ID='port' /
&VENT XB=15.01,15.47,2.82,3.28,4.88,4.88,SURF_ID='port' /
&VENT XB=2.82,3.28,8.91,9.37,4.88,4.88,SURF_ID='port' /
&VENT XB=8.91,9.37,8.91,9.37,4.88,4.88,SURF_ID='port' /
&VENT XB=15.01,15.47,8.91,9.37,4.88,4.88,SURF_ID='port' /
&VENT XB=11.79,12.60,5.69,6.50,0.30,0.30,SURF_ID='burner' / propylene burner
&VENT XB=0.10,0.61,5.18,7.01,6.10,6.10,SURF_ID='OPEN' / exhaust vent
```

```
&THCP XYZ=3.05,6.1,5.98,QUANTITY='TEMPERATURE',LABEL='Sector3 Ch11',DTSAM=5 /
&THCP XYZ=3.05,6.1,5.49,QUANTITY='TEMPERATURE',LABEL='Sector3 Ch12' /
&THCP XYZ=3.05,6.1,4.27,QUANTITY='TEMPERATURE',LABEL='Sector3 Ch13' /
&THCP XYZ=3.05,6.1,3.05,QUANTITY='TEMPERATURE',LABEL='Sector3 Ch14' /
&THCP XYZ=3.05,6.1,1.83,QUANTITY='TEMPERATURE',LABEL='Sector3 Ch15' /
&THCP XYZ=9.15,6.1,5.98,QUANTITY='TEMPERATURE',LABEL='Sector2 Ch6' /
&THCP XYZ=9.15,6.1,5.49,QUANTITY='TEMPERATURE',LABEL='Sector2 Ch7' /
&THCP XYZ=9.15,6.1,4.27,QUANTITY='TEMPERATURE',LABEL='Sector2 Ch8' /
&THCP XYZ=9.15,6.1,3.05,QUANTITY='TEMPERATURE',LABEL='Sector2 Ch9' /
&THCP XYZ=9.15,6.1,1.83,QUANTITY='TEMPERATURE',LABEL='Sector2 Ch10' /
&THCP XYZ=15.25,6.1,5.98,QUANTITY='TEMPERATURE',LABEL='Sector1 Ch1' /
&THCP XYZ=15.25,6.1,5.49,QUANTITY='TEMPERATURE',LABEL='Sector1 Ch2' /
&THCP XYZ=15.25,6.1,4.27,QUANTITY='TEMPERATURE',LABEL='Sector1 Ch3' /
&THCP XYZ=15.25,6.1,3.05,QUANTITY='TEMPERATURE',LABEL='Sector1 Ch4' /
&THCP XYZ=15.25,6.1,1.83,QUANTITY='TEMPERATURE',LABEL='Sector1 Ch5' /
&THCP XYZ=15.25,1.52,5.98,QUANTITY='TEMPERATURE',LABEL='Station1 Ch16' /
&THCP XYZ=15.25,1.52,5.49,QUANTITY='TEMPERATURE',LABEL='Station1 Ch41' /
&THCP XYZ=15.25,1.52,4.27,QUANTITY='TEMPERATURE',LABEL='Station1 Ch42' /
&THCP XYZ=15.25,1.52,3.05,QUANTITY='TEMPERATURE',LABEL='Station1 Ch43' /
&THCP XYZ=15.25,1.52,1.83,QUANTITY='TEMPERATURE',LABEL='Station1 Ch44' /
&THCP XYZ=9.14,1.52,5.98,QUANTITY='TEMPERATURE',LABEL='Station2 Ch17' /
&THCP XYZ=9.14,1.52,5.49,QUANTITY='TEMPERATURE',LABEL='Station2 Ch45' /
&THCP XYZ=9.14,1.52,4.27,QUANTITY='TEMPERATURE',LABEL='Station2 Ch46' /
&THCP XYZ=9.14,1.52,3.05,QUANTITY='TEMPERATURE',LABEL='Station2 Ch47' /
&THCP XYZ=9.14,1.52,1.83,QUANTITY='TEMPERATURE',LABEL='Station2 Ch48' /
&THCP XYZ=3.05,1.52,5.98,QUANTITY='TEMPERATURE',LABEL='Station3 Ch18' /
&THCP XYZ=3.05,1.52,5.49,QUANTITY='TEMPERATURE',LABEL='Station3 Ch49' /
&THCP XYZ=3.05,1.52,4.27,QUANTITY='TEMPERATURE',LABEL='Station3 Ch50' /
&THCP XYZ=3.05,1.52,3.05,QUANTITY='TEMPERATURE',LABEL='Station3 Ch51' /
&THCP XYZ=3.05,1.52,1.83,QUANTITY='TEMPERATURE',LABEL='Station3 Ch52' /
&THCP XYZ=12.19,3.05,5.98,QUANTITY='TEMPERATURE',LABEL='Station4 Ch19' /
&THCP XYZ=12.19,3.05,5.49,QUANTITY='TEMPERATURE',LABEL='Station4 Ch53' /
&THCP XYZ=12.19,3.05,4.27,QUANTITY='TEMPERATURE',LABEL='Station4 Ch54' /
&THCP XYZ=12.19,3.05,3.05,QUANTITY='TEMPERATURE',LABEL='Station4 Ch55' /
&THCP XYZ=12.19,3.05,1.83,QUANTITY='TEMPERATURE',LABEL='Station4 Ch56' /
&THCP XYZ=6.10,3.05,5.98,QUANTITY='TEMPERATURE',LABEL='Station5 Ch20' /
&THCP XYZ=6.10,3.05,5.49,QUANTITY='TEMPERATURE',LABEL='Station5 Ch57' /
&THCP XYZ=6.10,3.05,4.27,QUANTITY='TEMPERATURE',LABEL='Station5 Ch58' /
&THCP XYZ=6.10,3.05,3.05,QUANTITY='TEMPERATURE',LABEL='Station5 Ch59' /
&THCP XYZ=6.10,3.05,1.83,QUANTITY='TEMPERATURE',LABEL='Station5 Ch60' /
&THCP XYZ=12.19,9.14,5.98,QUANTITY='TEMPERATURE',LABEL='Station6 Ch21' /
&THCP XYZ=12.19,9.14,5.49,QUANTITY='TEMPERATURE',LABEL='Station6 Ch61' /
&THCP XYZ=12.19,9.14,4.27,QUANTITY='TEMPERATURE',LABEL='Station6 Ch62' /
&THCP XYZ=12.19,9.14,3.05,QUANTITY='TEMPERATURE',LABEL='Station6 Ch63' /
&THCP XYZ=12.19,9.14,1.83,QUANTITY='TEMPERATURE',LABEL='Station6 Ch64' /
&THCP XYZ=6.10,9.14,5.98,QUANTITY='TEMPERATURE',LABEL='Station7 Ch22' /
&THCP XYZ=6.10,9.14,5.49,QUANTITY='TEMPERATURE',LABEL='Station7 Ch65' /
&THCP XYZ=6.10,9.14,4.27,QUANTITY='TEMPERATURE',LABEL='Station7 Ch66' /
&THCP XYZ=6.10,9.14,3.05,QUANTITY='TEMPERATURE',LABEL='Station7 Ch67' /
&THCP XYZ=6.10,9.14,1.83,QUANTITY='TEMPERATURE',LABEL='Station7 Ch68' /
&THCP XYZ=15.24,10.67,5.98,QUANTITY='TEMPERATURE',LABEL='Station8 Ch23' /
&THCP XYZ=15.24,10.67,5.49,QUANTITY='TEMPERATURE',LABEL='Station8 Ch69' /
&THCP XYZ=15.24,10.67,4.27,QUANTITY='TEMPERATURE',LABEL='Station8 Ch70' /
&THCP XYZ=15.24,10.67,3.05,QUANTITY='TEMPERATURE',LABEL='Station8 Ch71' /
&THCP XYZ=15.24,10.67,1.83,QUANTITY='TEMPERATURE',LABEL='Station8 Ch72' /
&THCP XYZ=9.14,10.67,5.98,QUANTITY='TEMPERATURE',LABEL='Station9 Ch24' /
```

```
&THCP XYZ=9.14,10.67,5.49,QUANTITY='TEMPERATURE',LABEL='Station9 Ch73' /
&THCP XYZ=9.14,10.67,4.27,QUANTITY='TEMPERATURE',LABEL='Station9 Ch74' /
&THCP XYZ=9.14,10.67,3.05,QUANTITY='TEMPERATURE',LABEL='Station9 Ch75' /
&THCP XYZ=9.14,10.67,1.83,QUANTITY='TEMPERATURE',LABEL='Station9 Ch76' /
&THCP XYZ=3.05,10.67,5.98,QUANTITY='TEMPERATURE',LABEL='Station10 Ch25' /
&THCP XYZ=3.05,10.67,5.49,QUANTITY='TEMPERATURE',LABEL='Station10 Ch77' /
&THCP XYZ=3.05,10.67,4.27,QUANTITY='TEMPERATURE',LABEL='Station10 Ch78' /
&THCP XYZ=3.05,10.67,3.05,QUANTITY='TEMPERATURE',LABEL='Station10 Ch79' /
&THCP XYZ=3.05,10.67,1.83,QUANTITY='TEMPERATURE',LABEL='Station10 Ch80' /
&THCP XYZ=16.76,4.57,5.98,QUANTITY='TEMPERATURE',LABEL='Station11 Ch26' /
&THCP XYZ=1.52,4.57,5.98,QUANTITY='TEMPERATURE',LABEL='Station12 Ch27' /
&THCP XYZ=12.19,6.1,5.98,QUANTITY='TEMPERATURE',LABEL='Station13 Ch28' /
&THCP XYZ=6.10,6.10,5.98,QUANTITY='TEMPERATURE',LABEL='Station14 Ch29' /
&THCP XYZ=16.76,7.62,5.98,QUANTITY='TEMPERATURE',LABEL='Station15 Ch30' /
&THCP XYZ=1.52,7.62,5.98,QUANTITY='TEMPERATURE',LABEL='Station16 Ch31' /
```

A.6 Corner Fire (case1)

```
&HEAD CHID='OBSCOR1',TITLE='Obstructed Ceiling, corner, fast. fire, piecewise linear transformation' /
&GRID IBAR=113,JBAR=64,KBAR=40 /
&PDIM XBAR=9.20,YBAR=5.60,ZBAR=2.64 /
&TRNX CC= .326,PC= .368 /
&TRNX CC= .407,PC= .405 /
&TRNX CC= .733,PC= .773 /
&TRNX CC= .814,PC= .810 /
&TRNX CC=1.140,PC=1.178 /
&TRNX CC=1.221,PC=1.214 /
&TRNX CC=1.547,PC=1.582 /
&TRNX CC=1.628,PC=1.619 /
&TRNX CC=1.954,PC=1.987 /
&TRNX CC=2.035,PC=2.024 /
&TRNX CC=2.361,PC=2.392 /
&TRNX CC=2.442,PC=2.429 /
&TRNX CC=2.768,PC=2.797 /
&TRNX CC=2.850,PC=2.834 /
&TRNX CC=3.175,PC=3.202 /
&TRNX CC=3.257,PC=3.238 /
&TRNX CC=3.582,PC=3.606 /
&TRNX CC=3.664,PC=3.643 /
&TRNX CC=3.989,PC=4.011 /
&TRNX CC=4.071,PC=4.048 /
&TRNX CC=4.396,PC=4.416 /
&TRNX CC=4.478,PC=4.453 /
&TRNX CC=4.804,PC=4.821 /
&TRNX CC=4.885,PC=4.858 /
&TRNX CC=5.211,PC=5.226 /
&TRNX CC=5.292,PC=5.262 /
&TRNX CC=5.618,PC=5.630 /
&TRNX CC=5.699,PC=5.667 /
&TRNX CC=6.025,PC=6.035 /
&TRNX CC=6.106,PC=6.072 /
&TRNX CC=6.432,PC=6.440 /
&TRNX CC=6.513,PC=6.477 /
&TRNX CC=6.839,PC=6.845 /
&TRNX CC=6.920,PC=6.882 /
&TRNX CC=7.246,PC=7.250 /
```

```
&TRNX CC=7.327,PC=7.286 /
&TRNX CC=7.653,PC=7.654 /
&TRNX CC=7.735,PC=7.691 /
&TRNX CC=8.060,PC=8.059 /
&TRNX CC=8.142,PC=8.096 /
&TRNX CC=8.467,PC=8.464 /
&TRNX CC=8.549,PC=8.501 /
&TRNX CC=8.874,PC=8.869 /
&TRNX CC=8.956,PC=8.906 /
&TIME DT=0.50,TWFIN=150. /
&MISC TMPA=20.,DATABASE='database' /
&PART NPSAM=7,DTPAR=0.05,AGE=5. /
&SURF ID='BURNER',HRRPUA=2930.,TBO=0.30, RADIATIVE_FRACTION=0.14,RAMP_Q='fast' /
&SURF ID='WALL',ALPHA=0.00000016,KS=0.17,DELTA=0.0127,RADIATION=.FALSE. /
&SURF ID='CEILING',ALPHA=0.00000009,KS=0.11,DELTA=0.0254,RADIATION=.FALSE. /
&SURF ID='WOOD BEAM',ALPHA=0.00000009,KS=0.11,RADIATION=.FALSE. /
&SURF ID='STEEL BEAM',ALPHA=0.00001482,KS=54.0,DELTA=0.5,RADIATION=.FALSE. /
&OBST XB=0.00,0.70,0.00,1.00,0.00,0.30 /
&OBST XB=0.00,9.20,2.72,2.80,2.22,2.40,SURF_ID='STEEL BEAM' /
&OBST XB=0.3680,0.4048,0.00,5.60,2.40,2.64,SURF_ID='WOOD BEAM'  /
&OBST XB=0.7728,0.8096,0.00,5.60,2.40,2.64,SURF_ID='WOOD BEAM'  /
&OBST XB=1.1776,1.2144,0.00,5.60,2.40,2.64,SURF_ID='WOOD BEAM'  /
&OBST XB=1.5824,1.6192,0.00,5.60,2.40,2.64,SURF_ID='WOOD BEAM'  /
&OBST XB=1.9872,2.0240,0.00,5.60,2.40,2.64,SURF_ID='WOOD BEAM'  /
&OBST XB=2.3920,2.4288,0.00,5.60,2.40,2.64,SURF_ID='WOOD BEAM'  /
&OBST XB=2.7968,2.8336,0.00,5.60,2.40,2.64,SURF_ID='WOOD BEAM'  /
&OBST XB=3.2016,3.2384,0.00,5.60,2.40,2.64,SURF_ID='WOOD BEAM'  /
&OBST XB=3.6064,3.6432,0.00,5.60,2.40,2.64,SURF_ID='WOOD BEAM'  /
&OBST XB=4.0112,4.0480,0.00,5.60,2.40,2.64,SURF_ID='WOOD BEAM'  /
&OBST XB=4.4160,4.4528,0.00,5.60,2.40,2.64,SURF_ID='WOOD BEAM'  /
&OBST XB=4.8208,4.8576,0.00,5.60,2.40,2.64,SURF_ID='WOOD BEAM'  /
&OBST XB=5.2256,5.2624,0.00,5.60,2.40,2.64,SURF_ID='WOOD BEAM'  /
&OBST XB=5.6304,5.6672,0.00,5.60,2.40,2.64,SURF_ID='WOOD BEAM'  /
&OBST XB=6.0352,6.0720,0.00,5.60,2.40,2.64,SURF_ID='WOOD BEAM'  /
&OBST XB=6.4400,6.4768,0.00,5.60,2.40,2.64,SURF_ID='WOOD BEAM'  /
&OBST XB=6.8448,6.8816,0.00,5.60,2.40,2.64,SURF_ID='WOOD BEAM'  /
&OBST XB=7.2496,7.2864,0.00,5.60,2.40,2.64,SURF_ID='WOOD BEAM'  /
&OBST XB=7.6544,7.6912,0.00,5.60,2.40,2.64,SURF_ID='WOOD BEAM'  /
&OBST XB=8.0592,8.0960,0.00,5.60,2.40,2.64,SURF_ID='WOOD BEAM'  /
&OBST XB=8.4640,8.5008,0.00,2.80,2.40,2.64,SURF_ID='WOOD BEAM'  /
&OBST XB=8.8688,8.9056,0.00,2.80,2.40,2.64,SURF_ID='WOOD BEAM'  /
&VENT XB=0.00,0.60,0.00,0.60,0.30,0.30,SURF_ID='BURNER'  /
&VENT XB=8.30,9.20,2.90,5.60,2.64,2.64,SURF_ID='OPEN' /
&VENT CB='ZBAR' ,SURF_ID='CEILING' /
&VENT CB='XBAR' ,SURF_ID='WALL' /
&VENT CB='XBAR0',SURF_ID='WALL' /
&VENT CB='YBAR' ,SURF_ID='WALL' /
&VENT CB='YBAR0',SURF_ID='WALL' /
&SPRK XYZ=2.40,1.40,2.375,MAKE='VETTORI' /
&SPRK XYZ=6.80,1.40,2.375 /
&SPRK XYZ=6.80,4.20,2.375 /
&SPRK XYZ=2.40,4.20,2.375 /
&THCP XYZ=2.40,1.40,2.400,QUANTITY='TEMPERATURE',DTSAM=0.2 /
&THCP XYZ=2.40,1.40,2.375,QUANTITY='TEMPERATURE' /
&THCP XYZ=2.40,1.40,2.350,QUANTITY='TEMPERATURE' /
&THCP XYZ=2.40,1.40,2.325,QUANTITY='TEMPERATURE' /
```

```
&THCP XYZ=2.40,1.40,2.300,QUANTITY='TEMPERATURE' /
&THCP XYZ=2.40,1.40,2.275,QUANTITY='TEMPERATURE' /
&THCP XYZ=2.40,1.40,2.250,QUANTITY='TEMPERATURE' /
&THCP XYZ=2.40,1.40,2.150,QUANTITY='TEMPERATURE' /
&THCP XYZ=2.40,1.40,2.050,QUANTITY='TEMPERATURE' /
&THCP XYZ=2.40,1.40,1.950,QUANTITY='TEMPERATURE' /
&THCP XYZ=2.40,1.40,1.850,QUANTITY='TEMPERATURE' /
&THCP XYZ=2.40,1.40,1.500,QUANTITY='TEMPERATURE' /
&THCP XYZ=6.80,1.40,2.400,QUANTITY='TEMPERATURE' /
&THCP XYZ=6.80,1.40,2.375,QUANTITY='TEMPERATURE' /
&THCP XYZ=6.80,1.40,2.350,QUANTITY='TEMPERATURE' /
&THCP XYZ=6.80,1.40,2.325,QUANTITY='TEMPERATURE' /
&THCP XYZ=6.80,1.40,2.300,QUANTITY='TEMPERATURE' /
&THCP XYZ=6.80,1.40,2.275,QUANTITY='TEMPERATURE' /
&THCP XYZ=6.80,1.40,2.250,QUANTITY='TEMPERATURE' /
&THCP XYZ=6.80,1.40,2.150,QUANTITY='TEMPERATURE' /
&THCP XYZ=6.80,1.40,2.050,QUANTITY='TEMPERATURE' /
&THCP XYZ=6.80,1.40,1.950,QUANTITY='TEMPERATURE' /
&THCP XYZ=6.80,1.40,1.850,QUANTITY='TEMPERATURE' /
&THCP XYZ=6.80,1.40,1.500,QUANTITY='TEMPERATURE' /
&THCP XYZ=6.80,4.20,2.400,QUANTITY='TEMPERATURE' /
&THCP XYZ=6.80,4.20,2.375,QUANTITY='TEMPERATURE' /
&THCP XYZ=6.80,4.20,2.350,QUANTITY='TEMPERATURE' /
&THCP XYZ=6.80,4.20,2.325,QUANTITY='TEMPERATURE' /
&THCP XYZ=6.80,4.20,2.300,QUANTITY='TEMPERATURE' /
&THCP XYZ=6.80,4.20,2.275,QUANTITY='TEMPERATURE' /
&THCP XYZ=6.80,4.20,2.250,QUANTITY='TEMPERATURE' /
&THCP XYZ=6.80,4.20,2.150,QUANTITY='TEMPERATURE' /
&THCP XYZ=6.80,4.20,2.050,QUANTITY='TEMPERATURE' /
&THCP XYZ=6.80,4.20,1.950,QUANTITY='TEMPERATURE' /
&THCP XYZ=6.80,4.20,1.850,QUANTITY='TEMPERATURE' /
&THCP XYZ=6.80,4.20,1.500,QUANTITY='TEMPERATURE' /
&THCP XYZ=2.40,4.20,2.400,QUANTITY='TEMPERATURE' /
&THCP XYZ=2.40,4.20,2.375,QUANTITY='TEMPERATURE' /
&THCP XYZ=2.40,4.20,2.350,QUANTITY='TEMPERATURE' /
&THCP XYZ=2.40,4.20,2.325,QUANTITY='TEMPERATURE' /
&THCP XYZ=2.40,4.20,2.300,QUANTITY='TEMPERATURE' /
&THCP XYZ=2.40,4.20,2.275,QUANTITY='TEMPERATURE' /
&THCP XYZ=2.40,4.20,2.250,QUANTITY='TEMPERATURE' /
&THCP XYZ=2.40,4.20,2.150,QUANTITY='TEMPERATURE' /
&THCP XYZ=2.40,4.20,2.050,QUANTITY='TEMPERATURE' /
&THCP XYZ=2.40,4.20,1.950,QUANTITY='TEMPERATURE' /
&THCP XYZ=2.40,4.20,1.850,QUANTITY='TEMPERATURE' /
&THCP XYZ=2.40,4.20,1.500,QUANTITY='TEMPERATURE' /
&THCP XYZ=2.40,1.40,2.375,QUANTITY='VELOCITY' /
&THCP XYZ=2.40,1.40,2.325,QUANTITY='VELOCITY' /
&THCP XYZ=2.40,1.40,2.275,QUANTITY='VELOCITY' /
&THCP XYZ=2.40,1.40,2.150,QUANTITY='VELOCITY' /
&THCP XYZ=6.80,1.40,2.375,QUANTITY='VELOCITY' /
&THCP XYZ=6.80,1.40,2.325,QUANTITY='VELOCITY' /
&THCP XYZ=6.80,1.40,2.275,QUANTITY='VELOCITY' /
&THCP XYZ=6.80,1.40,2.150,QUANTITY='VELOCITY' /
```